LEVEL II

(12)

B.S.

LOW SPEED AERODYNAMIC CHARACTERISTICS OF WINGS OF ASPECT RATIOS 3 AND 4 EQUIPPED WITH HIGH LIFT SYSTEMS

by

Lynn A. Trobaugh
David G. Lee
Michael J. Harris

APPROVED FOR PUBLIC RELEASE: DISTRIBUTION UNLIMITED

AVIATION AND SURFACE EFFECTS DEPARTMENT

DTNSRDC/ASED-80/09

May 1980

DAVID W. TAYLOR NAVAL SHIP RESEARCH AND DEVELOPMENT CENTER

BETHESDA
MARYLAND
20084

UNCLASSIFIED

SECURITY CLASSIFICATION OF THIS PAGE *(When Data Entered)*

REPORT DOCUMENTATION PAGE

READ INSTRUCTIONS BEFORE COMPLETING FORM

1. REPORT NUMBER: DTNSRDC/ASED-80/09
2. GOVT ACCESSION NO.: AD-A087768
3. RECIPIENT'S CATALOG NUMBER:
4. TITLE (and Subtitle): LOW SPEED AERODYNAMIC CHARACTERISTICS OF WINGS OF ASPECT RATIOS 3 AND 4 EQUIPPED WITH HIGH LIFT SYSTEMS
5. TYPE OF REPORT & PERIOD COVERED:
6. PERFORMING ORG. REPORT NUMBER:
7. AUTHOR(s): Lynn A. Trobaugh; David G. Lee; Michael J. Harris
8. CONTRACT OR GRANT NUMBER(s):
9. PERFORMING ORGANIZATION NAME AND ADDRESS: David W. Taylor Naval Ship R&D Center, Aviation and Surface Effects Department, Bethesda, Maryland 20084
10. PROGRAM ELEMENT, PROJECT, TASK AREA & WORK UNIT NUMBERS: Program Element 62241N; Task Area WF41421091; Work Unit 1600-079
11. CONTROLLING OFFICE NAME AND ADDRESS: Naval Air Systems Command, AIR 320D, Washington, D.C. 20360
12. REPORT DATE: May 1980
13. NUMBER OF PAGES: 97
14. MONITORING AGENCY NAME & ADDRESS *(if different from Controlling Office)*: F41421
15. SECURITY CLASS. *(of this report)*: UNCLASSIFIED
15a. DECLASSIFICATION/DOWNGRADING SCHEDULE:
16. DISTRIBUTION STATEMENT *(of this Report)*: APPROVED FOR PUBLIC RELEASE: DISTRIBUTION UNLIMITED
17. DISTRIBUTION STATEMENT *(of the abstract entered in Block 20, if different from Report)*:
18. SUPPLEMENTARY NOTES:
19. KEY WORDS *(Continue on reverse side if necessary and identify by block number)*:
Circulation Control Wing; Double-Slotted Flaps; High Lift Systems; Lift Coefficient; Low Aspect Ratio Wings; Powered Lift Systems; Semispan Model; Trailing Edge Blowing; Upper Surface Blowing; Wing Tip Fences
20. ABSTRACT *(Continue on reverse side if necessary and identify by block number)*:

Low speed wind tunnel data show that wings of aspect ratios 3 and 4 can produce maximum lift coefficients twice that of conventional double-slotted flap configurations by using powered high lift systems. These high lift systems, which utilize either the circulation control or upper surface blowing concepts, were applied to a semispan wing-fuselage model having a supercritical airfoil section.

DD FORM 1 JAN 73 1473 EDITION OF 1 NOV 65 IS OBSOLETE S/N 0102-014-6601

UNCLASSIFIED

SECURITY CLASSIFICATION OF THIS PAGE *(When Data Entered)*

387695

TABLE OF CONTENTS

LIST OF FIGURES

Page

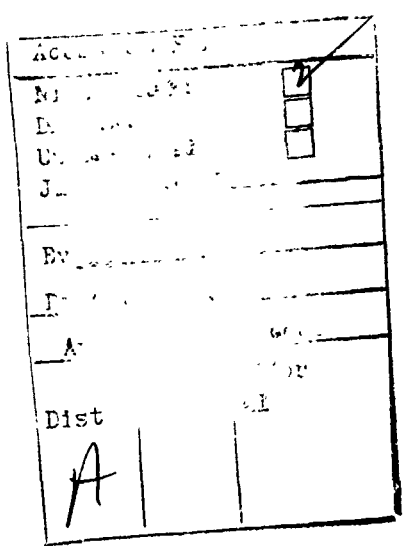

NOTATION

AR	Aspect ratio
b	Wing span, ft (m)
C_D	Drag coefficient
C_L	Lift coefficient
$C_{L_{max}}$	Maximum lift coefficient
C_R	Wing root chord, ft (m)
C_m	Pitching moment coefficient
C_t	Wing tip chord, ft (m)
C_μ	Momentum or thrust coefficient
c	Wing chord, ft (m)
$\bar{c}$	Mean aerodynamic chord, ft (m)
$\dot{m}$	Mass flow, slugs/sec (Kg/s)
P_d	Wing plenum total pressure, lb/in^2 (N/m^2)
P_∞	Free-stream static pressure, lb/in^2 (N/m^2)
q	Free-stream dynamic pressure, lb/in^2 (N/m^2)
R	Universal gas constant
S	Wing reference area, ft^2 (m^2)
T_d	Wing plenum total temperature, °R (°K)
V_j	Jet velocity, ft/sec (m/s)
Λ_{LE}	Leading edge sweep angle, deg
$\Lambda_{c/4}$	Quarter-chord sweep angle, deg

Λ_{te}	Trailing edge sweep angle, deg
γ	Ratio of specific heats
δ_{f_1}	Vane flap deflection angle, deg
δ_{f_2}	Aft flap deflection angle, deg

ABSTRACT

Low speed wind tunnel data show that wings of aspect ratios 3 and 4 can produce maximum lift coefficients twice that of conventional double-slotted flap configurations by using powered high lift systems. These high lift systems, which utilize either the circulation control or upper surface blowing concepts, were applied to a semispan wing-fuselage model having a supercritical airfoil section.

ADMINISTRATIVE INFORMATION

The experimental high lift aerodynamics work presented in this report was performed as part of the David W. Taylor Naval Ship Research and Development (DTNSRDC) Aerodynamics Block, and was sponsored by the Naval Air Systems Command (AIR-320D) under Program Element 62241N, Task Area WF41421091, Work Unit 1600-079.

INTRODUCTION

The concept of the air capable ship envisions at least one aircraft on each Navy surface combatant, perhaps down to destroyer size. Larger ships, such as the LPH, LHA, and others presently undefined, would carry a complement of several aircraft.

Operation of fixed wing aircraft from small ships, such as destroyers which may have only a relatively small landing platform, implies the necessity of some type of vertical takeoff and landing (VTOL) capability for these aircraft. When these aircraft operate from larger ships with enough free deck space to permit a short takeoff or landing (STOL) run, the STOL mode is preferred as it allows increased aircraft range and payload through greater takeoff gross weights. However, STOL operations from small ships pose a problem unique to the Navy, namely, wing span limitations to ensure adequate superstructure clearance. Adequate clearance considerations for an existing ship such as the LHA, for example, would limit wing spans to 62 ft (18.9 m).

Such constraints are at odds with aircraft design practice where good range and endurance generally dictate the use of large aspect ratio wings. These large span wings tend to make the airplane incompatible for operations

from small ships. By constraining wing spans for a given wing loading, the resulting low aspect ratios create the need for methods of increasing the effective aspect ratio.

An additional problem which results from reducing the aspect ratio is that the maximum lift developed by a given lift device is reduced, and for good STOL performance, high lift is needed. Conventional lift augmentation systems such as flaps are limited in the maximum lift they can provide. However, it is possible to generate higher lift by using powered lift augmentation systems to increase the circulation around the wing and to increase the thrust contribution to lift. It should, therefore, be possible to compensate for the relatively low lift produced by low aspect ratio wings with conventional lift augmentation systems by the addition of a powered lift system.

Unfortunately, the quantitative information which is available for powered high lift systems covers only wings of aspect ratios greater than 6. The notable exceptions are the XFV-12A and the A-6 Circulation Control Wing research vehicles. In order to address the problems associated with constraining wing spans, an experimental program has been established to evaluate the effectiveness of powered high lift systems and wing tip devices in providing both STOL and cruise/loiter performance enhancement for low aspect ratio wing aircraft. A more detailed description of this total program effort is provided in Reference 1.

This report presents the results from a series of experimental wind tunnel programs dealing with two powered high lift concepts applied to wings of aspect ratios 3 and 4. A conventional double-slotted flap system represents the state of the art in mechanical (unpowered) high lift systems and as such is evaluated to establish a baseline configuration. Two powered lift augmentation concepts - upper surface blowing (USB) and the circulation control wing (CCW) - are then compared against this baseline configuration.

MODEL AND APPARATUS

A semispan wing-fuselage model was used in this series of wind tunnel programs. The principal model dimensions are shown in Figure 1. The full-span double-slotted flap assembly and the CCW configurations are shown in Figures 2 and 3, respectively. To minimize wing leading edge flow

separation, a 15-percent chord full-span leading edge droop was employed with a deflection angle of 40 deg. The wing was configured for aspect ratios of 3 or 4 by the use of a tip panel to change wing spans.

The basic wing utilizes a 14-percent thick supercritical airfoil section. When configured for double-slotted flaps, the trailing edge flap assembly was designed so that in the retracted position the flap assembly is wholly within the airfoil envelope as would be required on a full scale wing. The gaps and overlaps for the flap assemblies are detailed in Figure 2. Flap deflection angles of 40 and 60 deg were used during these investigations. These angles refer to the angle that the aft flap makes with the horizontal. The vane or intermediate flap deflection angles are also presented in Figure 2. The double-slotted flap assembly in the USB configuration had both gaps filled and faired over with modeling clay to produce a single, continuous flap surface.

Removing the trailing edge flap assembly from the basic wing and substituting a round slotted trailing edge assembly having a wing plenum result in the CCW configuration shown in Figure 3. Details of the Coanda surface and gap dimensions are also shown in Figure 3.

A schematic of the major components of the USB configuration is presented in Figure 4. Two 5.5-in. (14.0-cm) diameter tip turbine fans are tandem mounted to the wing using a pylon assembly. The fan engines are driven by compressed air which is carried to the engines via internal piping inside the wing leading edge. Compressed air limitations restrict fan engine rpm to 70 percent of rated capacity. Consequently, the C_μ range for the USB configurations and, to a lesser degree, the CCW configurations are limited. The turning of the engine exhaust air is accomplished by the extended trailing edge flap acting as a Coanda surface. Three exhaust ducts, each having a "D" shaped cross section at the exit point, were fabricated and evaluated separately. The exhaust ducts have the same exit area but different width-to-height ratios. These dimensions are given in Figure 4.

Installation of the wind tunnel models in the double-slotted configuration and the USB configuration are presented as Figures 5 and 6, respectively.

Because the aspect ratio 4 wing is configured from the aspect ratio 3 wing by adding a tip panel to increase the span, the taper ratio of the two wings is slightly different.

The wing-fuselage model was mounted in the wind tunnel test section such that only the wing was attached to the balance frame. The fuselage was mounted to a boundary layer splitter plate and was independent of the balance frame with a small gap existing between wing root and fuselage body. The forces and moments measured by the balance frame are essentially wing alone data in the presence of a body.

Minor leakage developed through the wing-fuselage gap during testing of the CCW configuration. This leakage produced severe separation of the upper surface wing flow near the root area. Rather than attempt to seal the gap and thereby transmit loads to the fuselage, a large fence was installed around the wing close to the fuselage. This wing root fence and an additional wing tip fence used to explore tip flow are shown in Figure 7.

The circular boundary layer splitter plate, which was 8 ft (2.44 m) in diameter, also served as a reflection plane for the semispan model. The plate was mounted to the test section floor with a gap between the ground-board and tunnel floor to separate the boundary layer. Details of the splitter plate are shown in Figures 1, 4, and 6.

WIND TUNNEL EXPERIMENTS

The investigations were conducted in the 8- by 10-foot north subsonic wind tunnel at DTNSRDC.[2] This wind tunnel is of the single return closed-circuit type that is capable of continuous operation at atmospheric pressure. The rectangular shaped test section can achieve dynamic pressures up to 80 lb/ft^2 (3830 N/m^2). The majority of the data were recorded at a dynamic pressure of 20 lb/ft^2 (958 N/m^2), which corresponds to a Reynolds number of 0.8×10^6/ft (2.6×10^6/m).

For this series of investigations, the semispan model was floor-mounted in the wind tunnel in a vertical position using a base strut system. This strut system is located beneath the tunnel floor and transfers the aerodynamic loads of the model to an external Toledo mechanical balance system.

The Toledo balance measures six component force and moment data for recording on magnetic tape utilizing a Beckman 210 high speed acquisition system.

The CCW configuration was examined over a range of blowing coefficients (C_μ) from 0 to 0.60. Final C_μ values were calculated using wind tunnel data as Coanda slot height varied from actual measurements due to slot expansion caused by wing plenum pressure. The dashed curves presented in the figures represent nominal increments of C_μ obtained from crossplotting the wind tunnel data in order to facilitate comparisons of configurations. All of the data for the CCW configuration were recorded with the wing root fence installed. In addition, a wing tip fence was installed on several configurations to examine its effect on a portion of the data.

The momentum coefficient was calculated from the expression:

$$C_\mu = \frac{\dot{m} V_j}{qs}$$

where the jet mass flow ($\dot{m}$) was measured by a venturimeter located in the air supply line, and the jet velocity (V_j) was calculated assuming an isentropic expansion from the wing plenum total conditions to free-stream static conditions at the wing trailing edge. Under this assumption, the expression for V_j is:

$$V_j = \sqrt{\frac{2\gamma RT_d}{\gamma-1}\left[1-\left(\frac{P_\infty}{P_d}\right)^{\frac{\gamma-1}{\gamma}}\right]}$$

The expansion to local static conditions at the jet exit would give a more realistic value of V_j, and expansion to free-stream static pressure underestimates V_j. However, local exit conditions are functions of local geometry, and a comparison of two blown airfoils of unlike trailing edge geometry but identical mass flows and plenum pressures would yield unlike values of C_μ. The momentum coefficient based on expansion to free-stream conditions is thus accepted as a more "universal" parameter of blown systems and is consistent with previous DTNSRDC practice.

The USB configuration was examined over a range of thrust coefficients (C_μ) from 0 to 2.00. Final values of C_μ were obtained using the wind tunnel conditions and the expression:

$$C_\mu = \frac{T}{qs}$$

where the thrust T is measured statically and is the vector resultant of the forces in the drag and lift directions.

A thrust calibration was performed for each USB configuration used in these investigations with the model assembled on the balance frame in the wind tunnel. The thrust calibration was then programed into the data reduction routine. (Unless specifically noted, the 40-deg wing leading edge droop was retained as part of all the configurations examined.)

All forces and moments were resolved about the mean aerodynamic quarter chord point and reduced to standard coefficient form in the stability axis system. Coefficients were calculated based on measured wind tunnel loads and wing panel dimensions. Model weight and airline pressure tare corrections were applied to the balance data. The only aerodynamic corrections applied to the force and moment data consisted of the standard downwash corrections as outlined in Reference 3; angle of attack and drag coefficient were the two parameters affected.

Before recording data on both powered high lift concepts, the CCW and USB configurations were visually checked for the possibility of flow recirculation problems. Wool tufts were attached to the test section wall and groundboard in the vicinity of the model and observed during tunnel operation at maximum test conditions. No recirculation problems were found.

A static bench test of the three air turbine engine-duct combinations was also performed to examine the airflow as it exited the duct before impingement on the trailing edge flaps. A mixture of titanium oxide and oil was applied to the inside of the ducts to allow visual observations of the flow patterns. The three ducts have approximately the same exit area but have increasing aspect ratios B/H, where B is the duct exit width and H is the height. The ducts have aspect ratios of 2.2, 3.9, and 5.8, with other major dimensions shown in Figure 4. The general flow pattern was good; however, minor separation and turbulence occurred in the lower corners with the aspect ratio 5.8 duct exhibiting the most separation.

DISCUSSION OF RESULTS

DOUBLE-SLOTTED FLAPS

Figures 8 and 9 present the longitudinal aerodynamic characteristics of the full-span double-slotted flap configurations of the aspect ratio 3 and 4 wings, respectively. These configurations did not use either the wing root fence or the wing tip fence at any time. Both aspect ratio 3 and 4 wings begin to show evidence of flow separation for C_L values of 1.4 or greater. This flow separation is indicated by the change in the pitching moment characteristics of both double-slotted flap configurations. As previously noted, a portion of the separated flow on this semispan model is undoubtedly due to the leakage between the wing-fuselage gap which promotes spanwise flow in the wing root area. Unfortunately, the root fence constructed for the CCW configuration is incompatible with the trailing edge geometry of both the USB and double-slotted flap configurations. However, this problem will be addressed in a subsequent wind tunnel program and report. For this investigation, the maximum lift capability of both the USB and double-slotted flap configurations was therefore not fully realized. However, a comparison of the relative merits of the two high lift approaches is still valid.

With a flap deflection angle δ_{f_2} of 60 deg, the aspect ratio 3 wing produced a $C_{L_{max}}$ of 2.12 at an angle of attack α of 26 deg. With a δ_{f_2} of 40 deg, a $C_{L_{max}}$ of 1.87 was obtained at an α of 27 deg. The aspect ratio 4 wing produced a $C_{L_{max}}$ of 2.33 at an α of 26 deg for a δ_{f_2} of 60 deg. With a δ_{f_2} of 40 deg, the $C_{L_{max}}$ obtained was 2.10 at an α of 25 deg.

CIRCULATION CONTROL WING

Figures 10 and 11 present similar longitudinal data for the aspect ratio 4 wing in the CCW configuration with and without the wing tip fence installed. The addition of a tip fence is employed in an effort to reduce the tip vortex and to prevent separation of the Coanda surface near the tip. The wing root fence is utilized on all CCW configurations. The dashed curves shown are the interpolated values of C_μ which are used for comparison purposes with the other configurations. Values of C_μ are

presented in 0.05 increments from 0 to 0.20. The aerodynamic characteristics are presented for the aspect ratio 3 wing with the tip fence installed in Figure 12, and Figure 13 presents the wing with no tip fence.

For the aspect ratio 4 wing, increasing C_μ produces an increase in C_L for any angle of attack below stall up to a C_μ value of about 0.18. For C_μ greater than 0.18, $C_{L_{max}}$ decreases somewhat. The angle of attack to stall does not vary appreciably with an increase in C_μ, except at a C_μ of 0.26 where it drops 6 deg. In Figure 10a, for example, with a C_μ of 0.175, a $C_{L_{max}}$ of 3.35 occurs at an α of 21.6 deg. When C_μ is increased to 0.255, $C_{L_{max}}$ is 3.30 and occurs at an α of only 15.8 deg. A similar trend is displayed in Figure 11a for the aspect ratio 4 wing without the tip fence installed. Examination of the C_M-C_L plots shows the pitching moment rapidly becoming more positive at stall. This would tend to indicate flow separation at the wing trailing edge and flow visualization using wool tufts confirmed this. The trailing edge Coanda surface separates at the wing tip as the stall angle of attack is approached and progresses inboard as the angle of attack is increased further. Stall angle of attack is generally reduced and $C_{L_{max}}$ increases with the addition of a tip fence.

Results for the aspect ratio 3 wing in the CCW configuration are shown in Figures 12 and 13 with and without the wing tip fence installed. The aspect ratio 3 wing exhibits similar trends displayed by the aspect ratio 4 wing. The $C_{L_{max}}$ increases with C_μ until a C_μ of 0.20 is reached. A higher value of C_μ produces a lower $C_{L_{max}}$ and a significantly lower stall angle. This is shown in Figure 13a where a C_μ of 0.285 produces a sudden stall at an α of 12 deg due to detachment of the flow from the Coanda surface.

The aspect ratio 3 CCW wing was found to have a noncircular trailing edge after model fabrication. While the Coanda surface did not have sharp steps or surface discontinuities, it did have a varying radius of curvature. To determine the sensitivity of the CCW performance to this type of irregularity, wind tunnel data were obtained on this configuration before the Coanda surface was reworked. These data are presented in Figures 14 and 15 for the aspect ratio 3 wing with and without the tip fence installed. Figure 16 summarizes the effect of the noncircular Coanda surface on the lift characteristics. The aerodynamic characteristics of the aspect ratio

3 wing show evidence of trailing edge separation. This separation occurs over the C_μ range at approximately 10-deg angle of attack and is evident from the change in the slope of the C_L-α curve and from the break in the C_M-C_L curve. Visual observations of wool tufts attached to the Coanda surface verified the separation of the flow. The angle of stall again decreases with increasing C_μ. The flow separation begins at the wing tip and progresses inboard as C_μ and/or α is increased. For C_μ values greater than about 0.20, a relatively abrupt change in pitching moment occurs with little or no change in C_L, indicating a sudden change in the shape of the chordwise pressure distribution curve with no change of volume under the wing pressure distribution envelope. As expected, the CCW configuration with the nonround Coanda trailing edge produces lower lift over the range of α and C_μ investigated as compared to the round Coanda surface. The addition of a tip fence to the configurations generally lowers the angle of stall for the nonround Coanda trailing edge as compared to the round Coanda surface; however, this addition may also result in a higher lift coefficient than that of the round Coanda trailing edge depending on the value of α and C_μ.

Figure 17 is a crossplot of all of the CCW data showing the effect of a wing tip fence on $C_{L_{max}}$ of both the aspect ratio 3 and 4 wings. For the aspect ratio 4 wing, there is an increase in $C_{L_{max}}$ resulting from the addition of a tip fence. This increase is about 10 percent and occurs over the range of values of C_μ investigated. The same percentage increase in $C_{L_{max}}$ occurs with the addition of a tip fence on the aspect ratio 3 wing; however, little or no effect occurs at the low end of the C_μ range. Flow visualization shows that the tip fence delays jet detachment from the Coanda surface at the wing tip. Flow entrainment by the jet produces a strong inboard spanwise flow at the wing tip which tends to detach the flow. Englar[4,5] noted similar flow characteristics with other CCW configurations. The addition of an endplate (wing tip fence) helps prevent spanwise tip flow and the resulting flow detachment from the Coanda surface.

UPPER SURFACE BLOWING

The longitudinal characteristics for the aspect ratio 3 wing in the USB configuration are presented in Figures 18 and 19. The data show that

a $C_{L_{max}}$ of 4.20 was obtained for a δ_{f_2} of 60 deg, while a δ_{f_2} of 40 deg produced a $C_{L_{max}}$ of 3.86. Both $C_{L_{max}}$ values were obtained at a thrust coefficient C_μ of approximately 1.60. In the stall region near $C_{L_{max}}$, there is an abrupt change in the pitching moment to a more positive value similar to the condition present for the CCW configuration - although not as abrupt at the higher value of C_μ. The aspect ratio 4 wing data presented in Figures 20 and 21 show a $C_{L_{max}}$ of 4.31 for a δ_{f_2} of 60 deg and a $C_{L_{max}}$ of 4.05 for a δ_{f_2} of 40 deg. These values of maximum lift coefficient were recorded for C_μ values in the range of 1.40. Contrary to the trends observed for the CCW and at least for the range of C_μ values investigated for the USB configurations, $C_{L_{max}}$ continues to increase with C_μ, and the angle of attack for stall remains approximately the same - even increasing in some cases.

The lift characteristics for the remainder of the USB configurations are presented in Figures 22 through 25. The three duct designs for the tip turbine engines in the USB configurations generally confirm the trends reported by Phelps et al.[6,7] (The overall geometry of the exhaust ducts shown in Figure 4 are based on the data of these references.) The aspect ratio 5.8 duct having the largest roof and spread angles tends to flatten and spread the exhaust jet sheet over the trailing edge flap to cover a greater part of the flap and produce better turning of the flow. This was confirmed from data obtained during static thrust calibrations in the wind tunnel where flow turning angles were calculated for each engine duct-flap configuration. As expected, the lift data show the aspect ratio 5.8 duct consistently produces the highest $C_{L_{max}}$, with the aspect ratio 2.2 duct consistently producing the lowest $C_{L_{max}}$. As the exit area of the three duct designs are approximately the same, increasing the duct width-to-height exit ratio (aspect ratio) likewise produces an increase in the root and spread angles. The duct designs all used "D" shaped exit cross sections with well rounded corners to minimize the creation of external vortices. The lift data of Figures 22 through 25 show that as duct aspect ratio increases and spreads out the jet sheet over the trailing edge flap, $C_{L_{max}}$ generally increases and the angle of attack for stall decreases.

For all USB configurations at the lower values of C_μ, the addition of a tip fence increases $C_{L_{max}}$. However, at the higher values of C_μ only the 60-deg flap configuration is affected by the tip fence, where the addition reduces $C_{L_{max}}$.

Figures 26 and 27 present the lift characteristics of the aspect ratio 3 and 4 wing in the USB configuration with a "clean" trailing edge, i.e., no flap deflection. A significant difference in the lift capability between the two aspect ratios exists only at the highest C_μ investigated.

The effect of using a slotted flap system as opposed to the single continuous flap surface for USB configurations is shown in Figure 28. Modeling clay used to form a single continuous flap system was removed to create a double-slotted flap configuration. The aspect ratio 3 wing with the double-slotted flap reached a $C_{L_{max}}$ of 3.06. By using the continuous flap surface, a $C_{L_{max}}$ of 3.58 was obtained for the same value of C_μ. For the aspect ratio 4 wing, the corresponding values of $C_{L_{max}}$ were 3.24 and 4.00. These configurations had wing tip fences installed and used a 60-deg flap deflection. The continuous flap surface stalls at a lower angle of attack; however, for the same value of C_μ, a greater static flow turning is produced with a resulting higher $C_{L_{max}}$.

A summary of the $C_{L_{max}}$ data for the USB configurations with the 5.8 aspect ratio duct is presented in Figure 29. Additional increases in $C_{L_{max}}$ could be expected with an increase in C_μ beyond the maximum value investigated in this program. For both aspect ratio 3 and 4 wings, increasing the flap deflection angle from 40 to 60 deg does not increase $C_{L_{max}}$ an appreciable amount, except at C_μ values greater than about 1.20.

SUMMARY

Analysis of the data from these investigations indicates the following:

1. Full-span double-slotted flaps using a 60-deg deflection produce a $C_{L_{max}}$ of 2.12 with an aspect ratio 3 wing and a $C_{L_{max}}$ of 2.33 for an aspect ratio 4 wing. Both aspect ratio wings experience a reduction in $C_{L_{max}}$ of approximately 10 percent for a flap setting of 40 deg.

2. In a CCW configuration, the aspect ratio 3 wing produces a $C_{L_{max}}$ of 2.6, while the aspect ratio 4 wing reaches a $C_{L_{max}}$ of 3.0. Although lift coefficient increases with C_μ, values of C_μ greater than 0.20 produce little or no additional improvements in lift.

3. For a CCW configuration, the stall angle of attack decreases with an increase in C_μ. In the stall area, a sudden change in the pressure distribution produces a relatively large change in the pitching moment with little or no change in the lift.

4. The Coanda surface of a CCW is highly sensitive to irregularities in surface curvature which cause jet detachment at low values of C_μ and low angles of attack. The addition of a wing tip fence reduces spanwise flow, which results in increased $C_{L_{max}}$ due to reduced flow detachment.

5. The USB configuration with an aspect ratio 3 wing produces a $C_{L_{max}}$ of 3.86 and 4.20 for flap deflections of 40 and 60 deg, respectively. The corresponding values of $C_{L_{max}}$ for the aspect ratio 4 wing are 4.05 and 4.31. Lift coefficient increases with C_μ up to a value of 1.6, the maximum value of C_μ obtained during this investigation.

6. For the USB configurations, the stall angle of attack remains approximately the same with increases in C_μ and in some cases increases slightly. Similar to the CCW case, there is a sudden but even larger change in the pitching moment characteristics occurring at high values of C_μ with little or no change in lift coefficient.

7. In the USB configurations, a continuous flap surface - though stalling at lower angles of attack - produces significantly higher values of $C_{L_{max}}$ than the slotted flap surfaces at the same flap angle.

8. The addition of wing tip fences on USB configurations does not produce as consistent a beneficial effect as is the case in the CCW configurations.

CONCLUSIONS

Wind tunnel results indicate that V/STOL configurations employing low aspect ratio wings can produce up to twice the lift coefficient available from conventional double-slotted flap configurations when powered lift augmentation is utilized. The effective aspect ratio of these wings is increased through additional circulation gained from Coanda trailing edge

blowing or upper surface wing blowing using engine exhaust air. In the case of the upper surface blowing technique, additional lift is achieved through rotation of the engine thrust vector from a horizontal to more of a vertical direction by proper design of the engine exhaust duct.

The stall characteristics of power-augmented low aspect ratio wings tend to be rather sudden and abrupt, indicating leading edge flow separation. The addition of a tip fence reduces tip spanwise flow in the case of the trailing edge Coanda blowing wing and results in higher maximum lift coefficients. However, for the upper surface blowing, little or no beneficial effects occur with a tip fence addition as the lift augmenting high energy airflow is concentrated near the wing midspan as opposed to the tip-to-root distribution of the trailing edge Coanda blowing.

REFERENCES

1. Nichols, J.H. Jr., "Development of High Lift Devices for Application to Advanced Navy Aircraft," David W. Taylor Naval Ship R&D Center Report DTNSRDC-80/058 (Apr 1980).

2. Kidd, M. A., "Subsonic Wind Tunnel Facilities," Naval Ship Research and Development Center Report 3782 (Jan 1972).

3. Pope, A. and J.J. Harper, "Low-Speed Wind Tunnel Testing," John Wiley and Sons, Inc., New York, pp. 337-342 (1966).

4. Englar, R.J., "Circulation Control for High Lift and Drag Generation on STOL Aircraft," Journal of Aircraft, Vol. 12, No. 5, pp. 457-463 (1975).

5. Englar, R.J. et al., "STOL Potential of the Circulation Control Wing for High Performance Aircraft," Journal of Aircraft, Vol. 5, No. 3, pp. 175-181 (1978).

6. Phelps, A.E., III, and W.C. Sleeman, Jr., "Upper-Surface-Blowing Flow-Turning Performance," National Aeronautics and Space Administration, SP-406, pp. 29-43 (1976).

7. Phelps, A.E., III, et al., "Summary of Low-Speed Aerodynamic Characteristics of Upper-Surface-Blown Jet-Flap Configurations," National Aeronautics and Space Administration, SP-406, pp. 63-87 (1976).

NOMINAL ASPECT RATIO	CHORD		SWEEP (deg)		
	TIP	ROOT	L.E.	T.E.	SEMISPAN
3	8.40 in. (21.34 cm)	18.34 in. (46.58 cm)	25.8	0	1.91 ft (0.582 m)
4	6.42 in. (16.31 cm)	18.34 in. (46.58 cm)	25.8	0	2.12 ft (0.646 m)

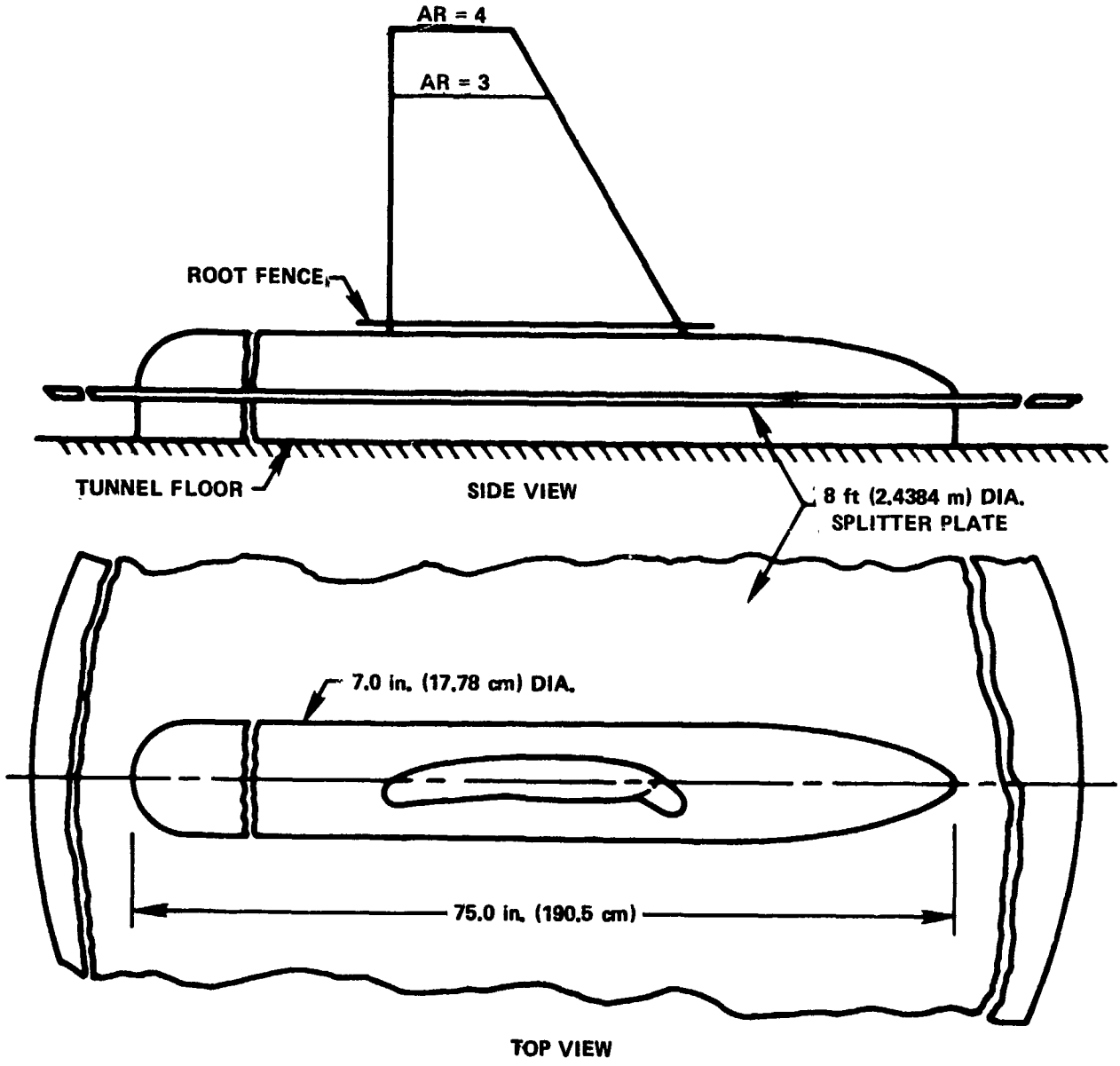

Figure 1 - Semispan Wing - Fuselage Model and Groundboard

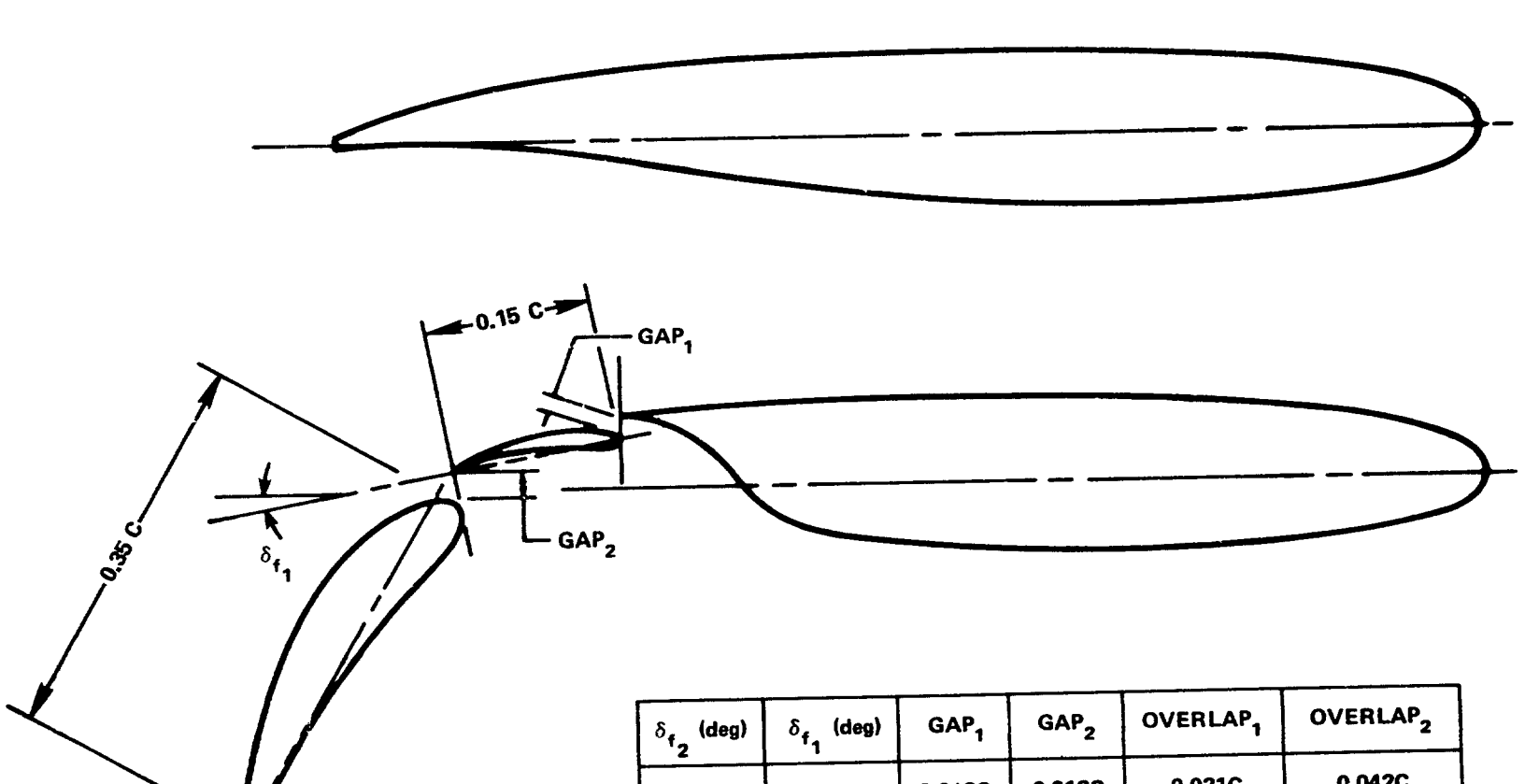

δ_{f_2} (deg)	δ_{f_1} (deg)	GAP_1	GAP_2	$OVERLAP_1$	$OVERLAP_2$
40	9.8	0.012C	0.012C	0.021C	0.042C
60	10.4	0.020C	0.020C	0	0

Figure 2 - Double-Slotted Flap Configuration

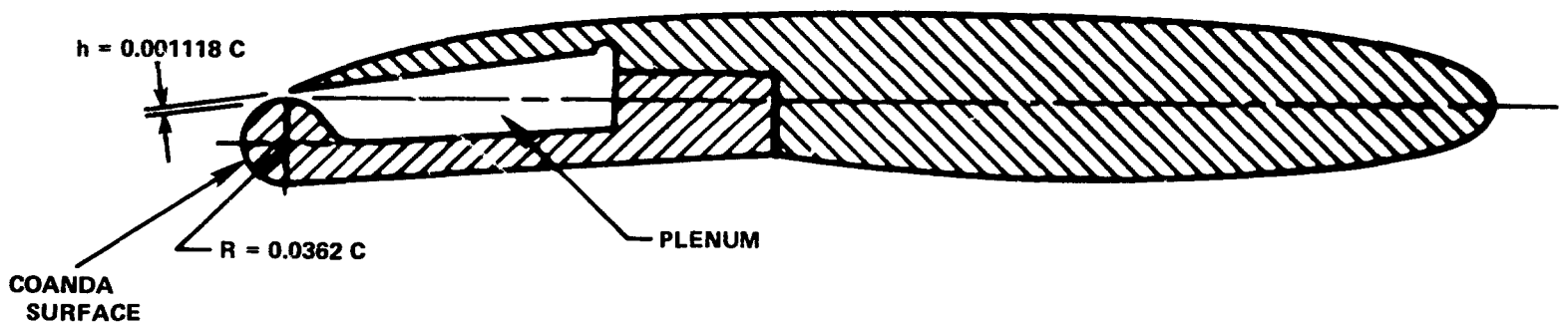

Figure 3 - Circulation Control Wing Configuration

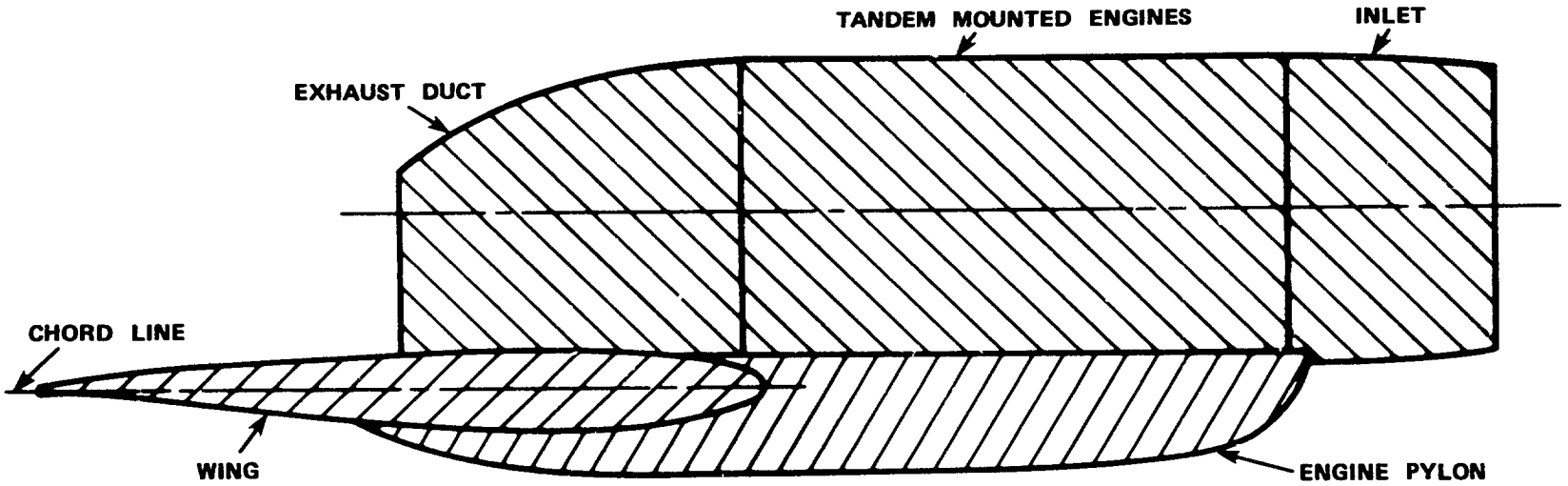

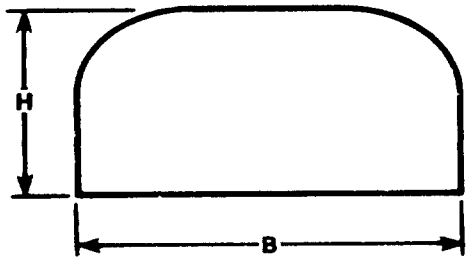

DUCT	B	B/H	ROOF ANGLE (DEGREES)	OUTBOARD SPREAD ANGLE (DEGREES)
1	7.6 in. (19.3 cm)	2.2	27	7
2	10.5 in. (26.7 cm)	3.9	34	30
3	12.8 in. (32.5 cm)	5.8	37	45

Figure 4 - Upper Surface Blowing Configuration

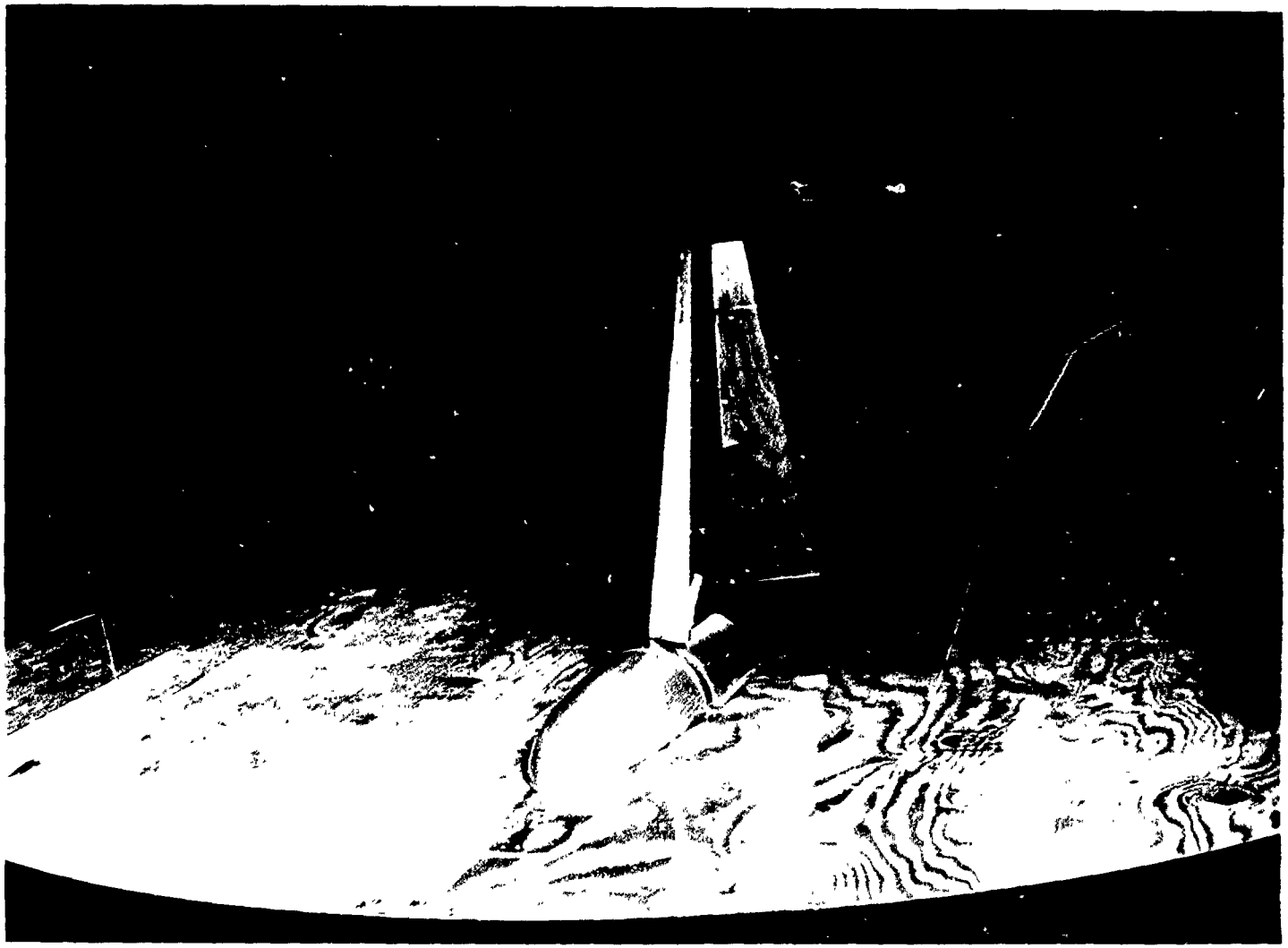

Figure 5 - Wind Tunnel Model with Double-Slotted Flaps

Figure 6 - Wind Tunnel Model with Upper Surface Blowing

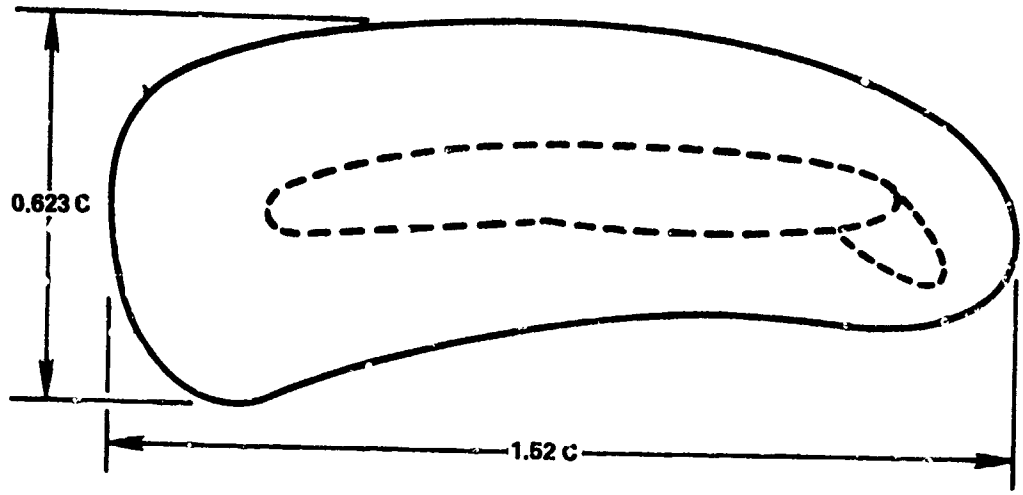

WING TIP PLATE

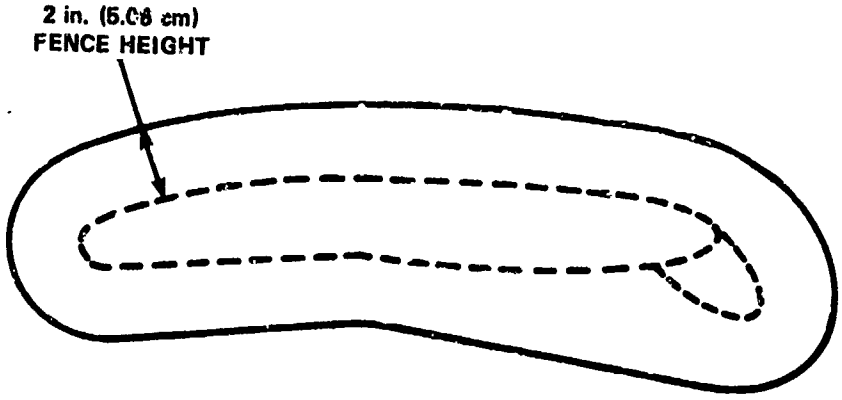

WING ROOT PLATE

Figure 7 - Wing Tip and Wing Root Fence Configurations

Figure 8 - Aspect Ratio 3 Wing With D uble-Slotted Flaps

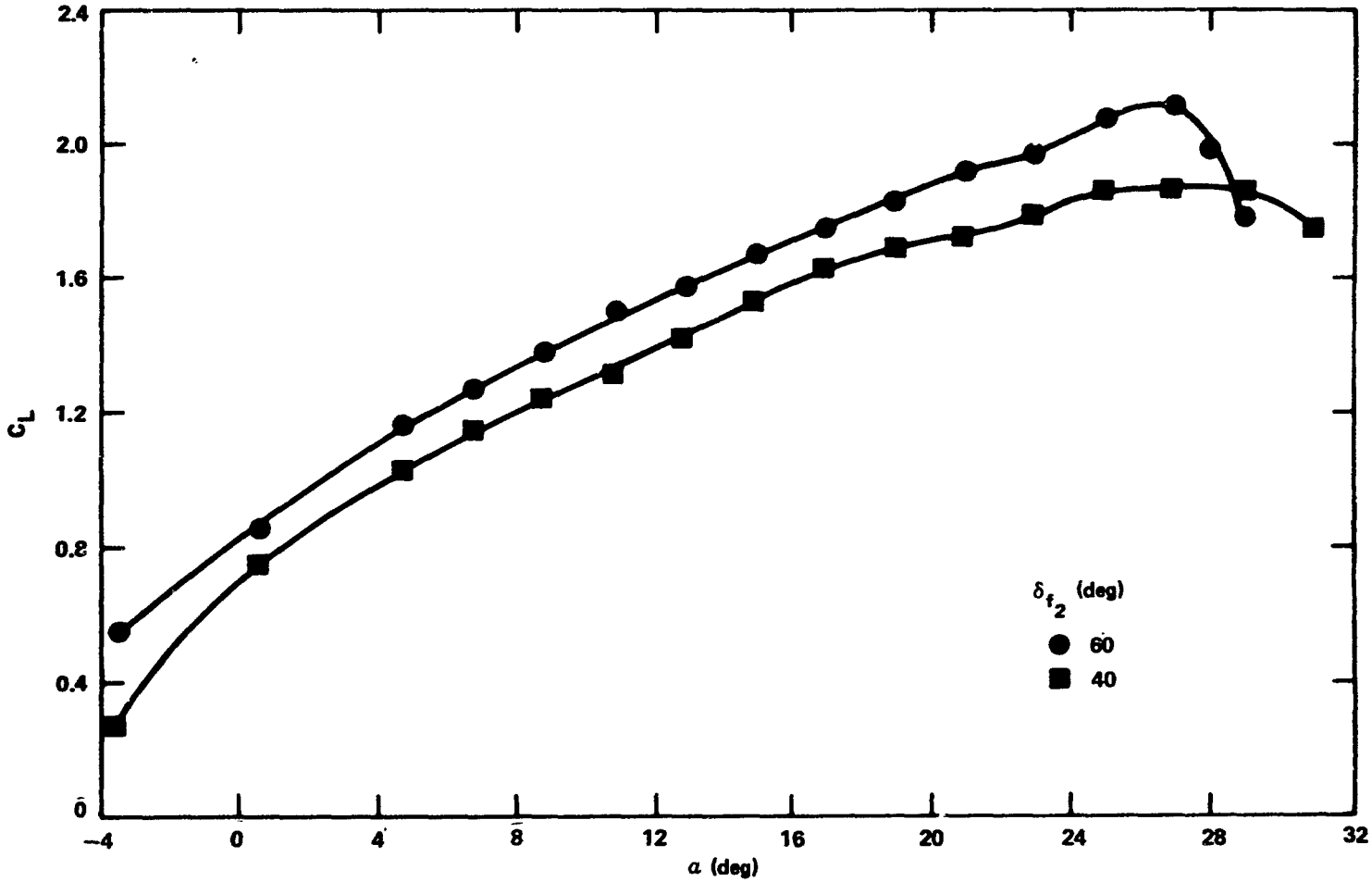

Figure 8a - Lift Characteristics

Figure 8 (Continued)

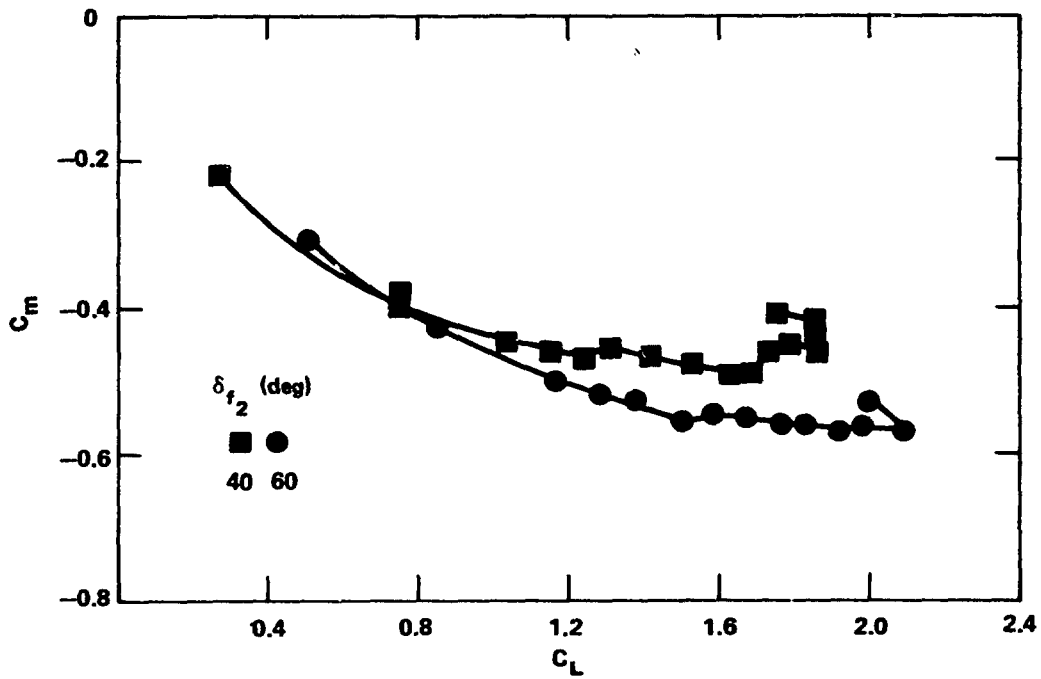

Figure 8b - Pitching Moment Characteristics

Figure 8 (Continued)

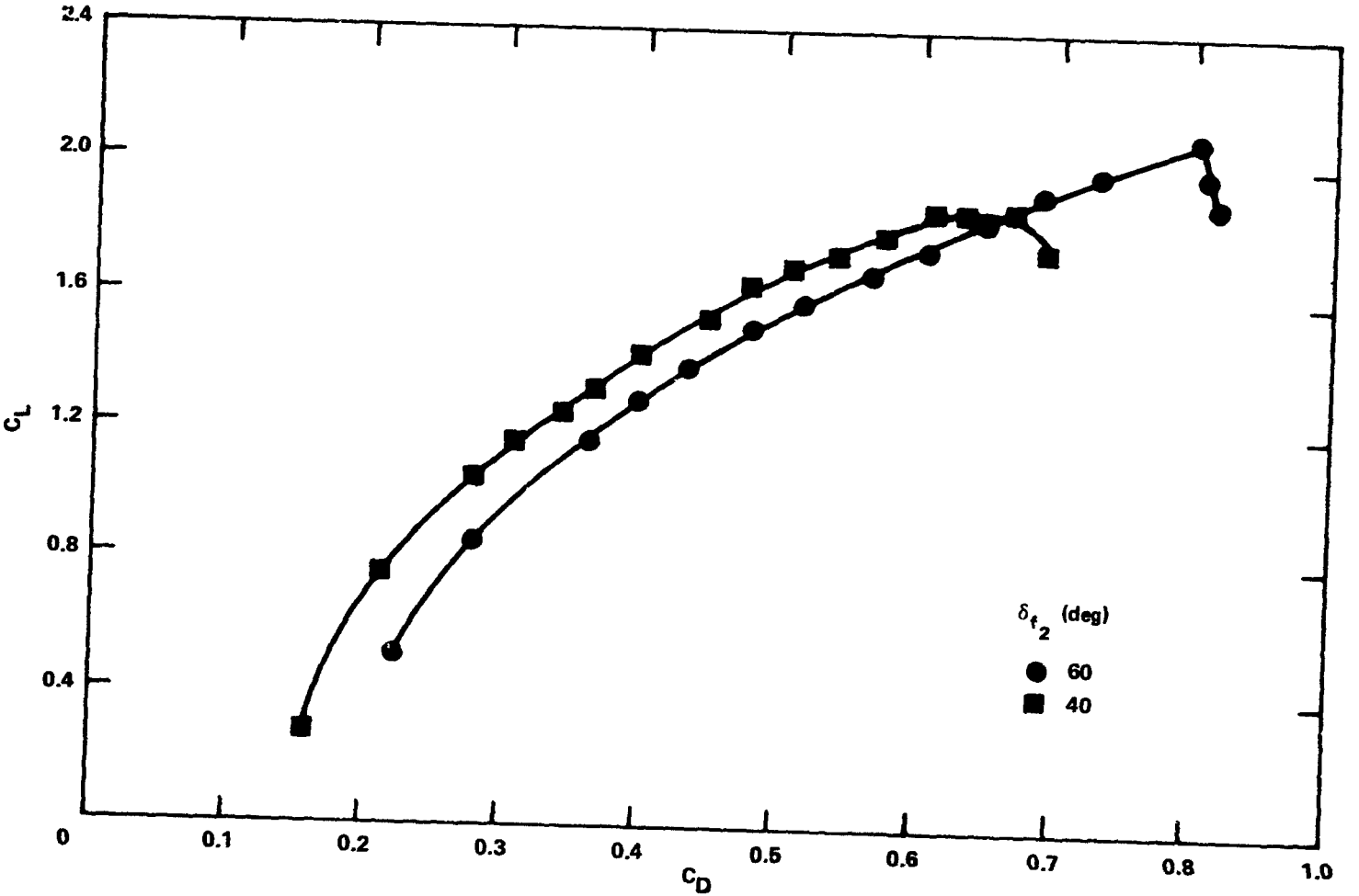

Figure 8c - Drag Polar

Figure 9 - Aspect Ratio 4 Wing with Double-Slotted Flaps

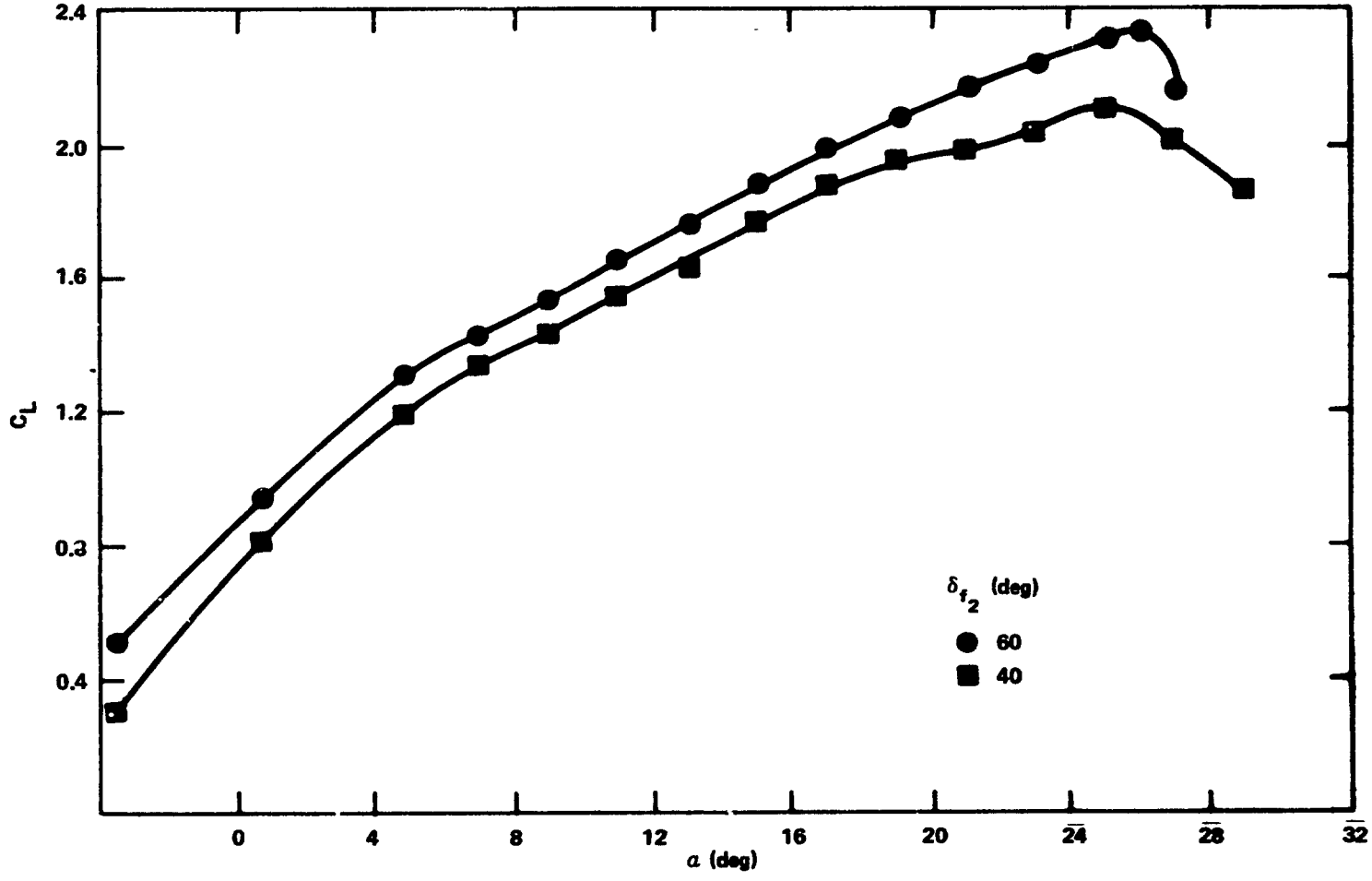

Figure 9a - Lift Characteristics

Figure 9 (Continued)

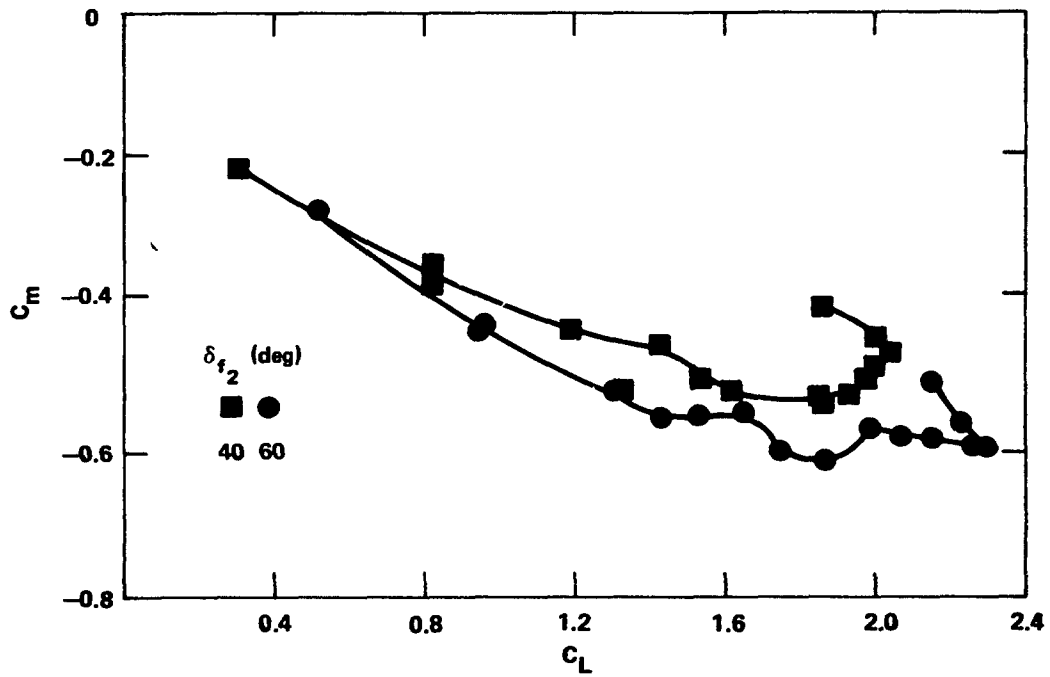

Figure 9b - Pitching Moment Characteristics

Figure 9 (Continued)

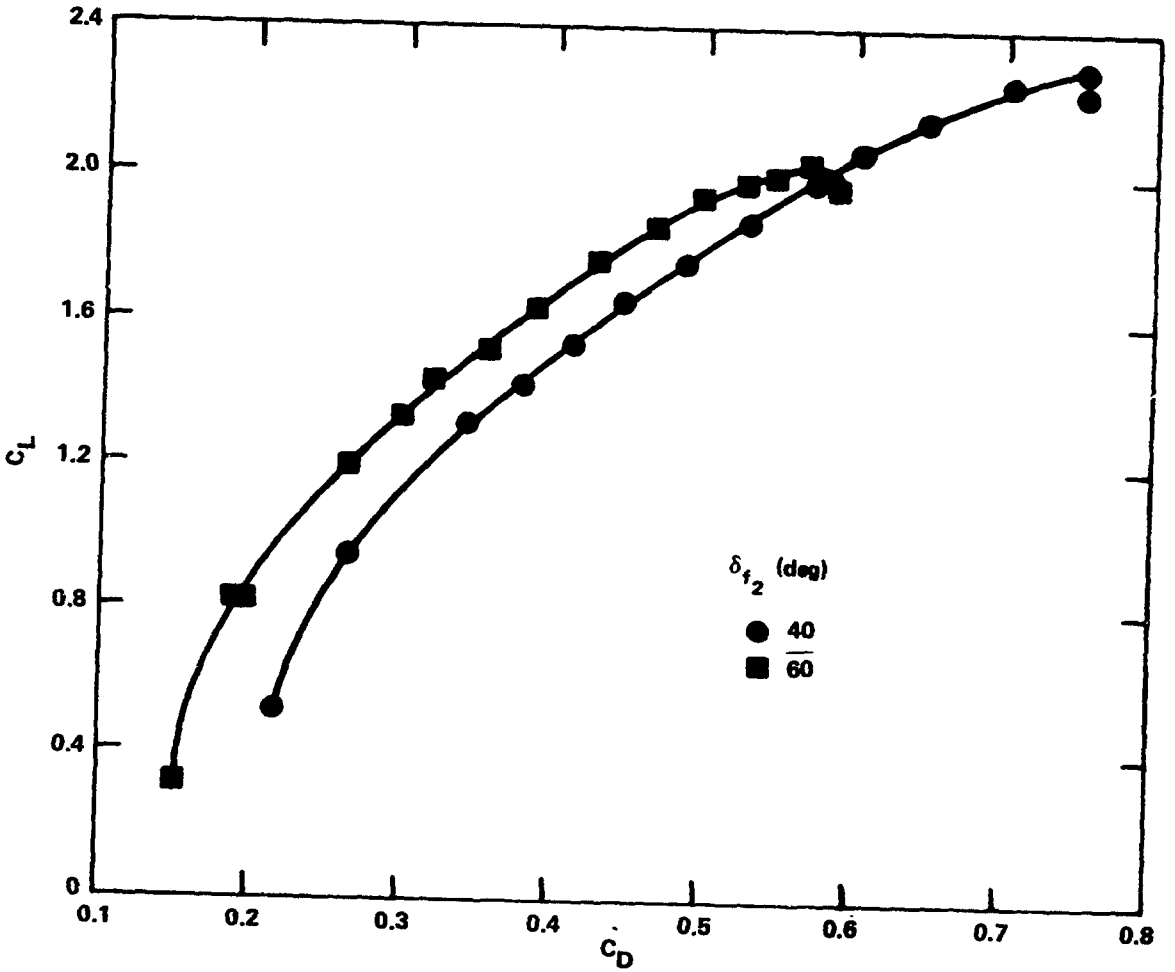

Figure 9c - Drag Polar

Figure 10 - Aspect Ratio 4 Wing in CCW Configuration with Wing Tip Fence Installed

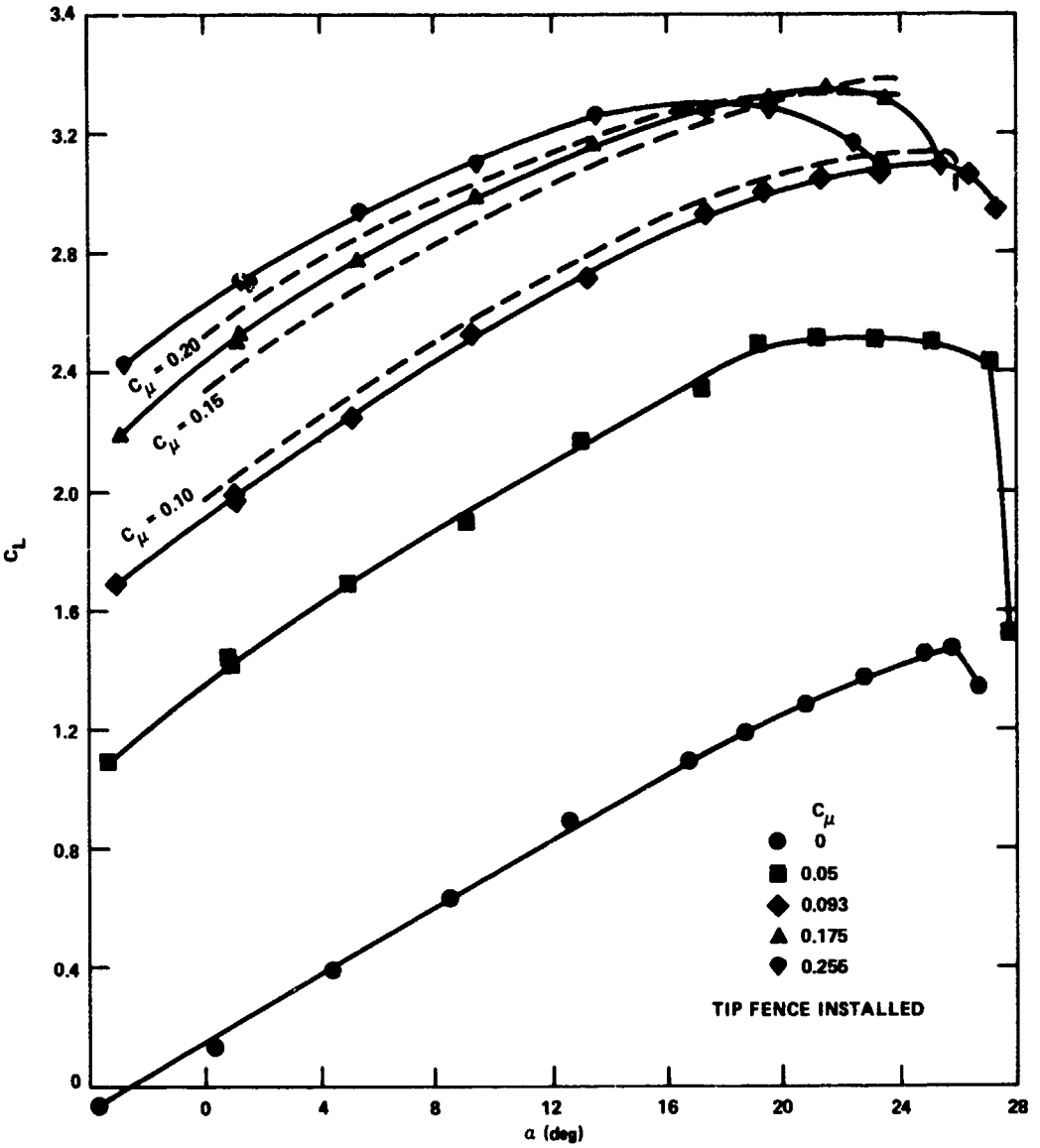

Figure 10a - Lift Characteristics

Figure 10 (Continued)

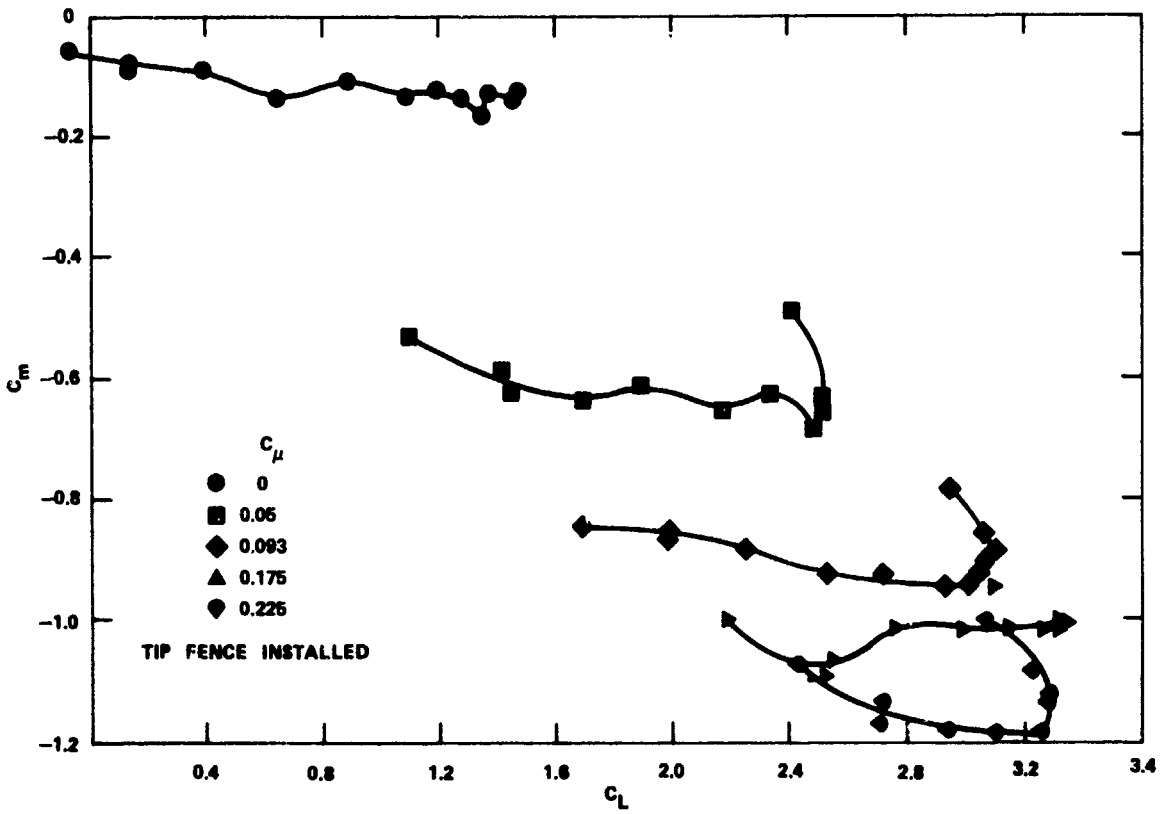

Figure 10b - Pitching Moment Characteristics

Figure 10 (Continued)

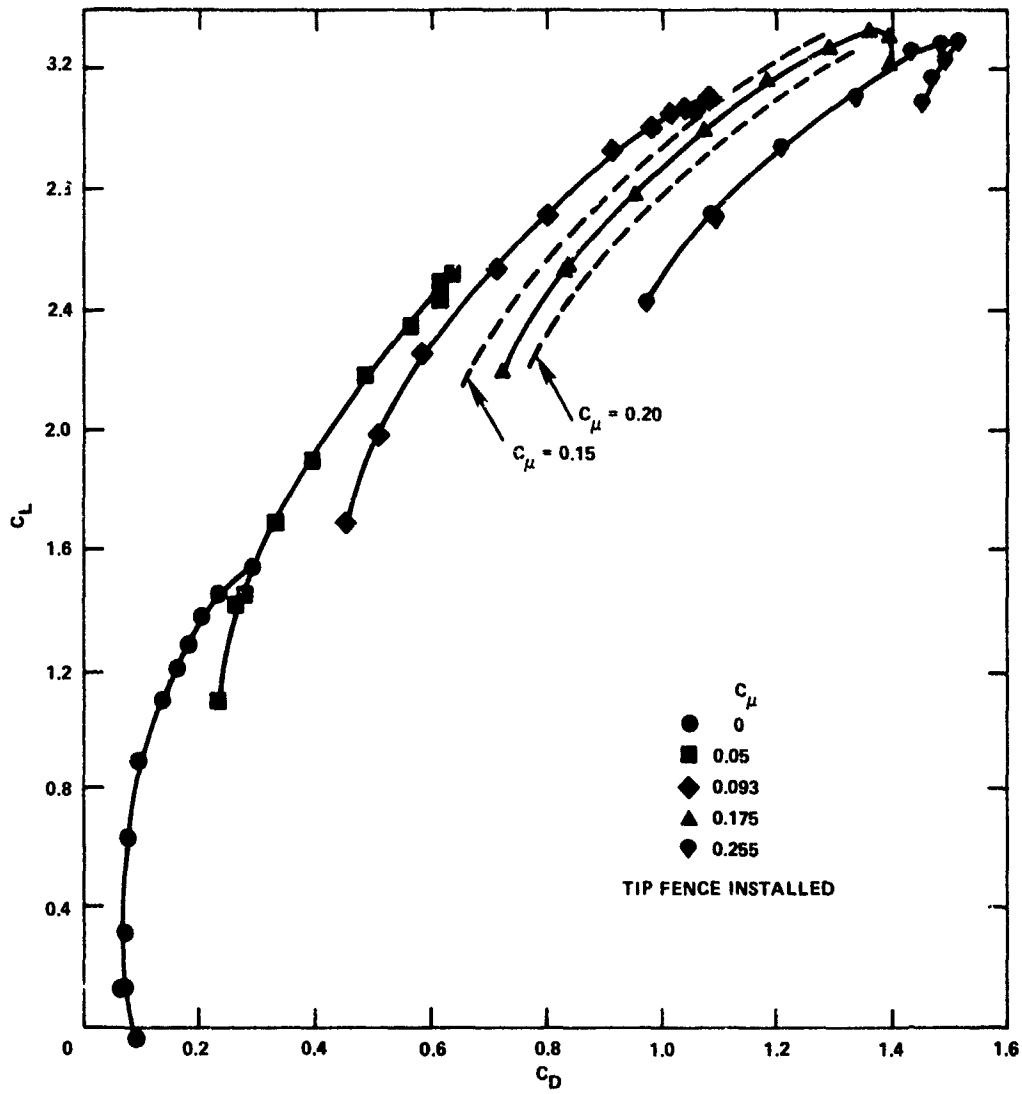

Figure 10c - Drag Pola:

Figure 11 - Aspect Ratio 4 Wing in CCW Configuration without Wing Tip Fence

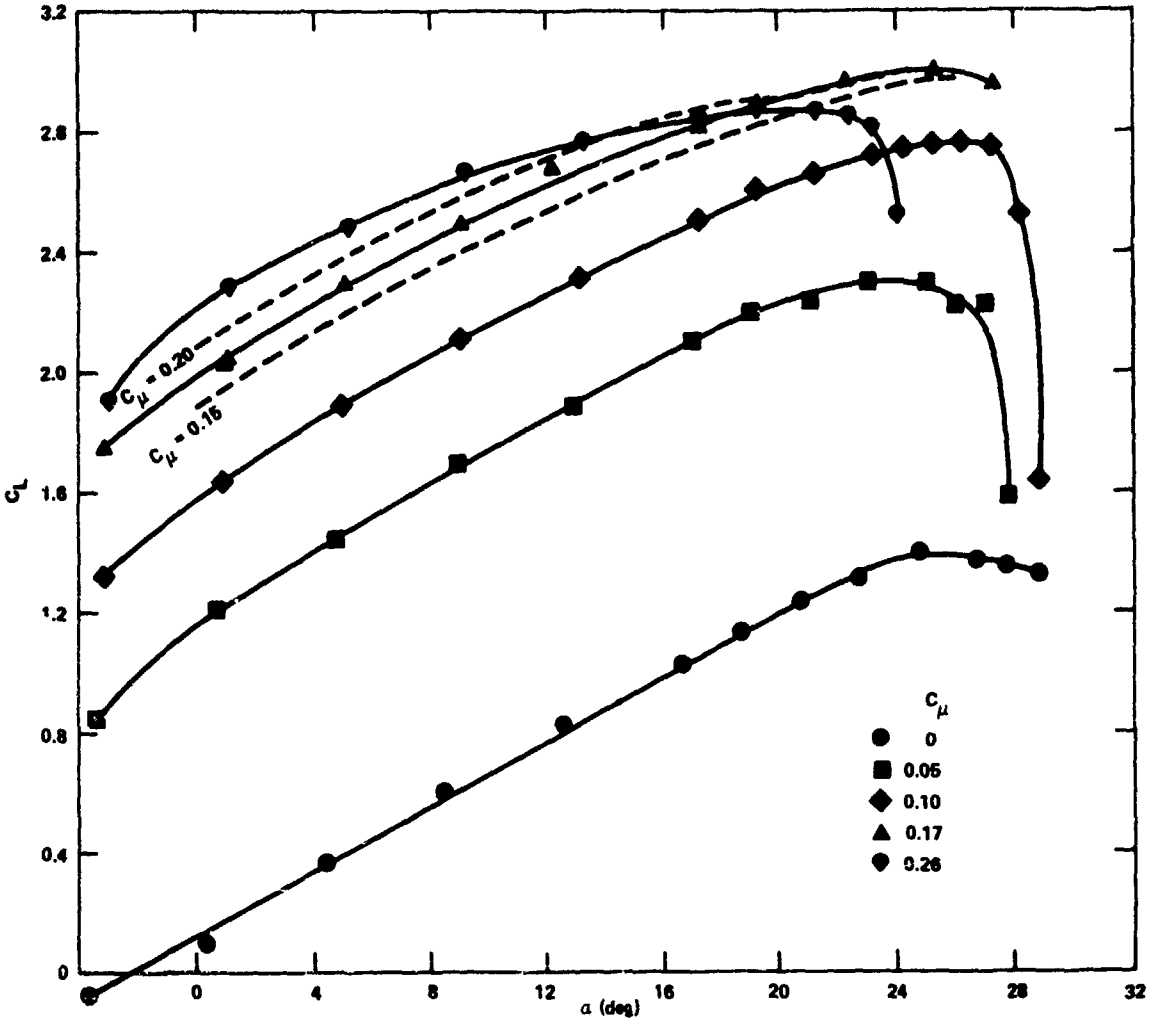

Figure 11a - Lift Characteristics

Figure 11 (Continued)

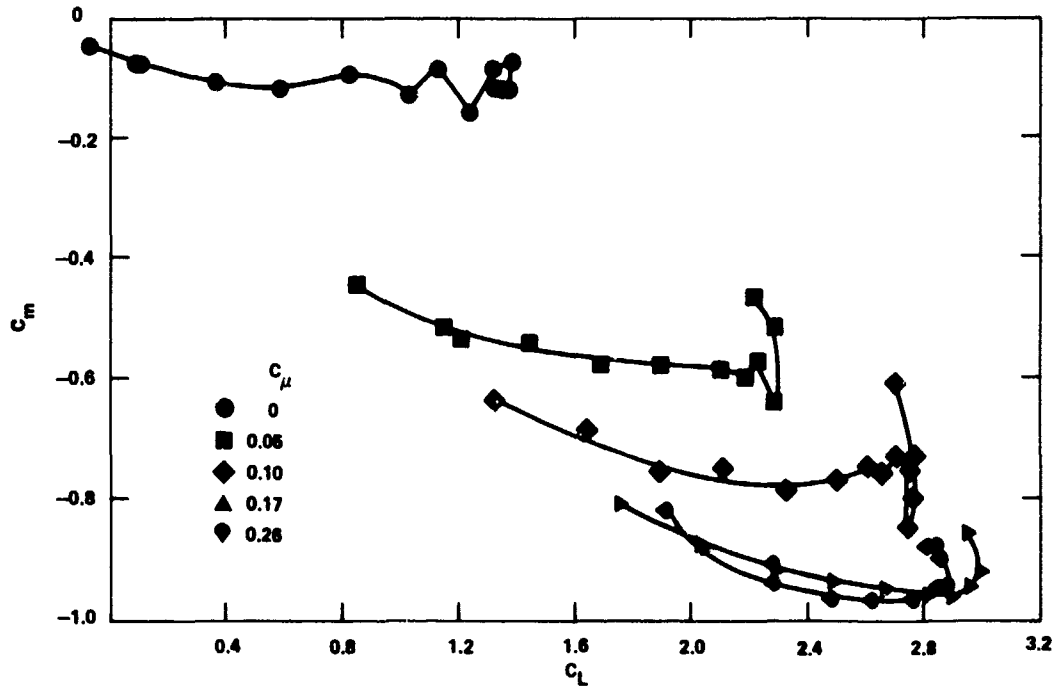

Figure 11b - Pitching Moment Characteristics

Figure 11 (Continued)

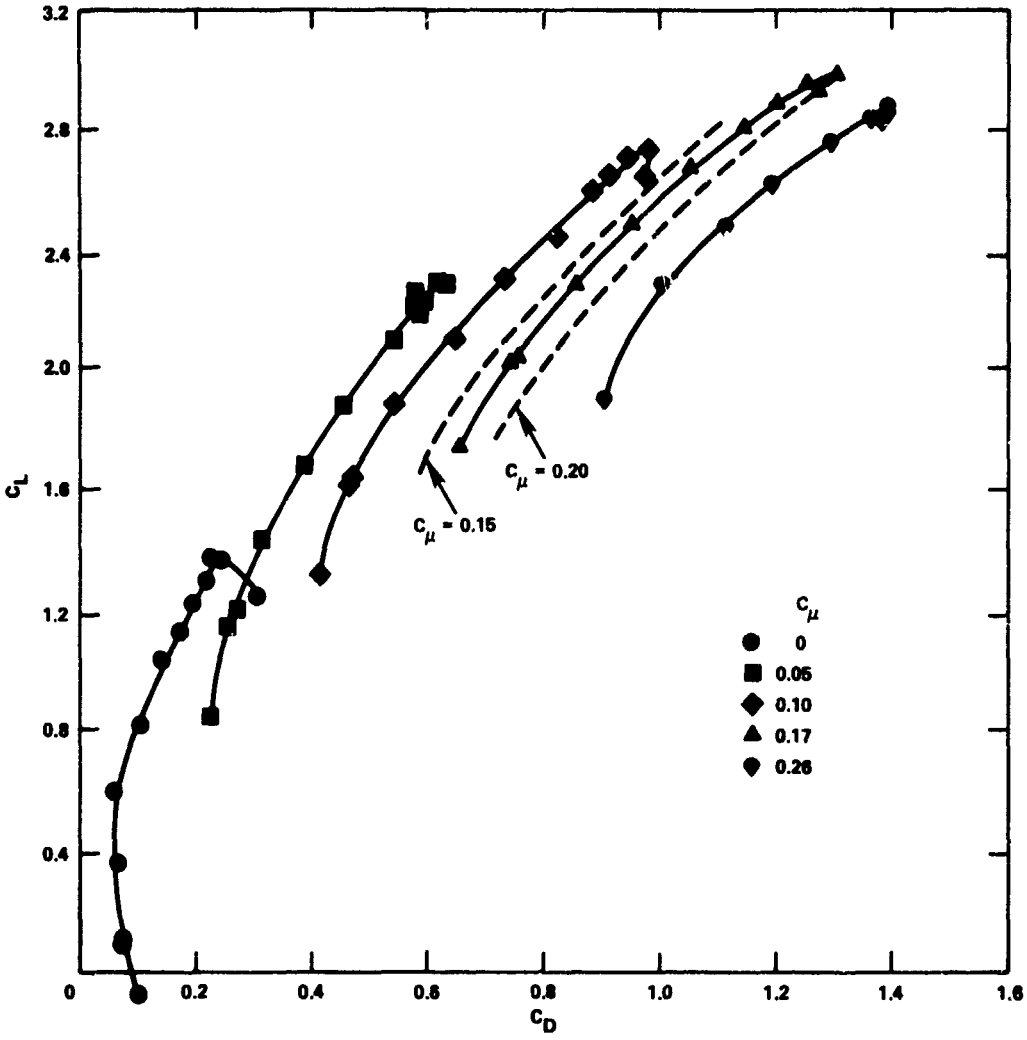

Figure 11c - Drag Polar

Figure 12 - Aspect Ratio 3 Wing in CCW Configuration with Wing Tip Fence Installed

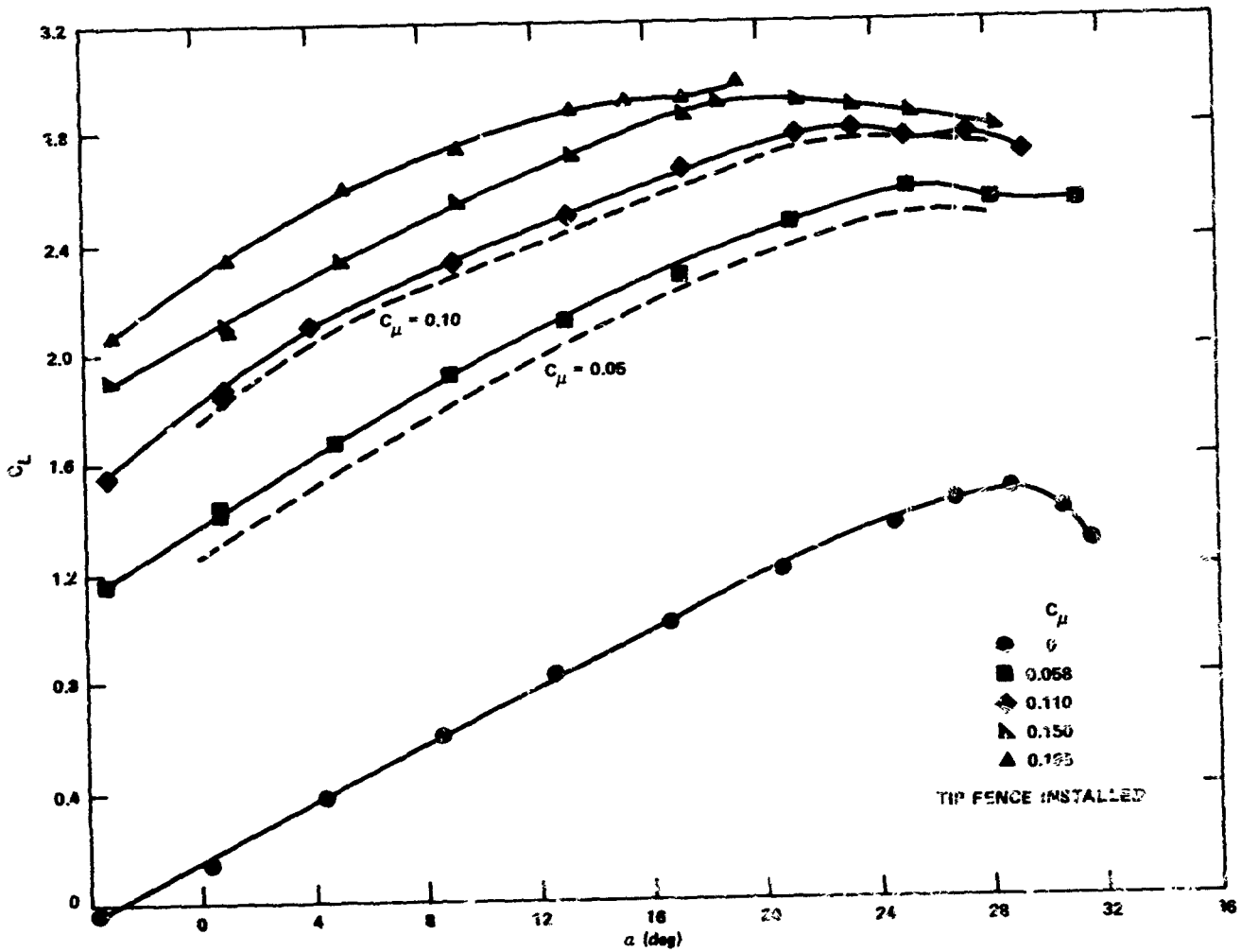

Figure 12a - Lift Characteristics

Figure 12 (Continued)

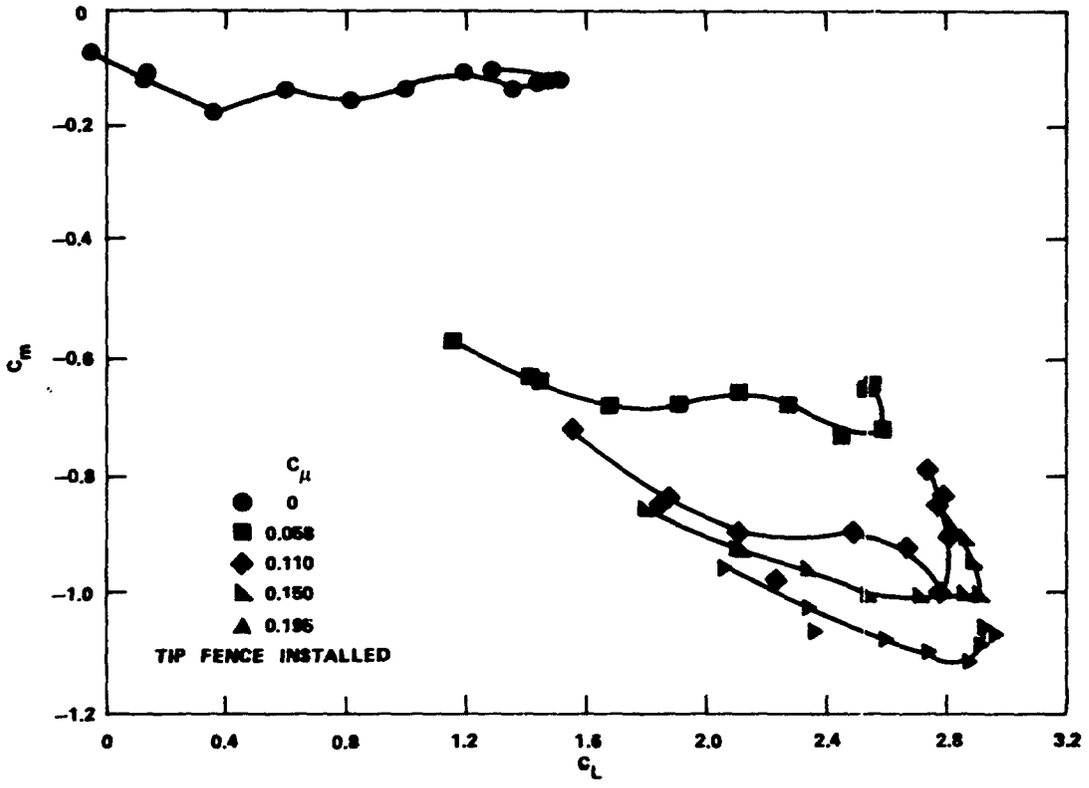

Figure 12b - Pitching Moment Characteristics

Figure 12 (Continued)

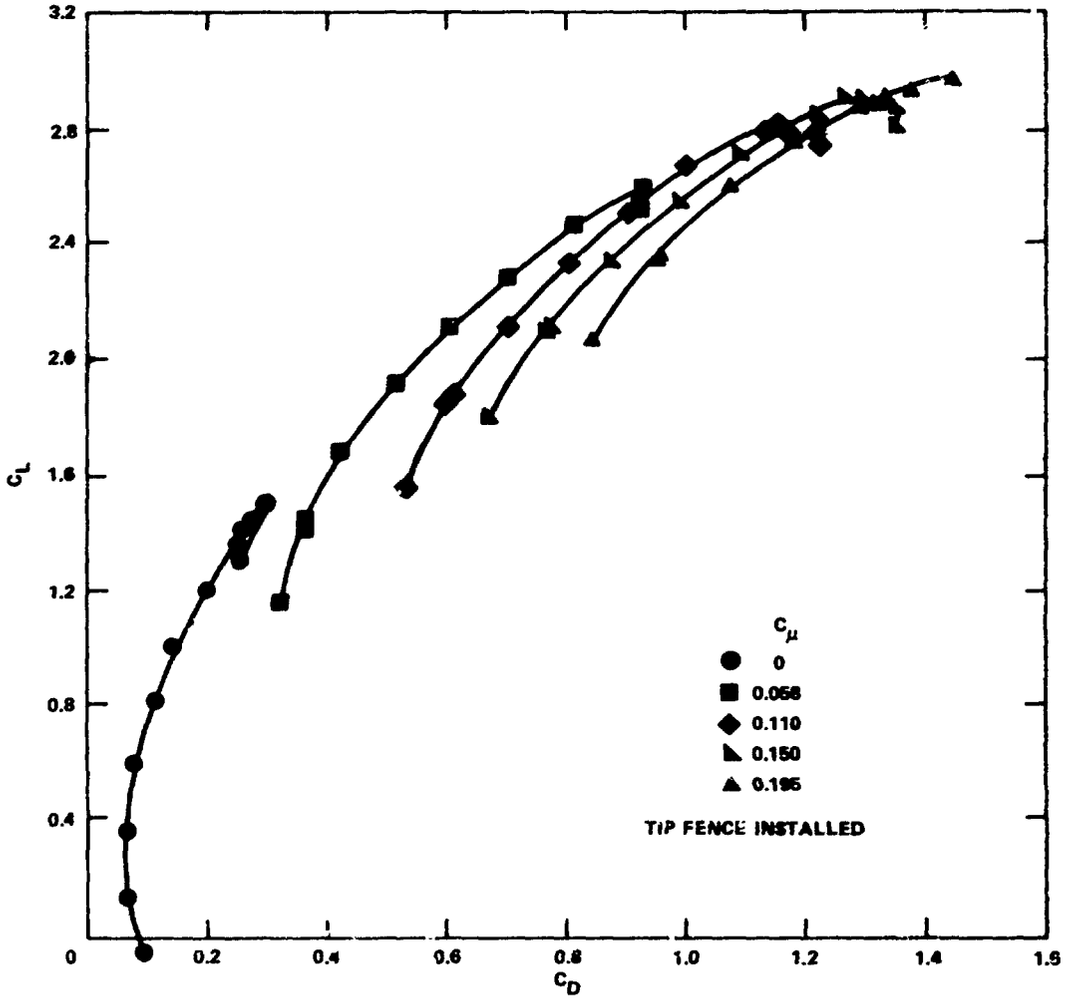

Figure 12c - Drag Polar

Figure 13 - Aspect Ratio 3 Wing in CCW Configuration without Wing Tip Fence

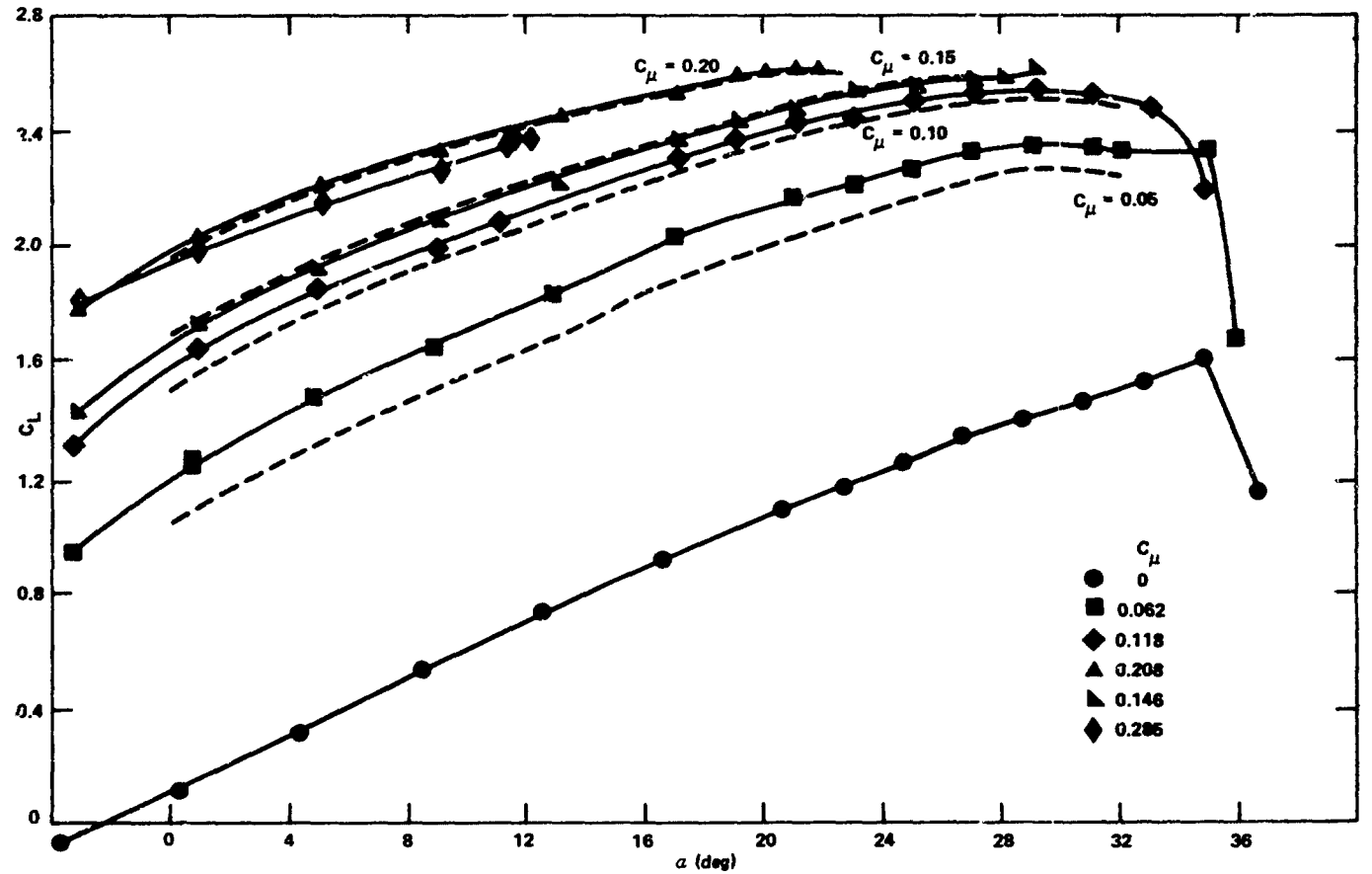

Figure 13a - Lift Characteristics

Figure 13 (Continued)

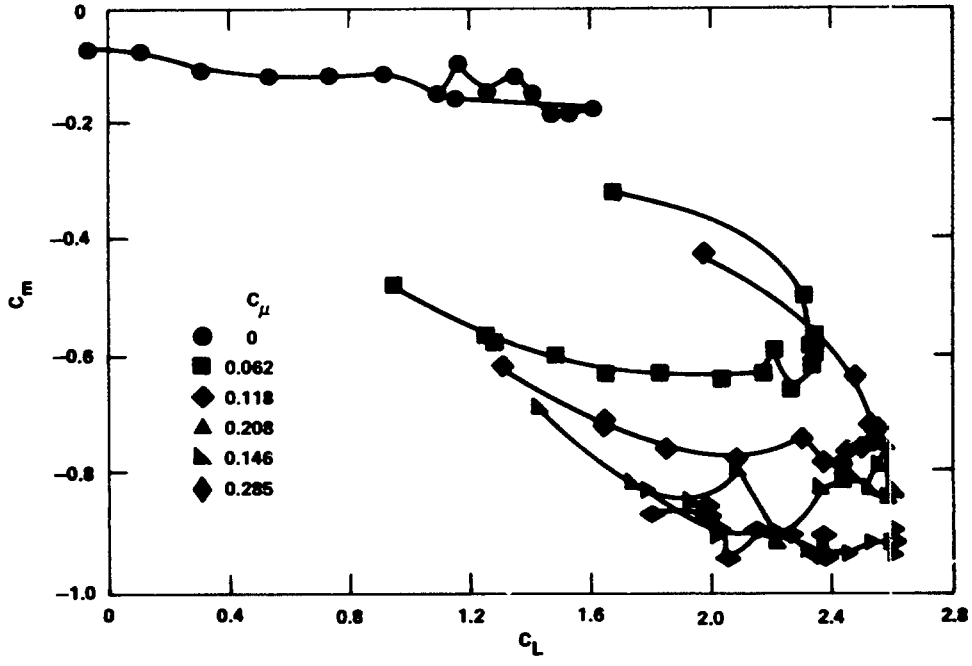

Figure 13b - Pitching Moment Characteristics

Figure 13 (Continued)

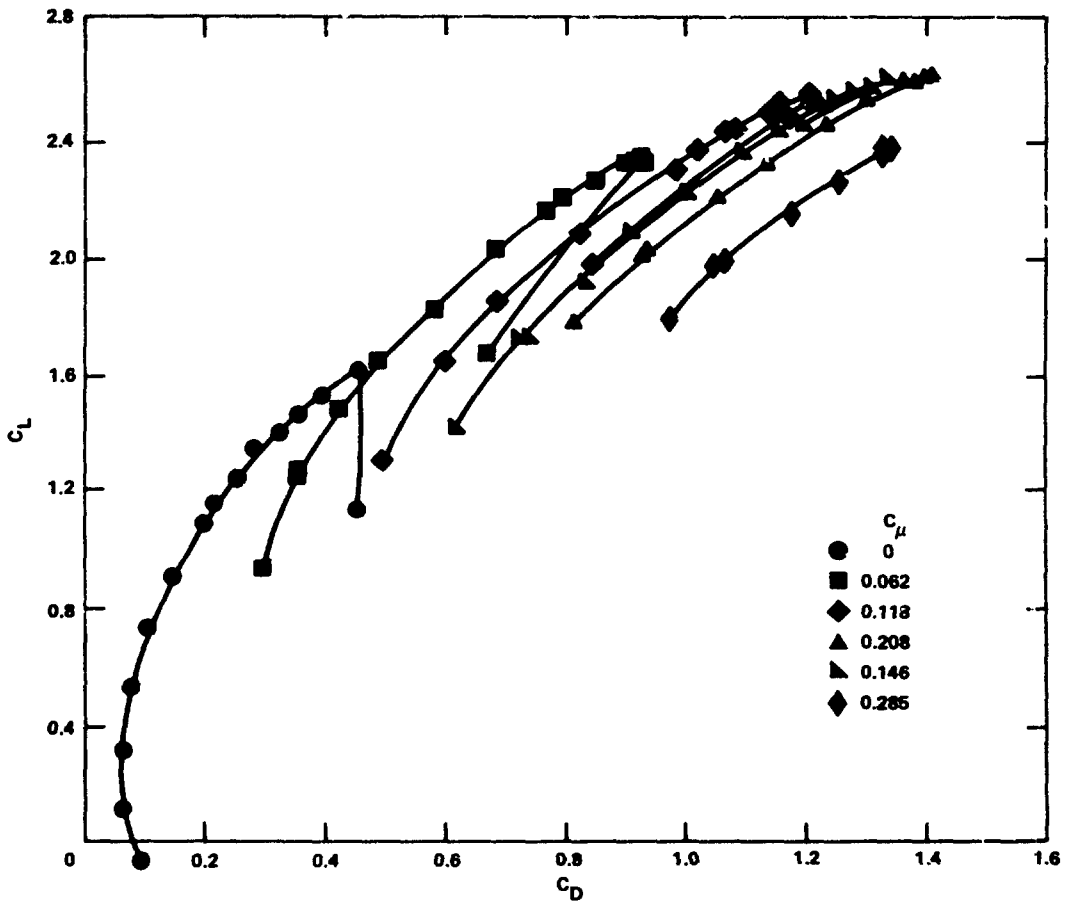

Figure 13c - Drag Polar

Figure 14 - Aspect Ratio 3 Wing with Nonround Trailing Edge in CCW Configuration with Tip Fence Installed

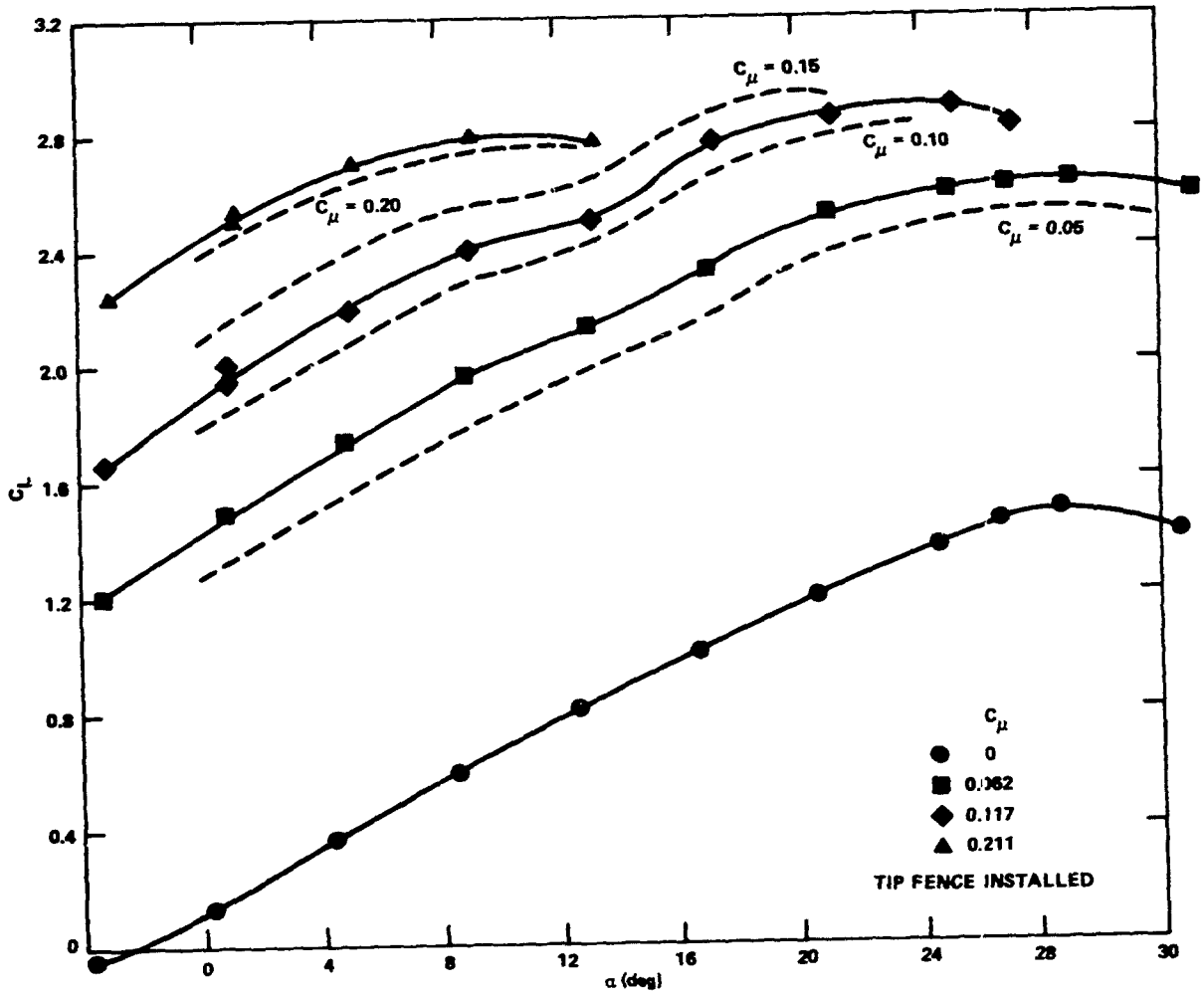

Figure 14a - Lift Characteristics

Figure 14 (Continued)

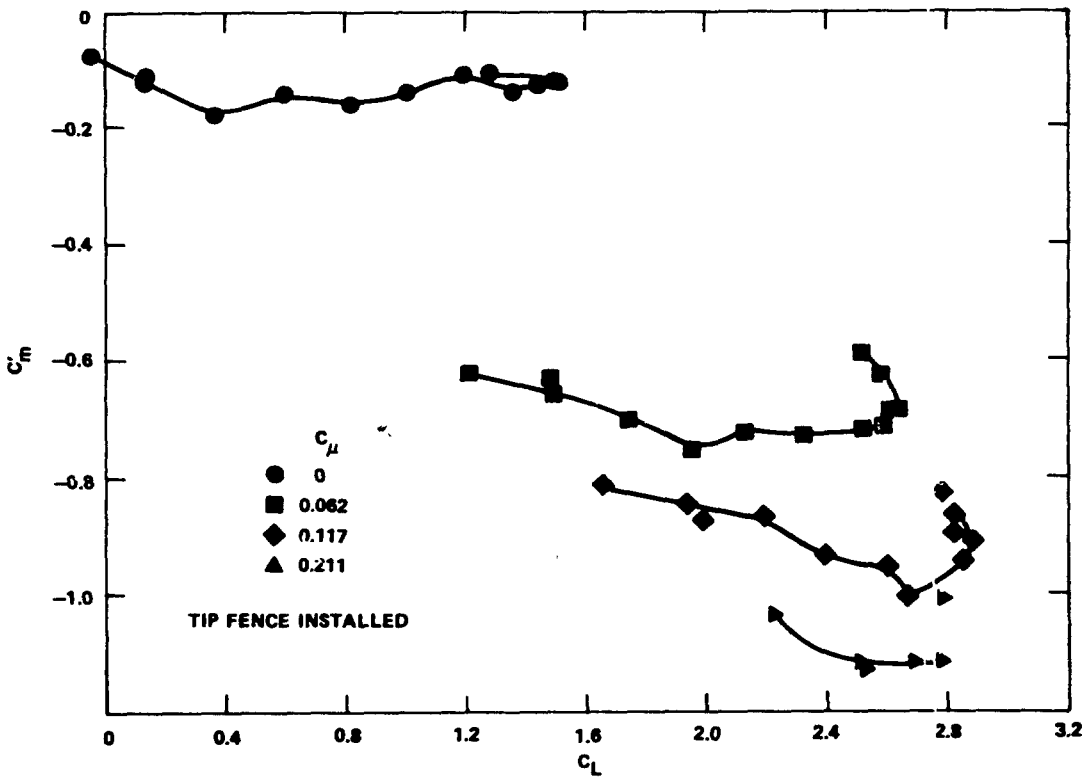

Figure 14b - Pitching Moment Characteristics

Figure 14 (Continued)

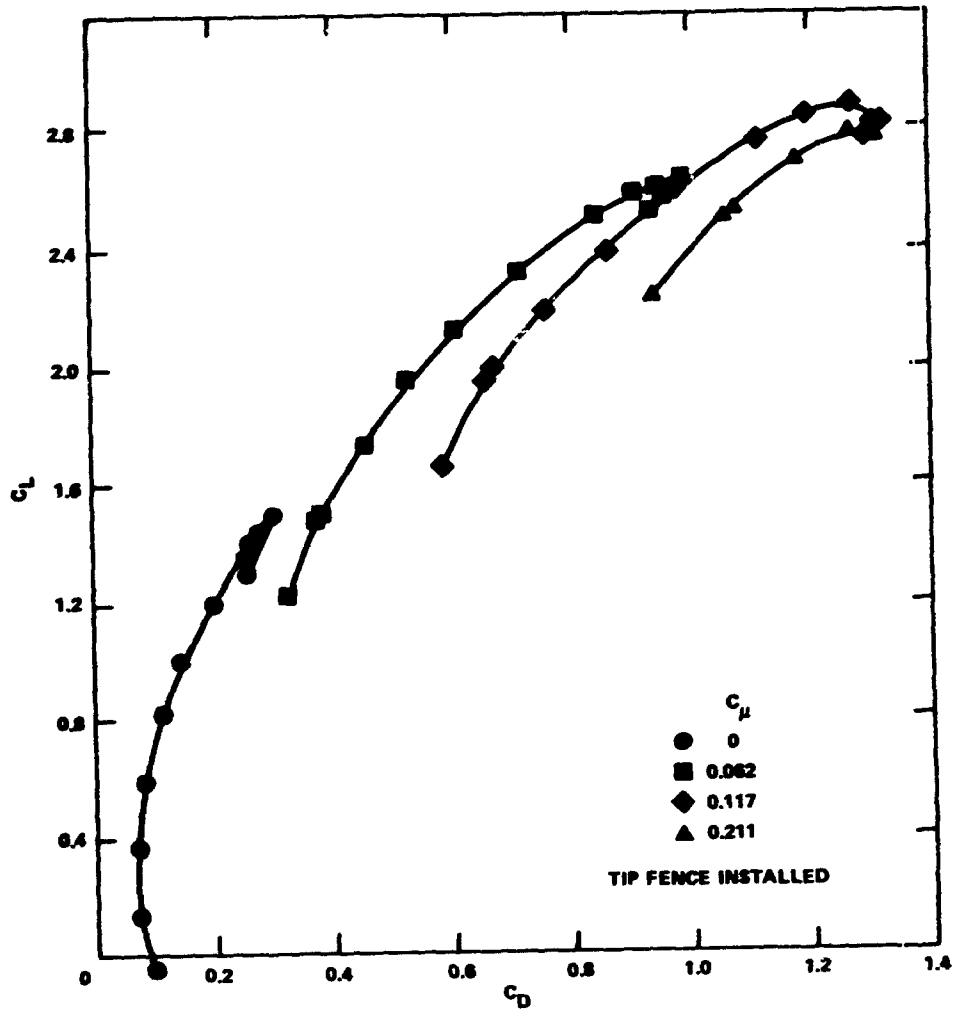

Figure 14c - Drag Polar

Figure 15 - Aspect Ratio 3 Wing with Nonround Trailing Edge in CCW Configuration without Tip Fence

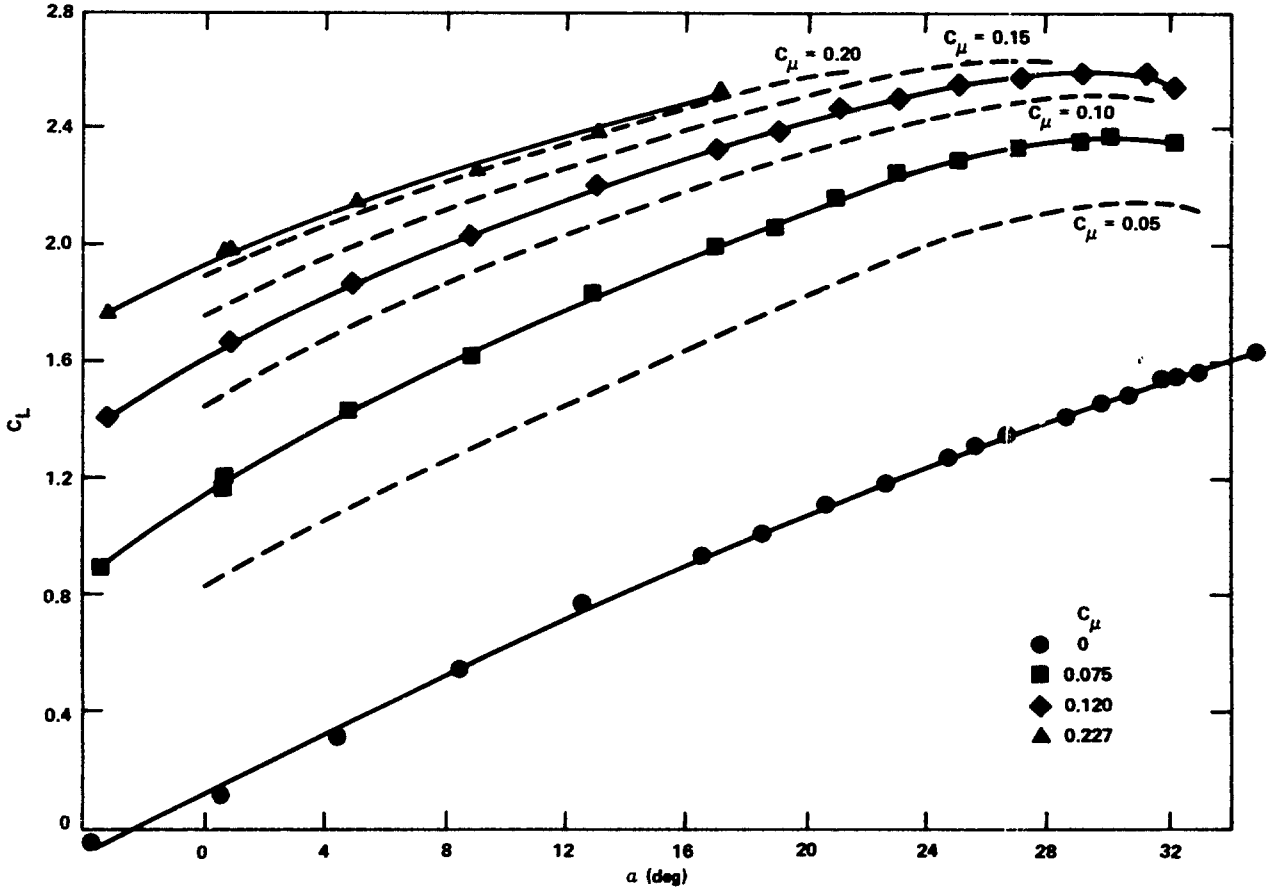

Figure 15a - Lift Characteristics

Figure 15 (Continued)

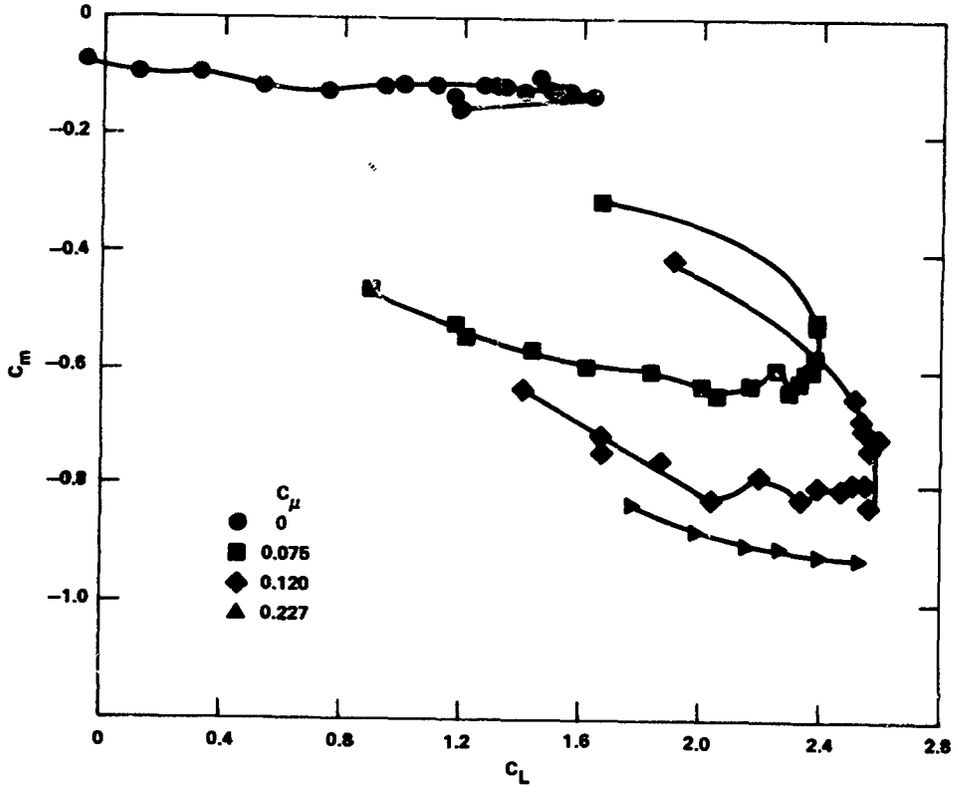

Figure 15b - Pitching Moment Characteristics

Figure 15 (Continued)

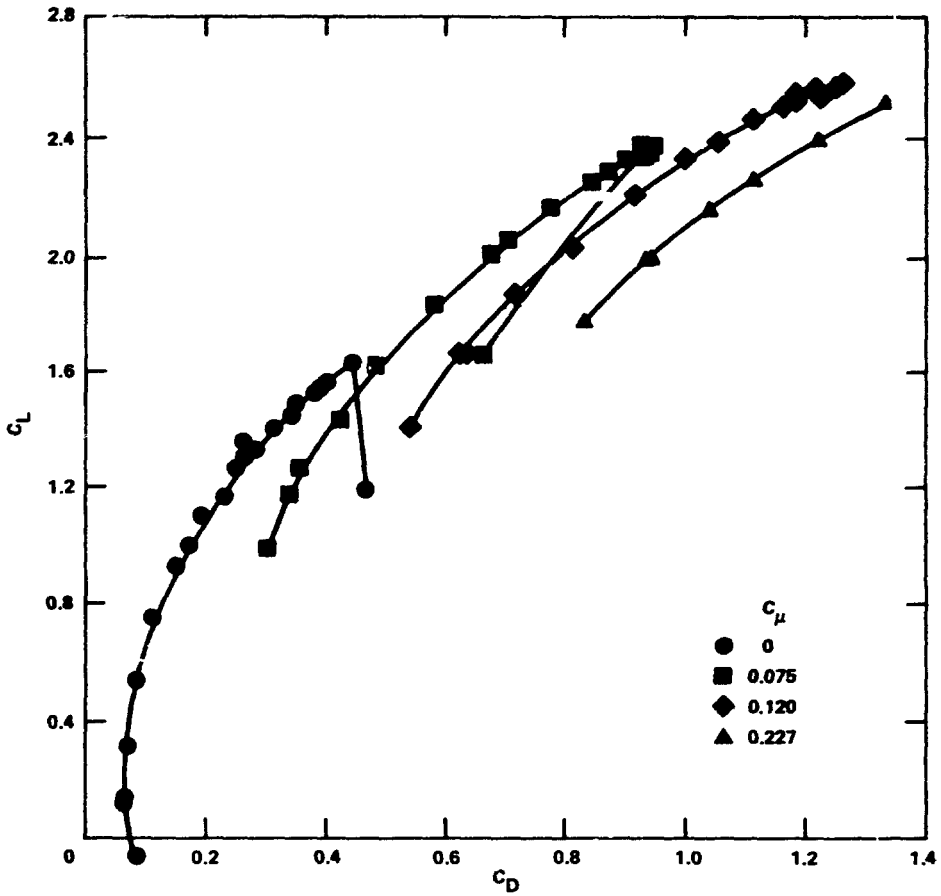

Figure 15c - Drag Polar

Figure 16 - Effect of a Nonround Coanda Trailing Edge on an Aspect Ratio 3 Wing in CCW Configuration

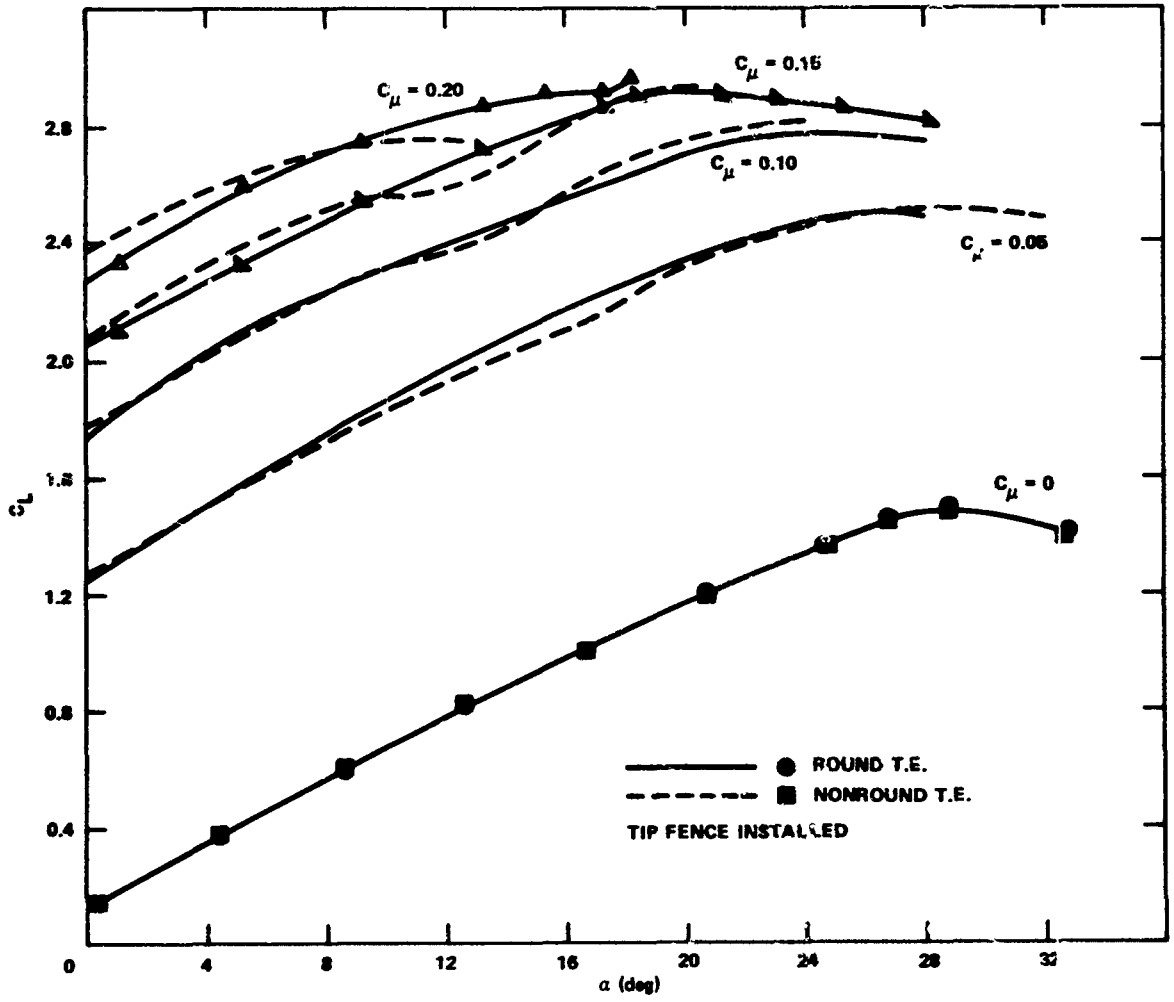

Figure 16a - Lift Characteristics with Wing Tip Fence

Figure 16 (Continued)

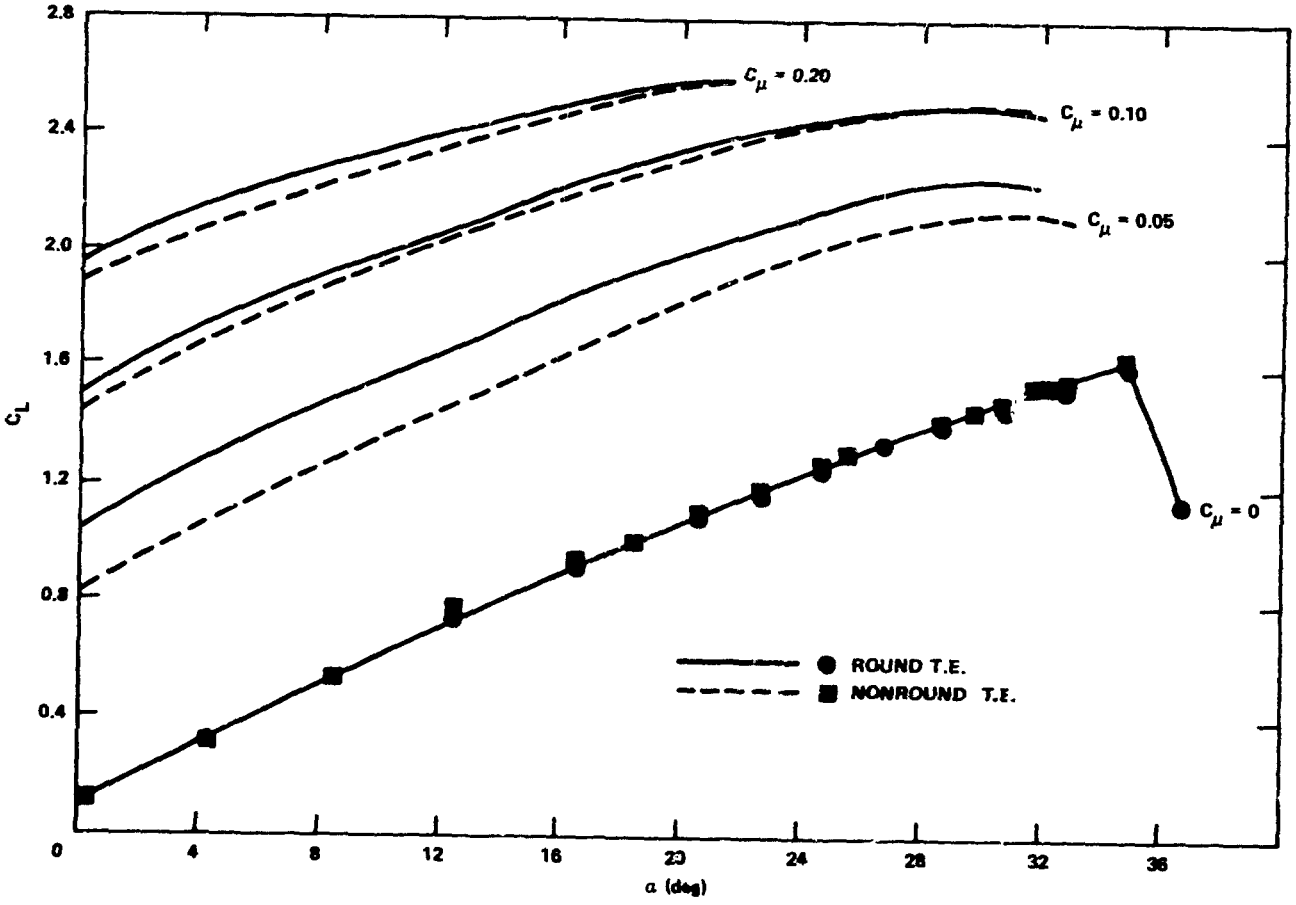

Figure 16b - Lift Characteristics without Wing Tip Fence

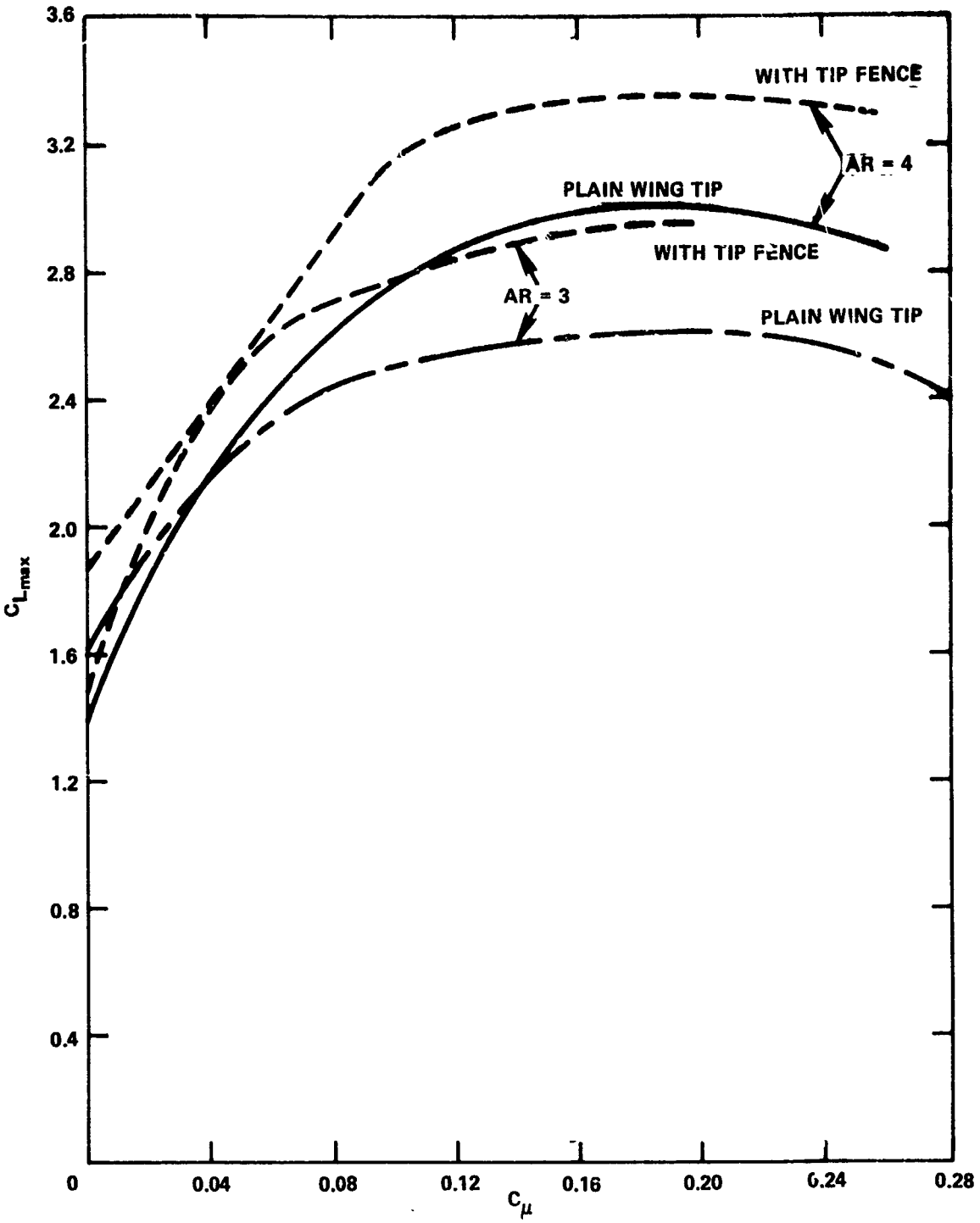

Figure 17 - Effect of a Wing Tip Fence on a CCW Configuration

Figure 18 - Aspect Ratio 3 Wing in USB Configuration
with 5.8 Aspect Ratio Duct and 40-Degree Flaps

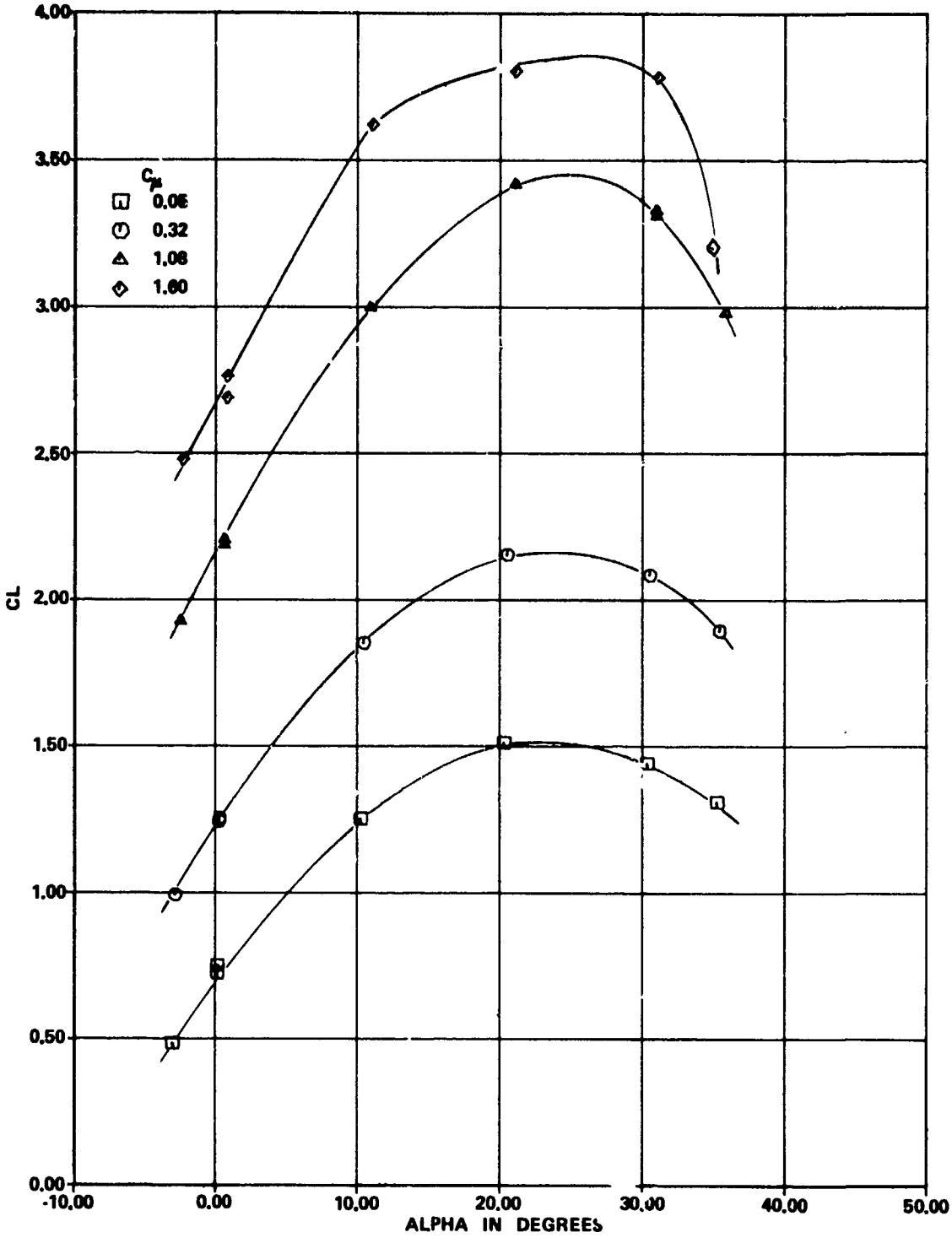

Figure 18a - Lift Characteristics

Figure 18 (Continued)

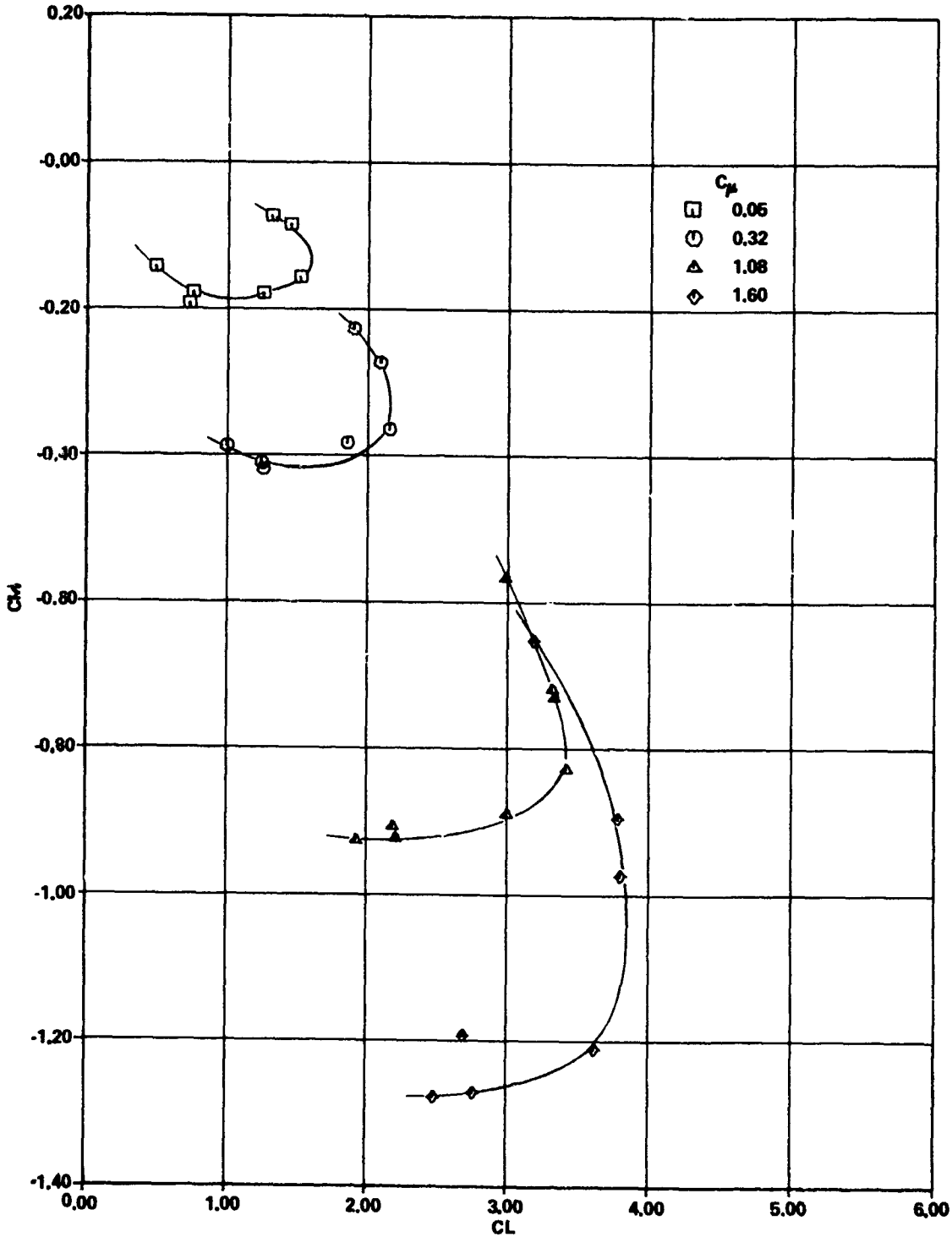

Figure 18b - Pitching Moment Characteristics

Figure 18 (Continued)

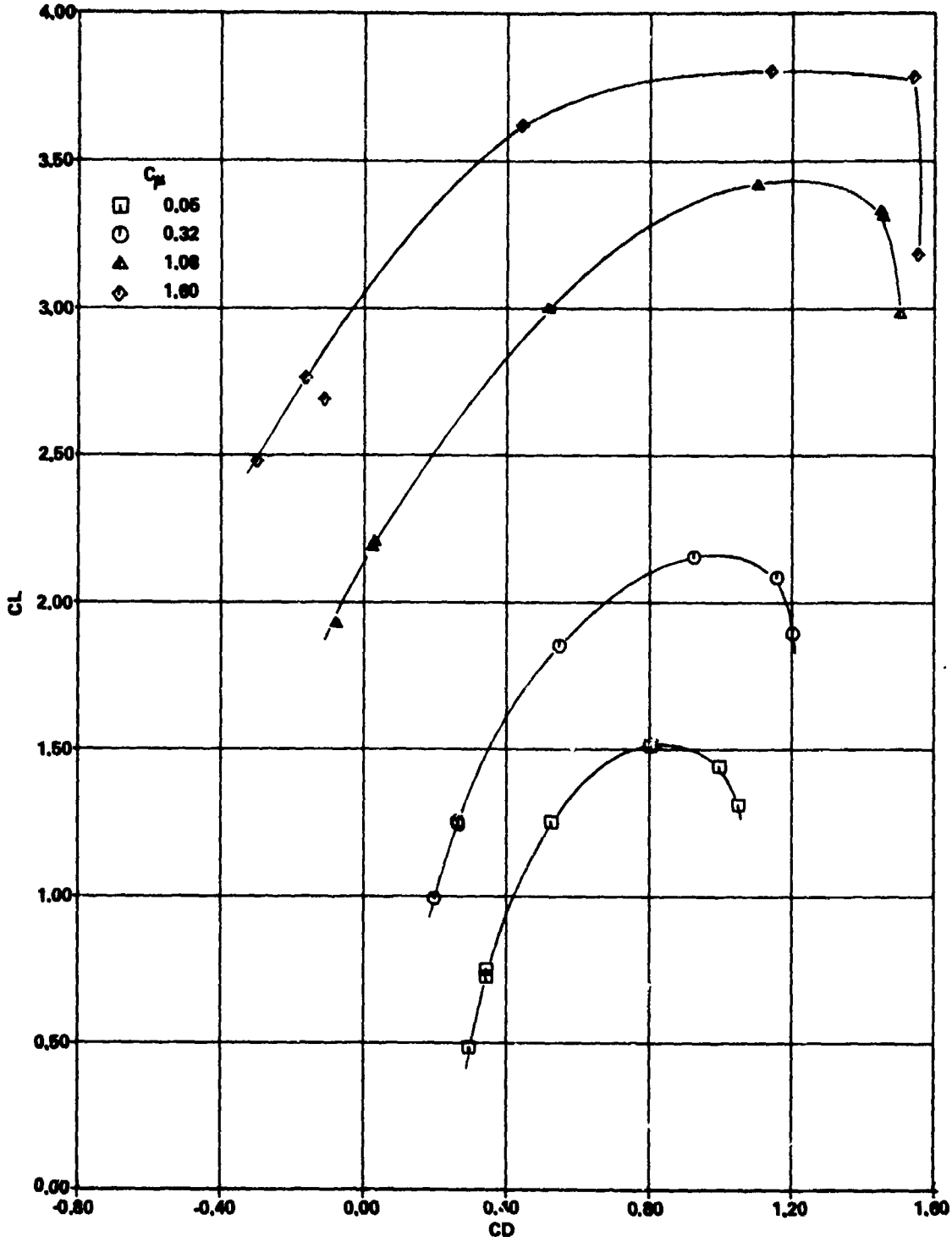

Figure 18c - Drag Polar

Figure 19 - Aspect Ratio 3 Wing in USB Configuration with 5.8 Aspect Ratio Duct and 60-Degree Flaps

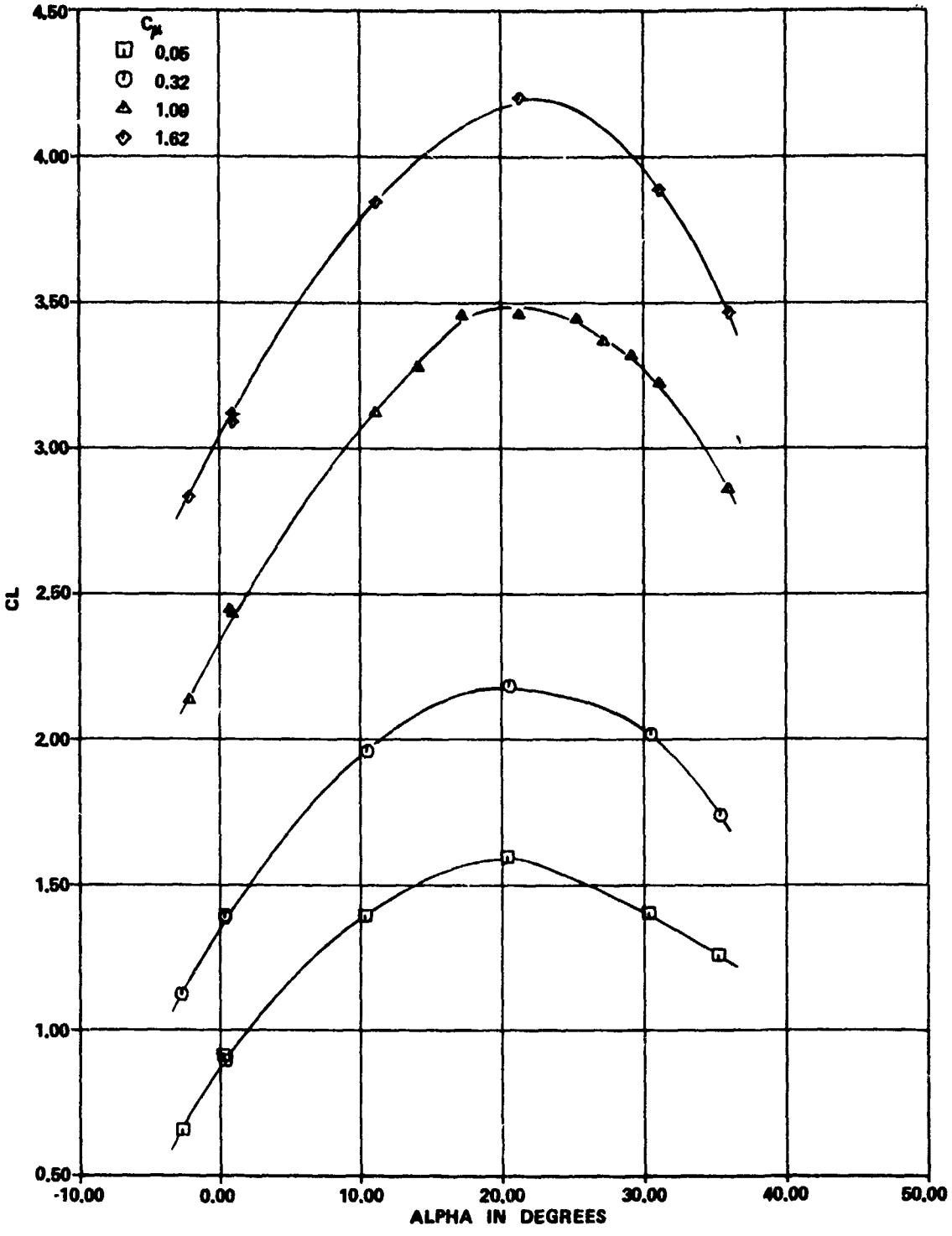

Figure 19a - Lift Characteristics

Figure 19 (Continued)

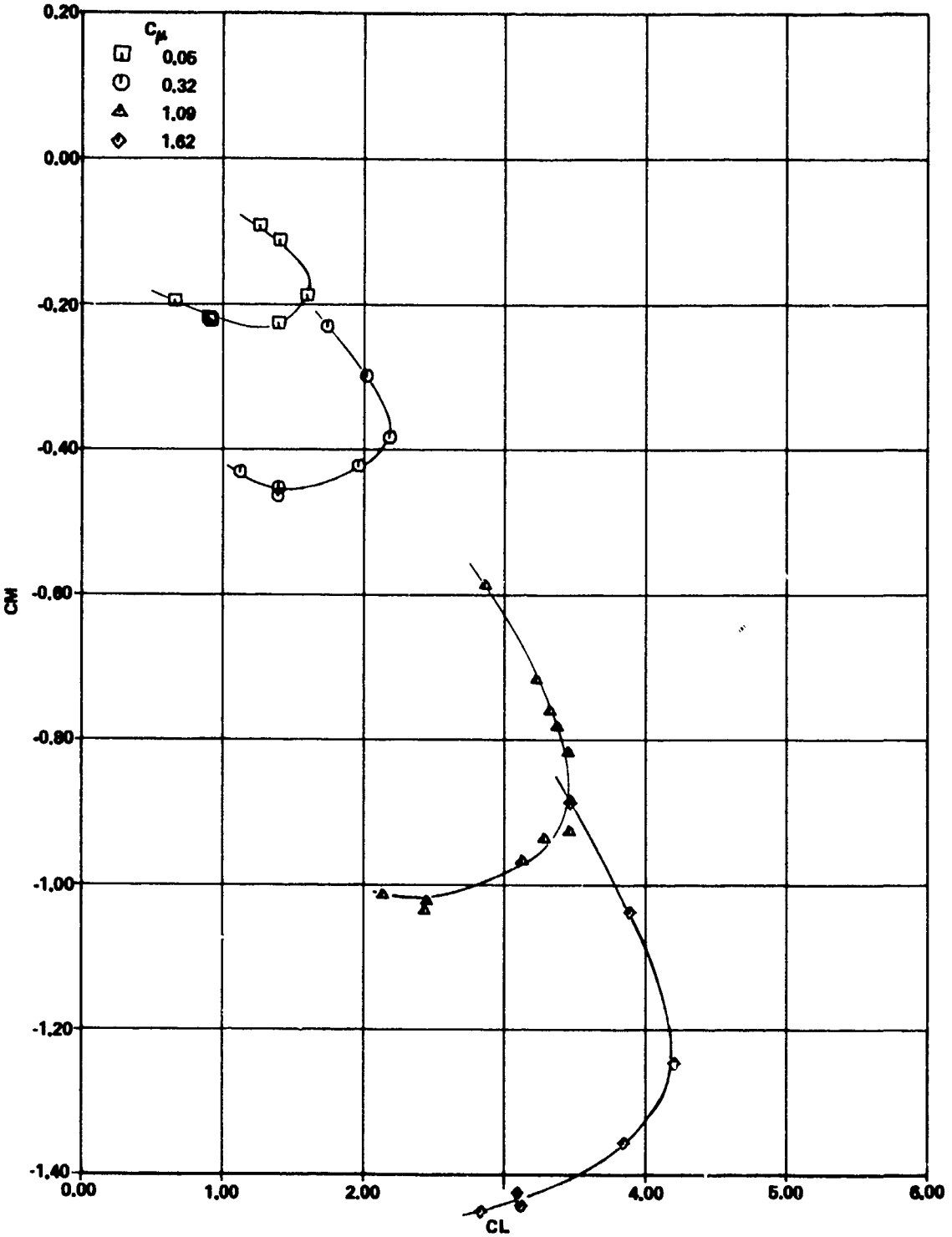

Figure 19b - Pitching Moment Characteristics

Figure 19 (Continued)

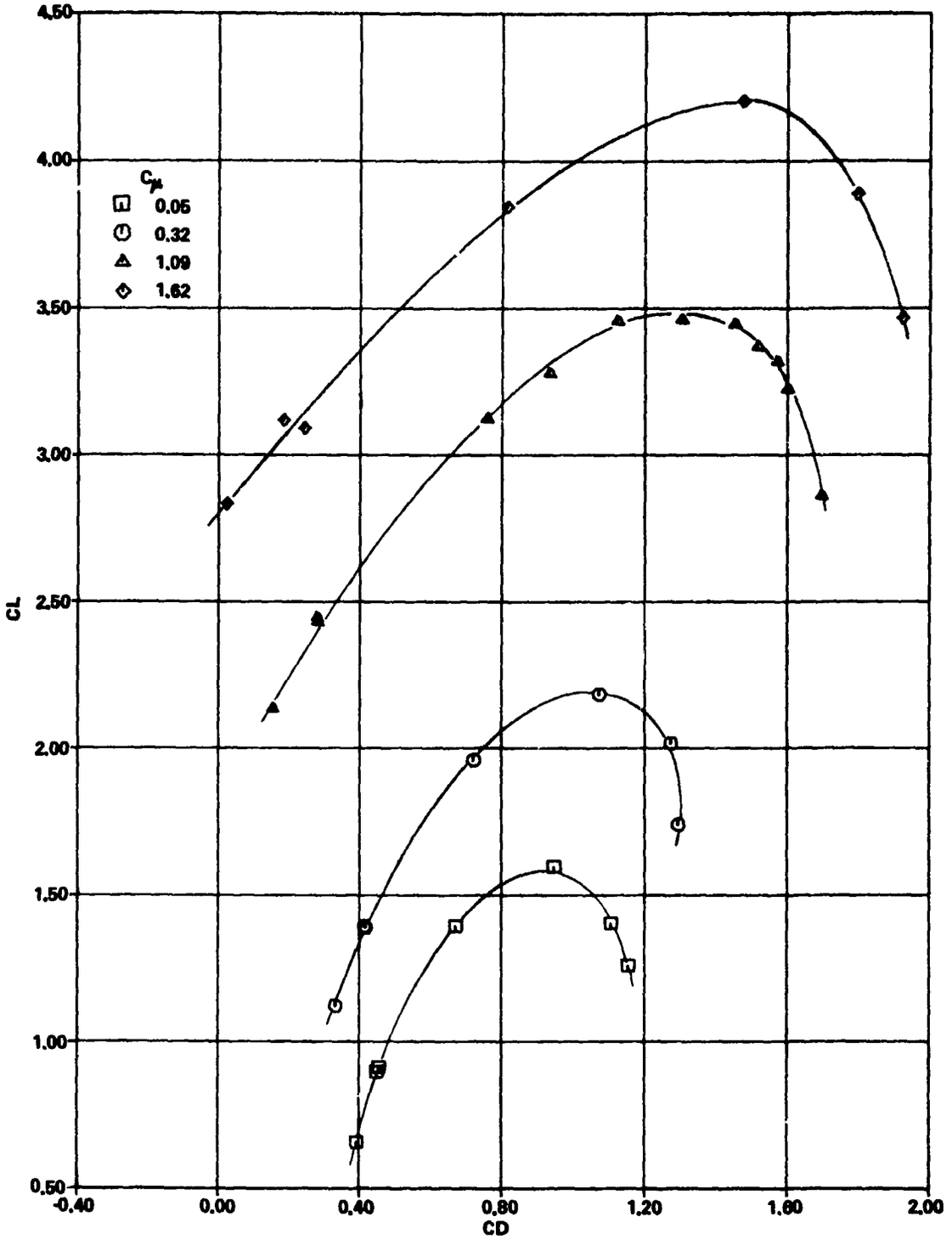

Figure 19c - Drag Polar

Figure 20 - Aspect Ratio 4 Wing in USB Configuration
with 5.8 Aspect Ratio Duct and 40-Degree Flaps

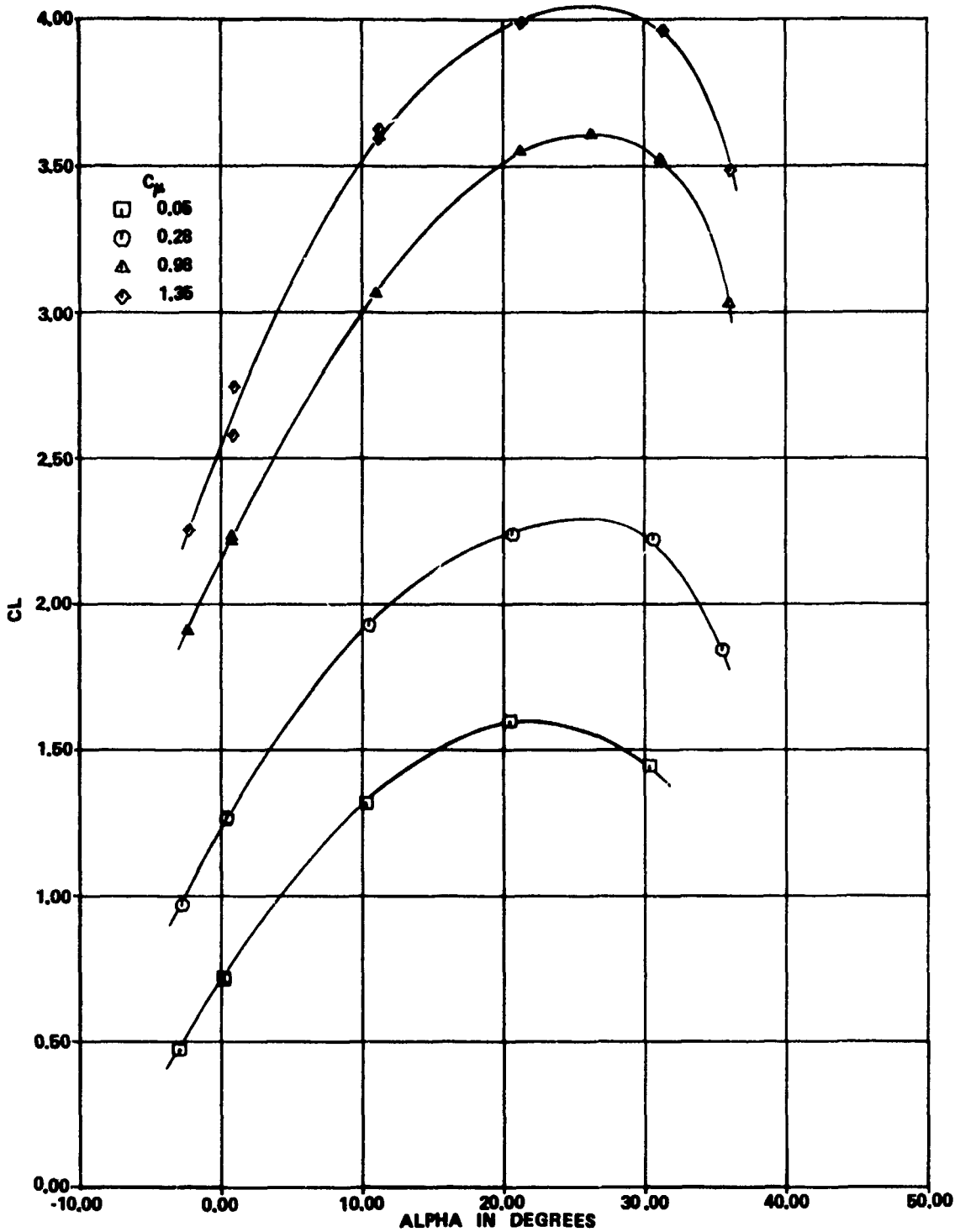

Figure 20a - Lift Characteristics

Figure 20 (Continued)

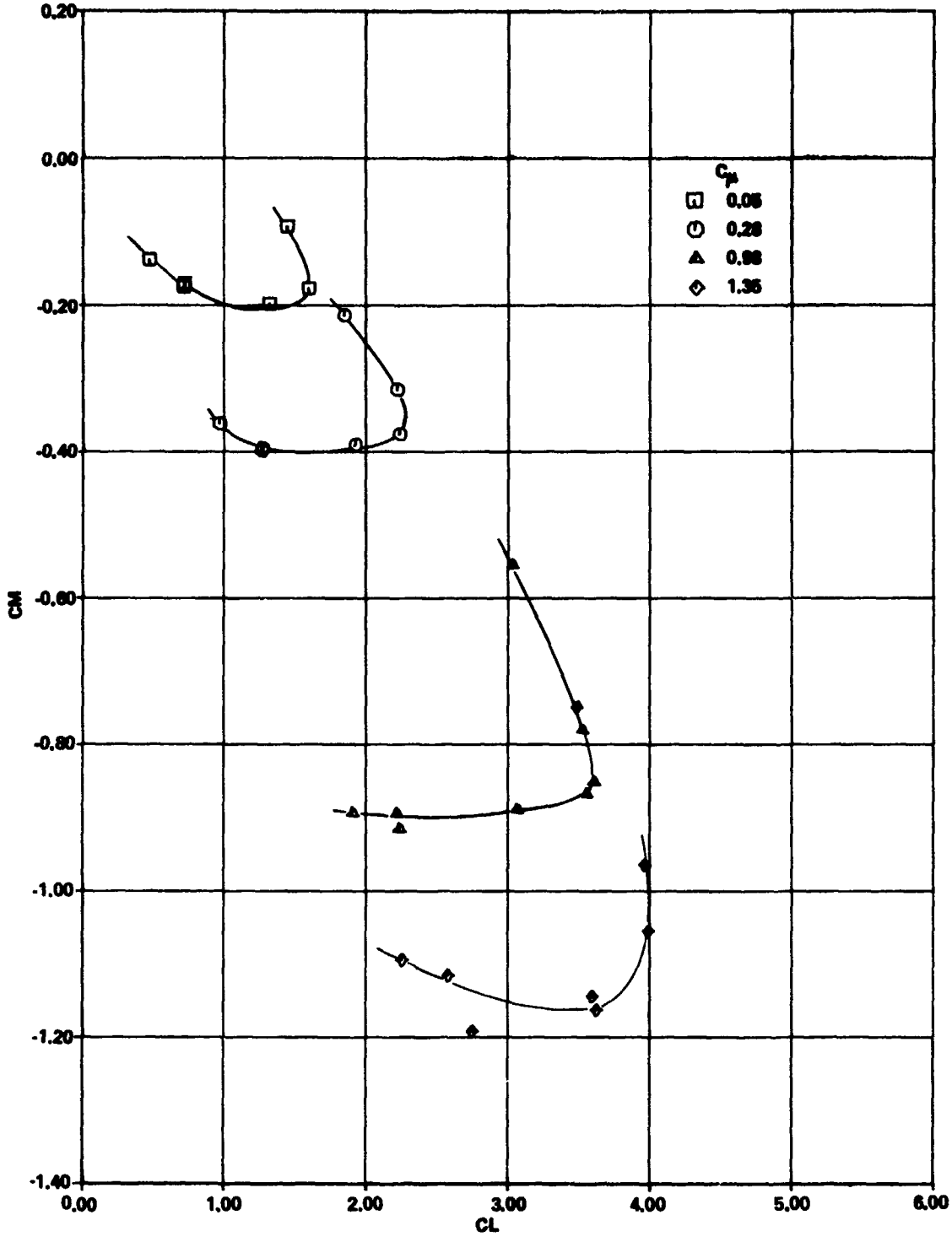

Figure 20b - Pitching Moment Characteristics

Figure 20 (Continued)

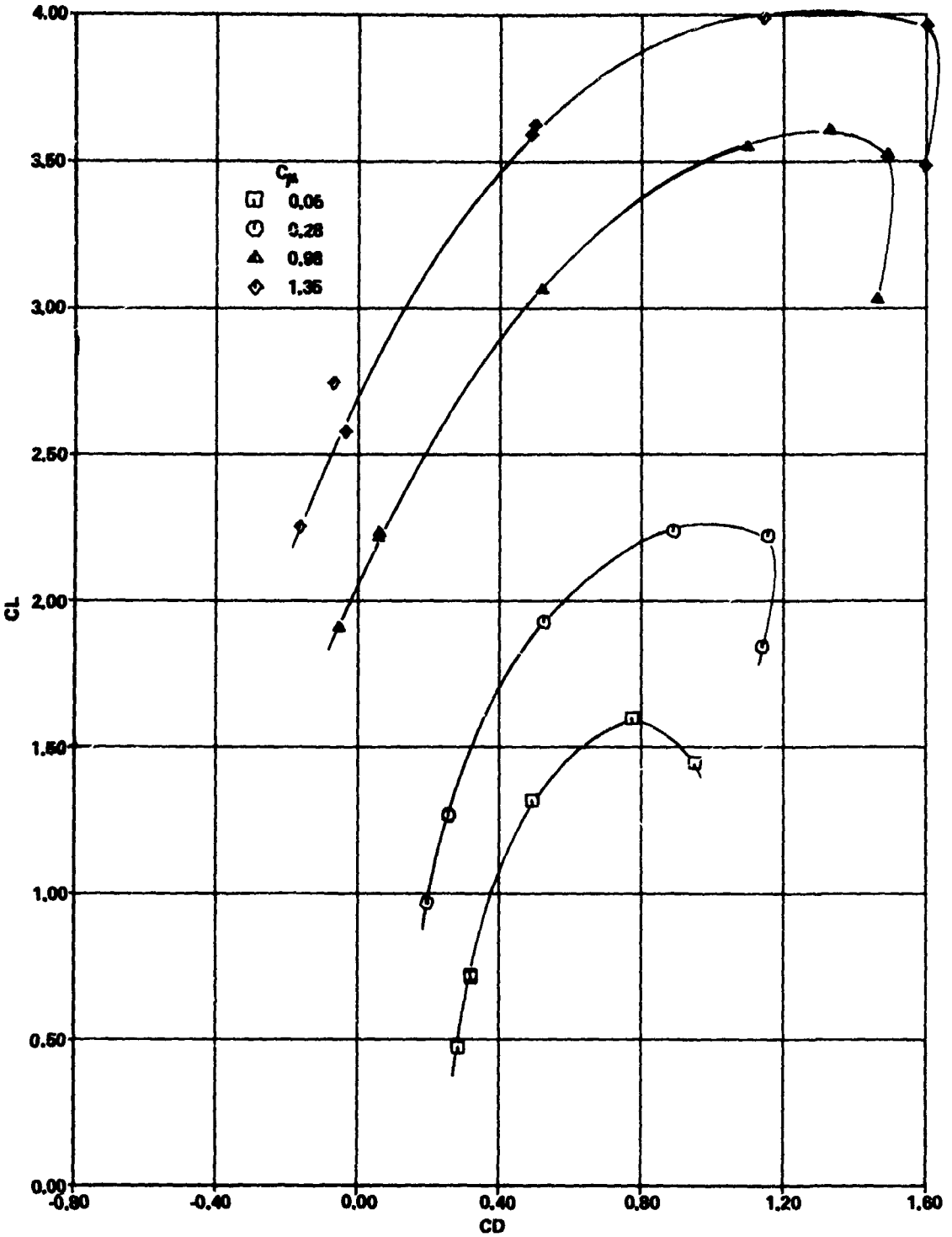

Figure 20c - Drag Polar

Figure 21 - Aspect Ratio 4 Wing in USB Configuration with 5.8 Aspect Ratio Duct and 60-Degree Flaps

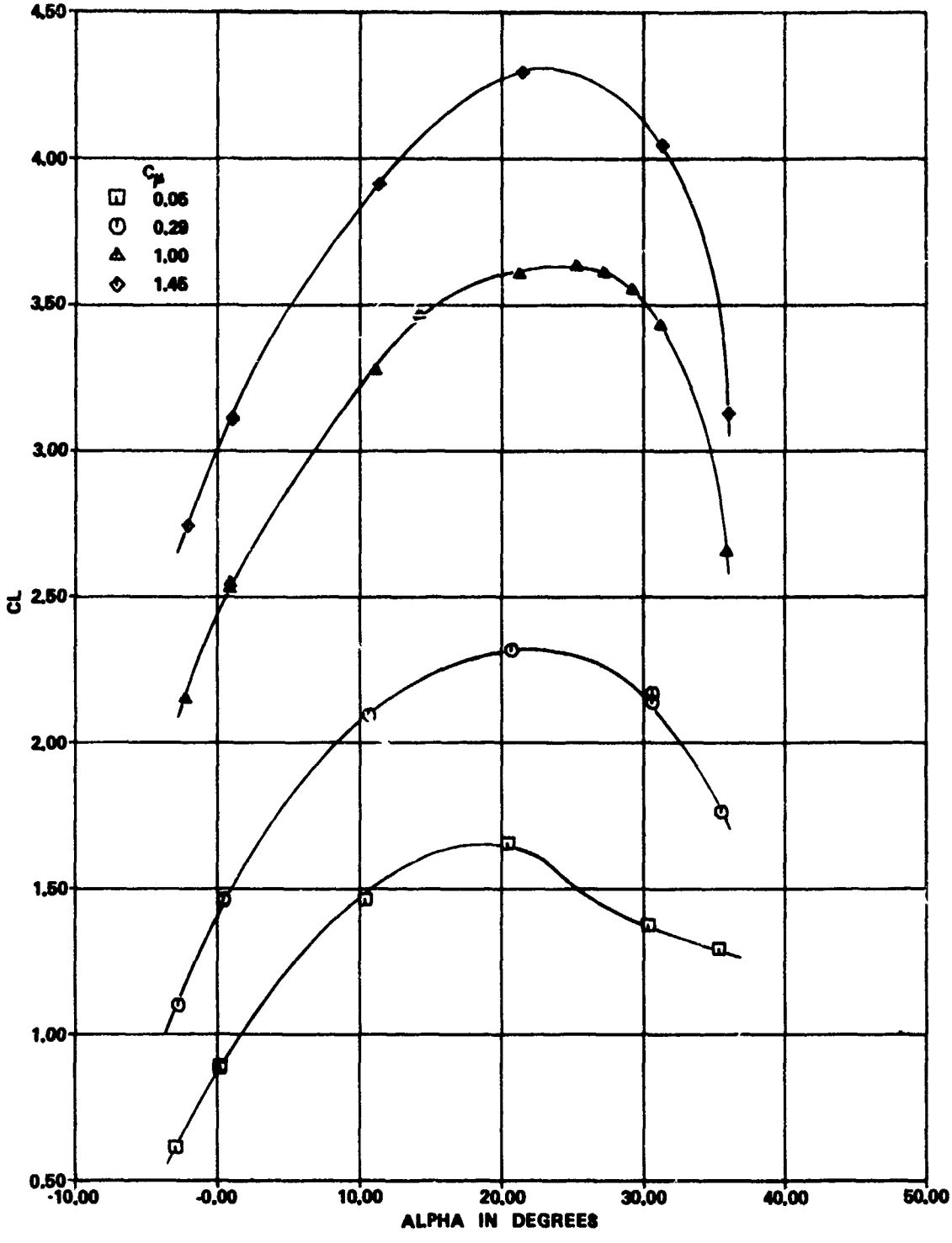

Figure 21a - Lift Characteristics

Figure 21 (Continued)

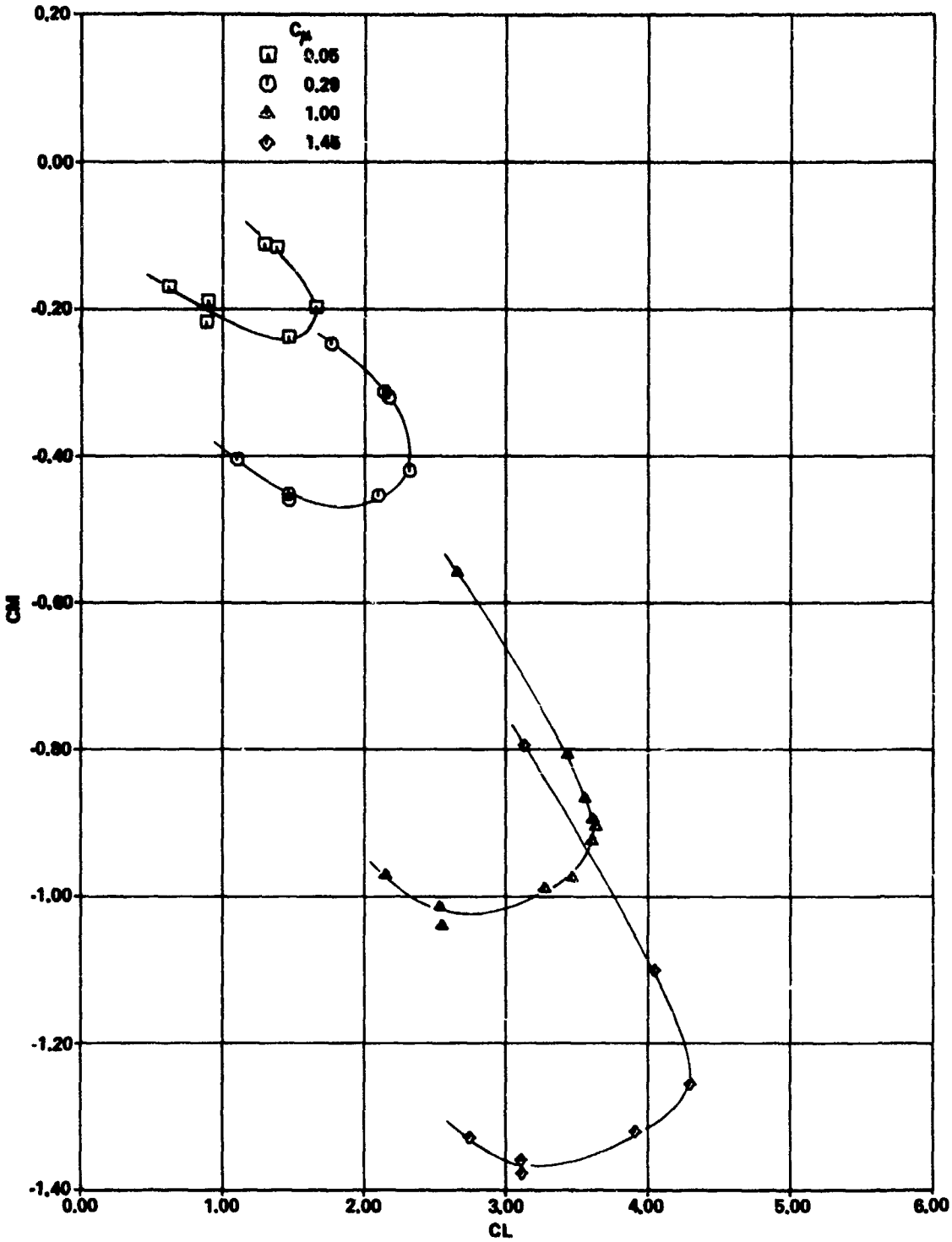

Figure 21b - Pitching Moment Characteristics

Figure 21 (Continued)

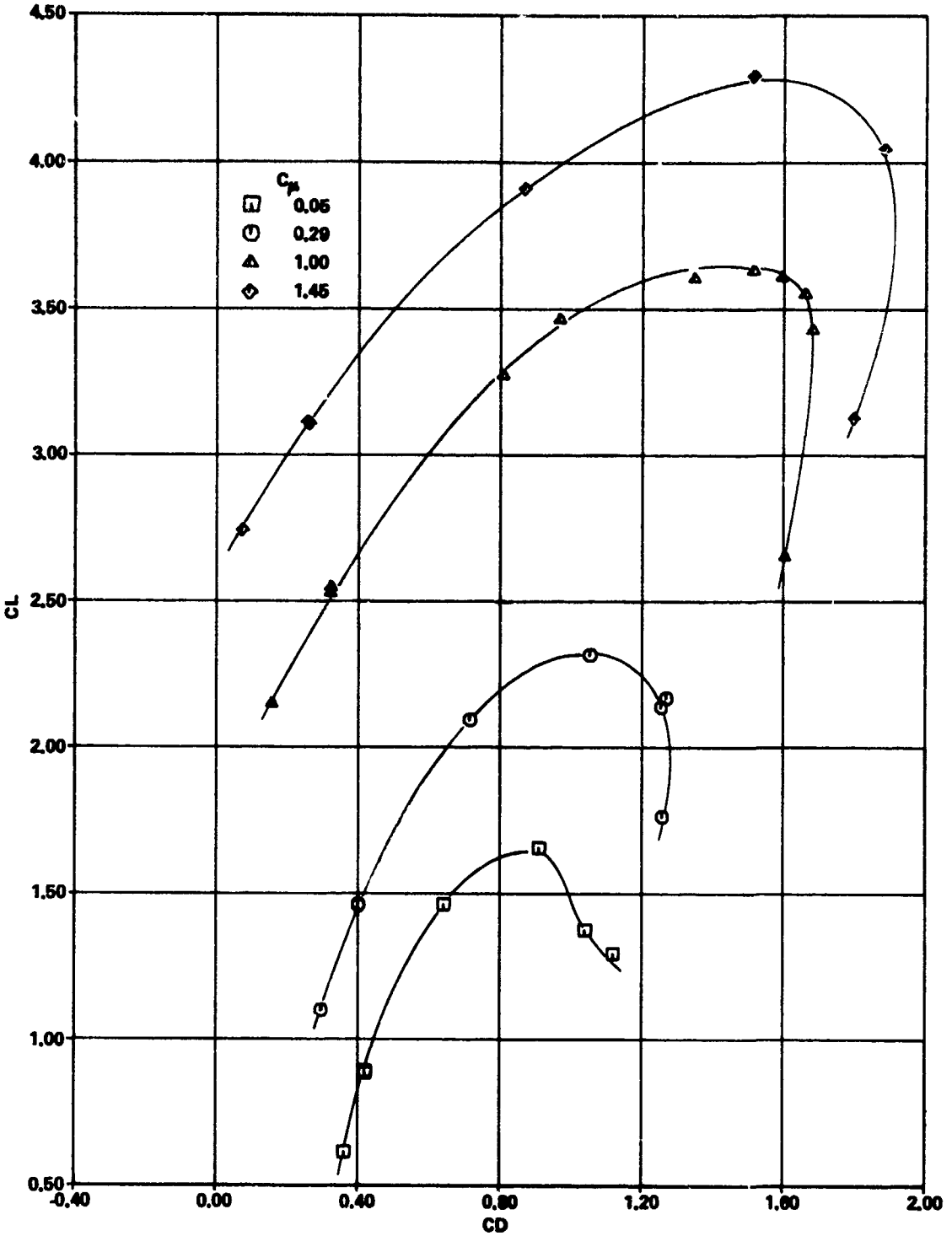

Figure 21c - Drag Polar

Figure 22 - Lift Characteristics of Aspect Ratio Wing in USB Configuration with 40-Degree Flap

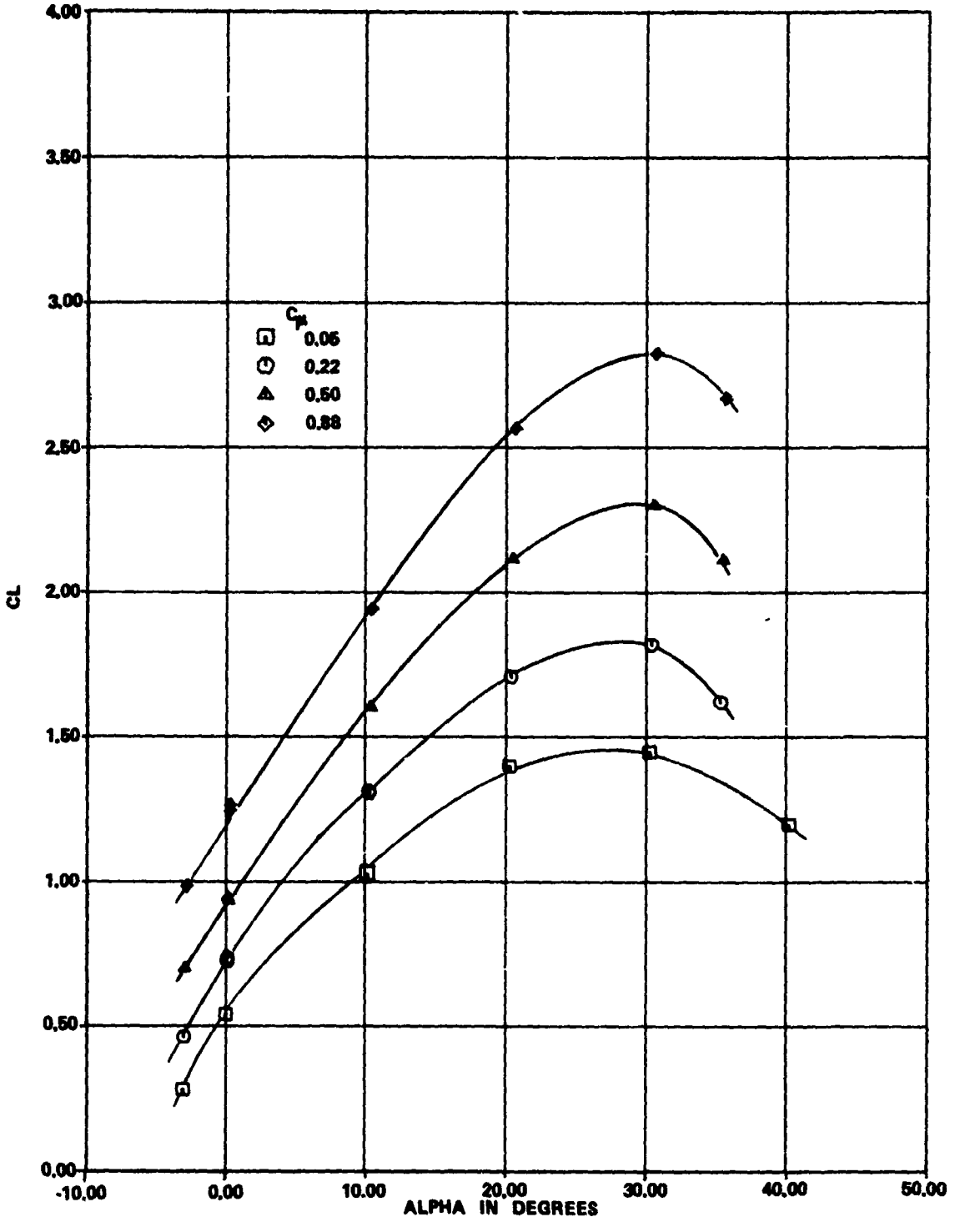

Figure 22a - Aspect Ratio 2.2 Duct

Figure 22 (Continued)

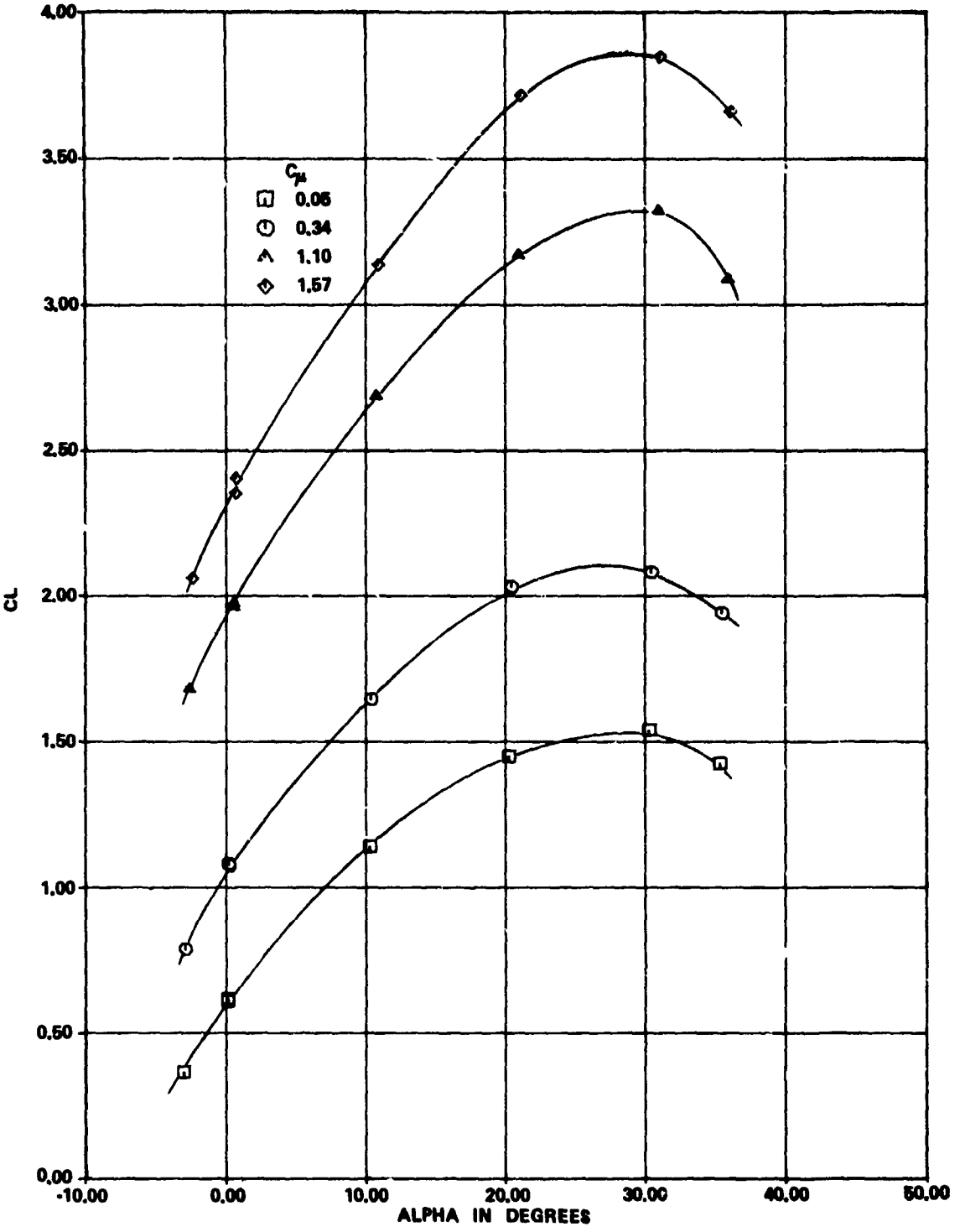

Figure 22b - Aspect Ratio 3.9 Duct

Figure 22 (Continued)

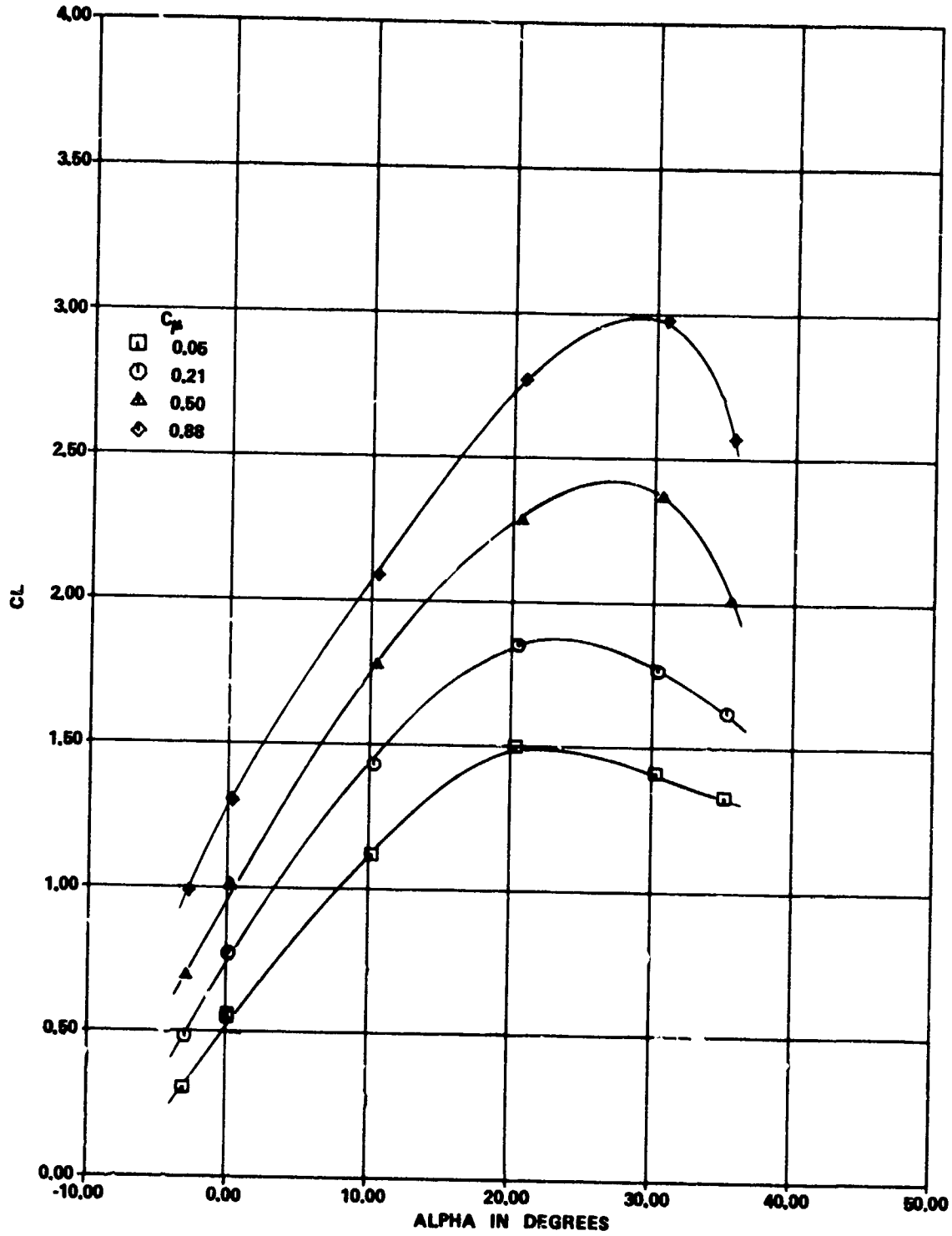

Figure 22c - Aspect Ratio 2.2 Duct with Tip Fence Installed

Figure 22 (Continued)

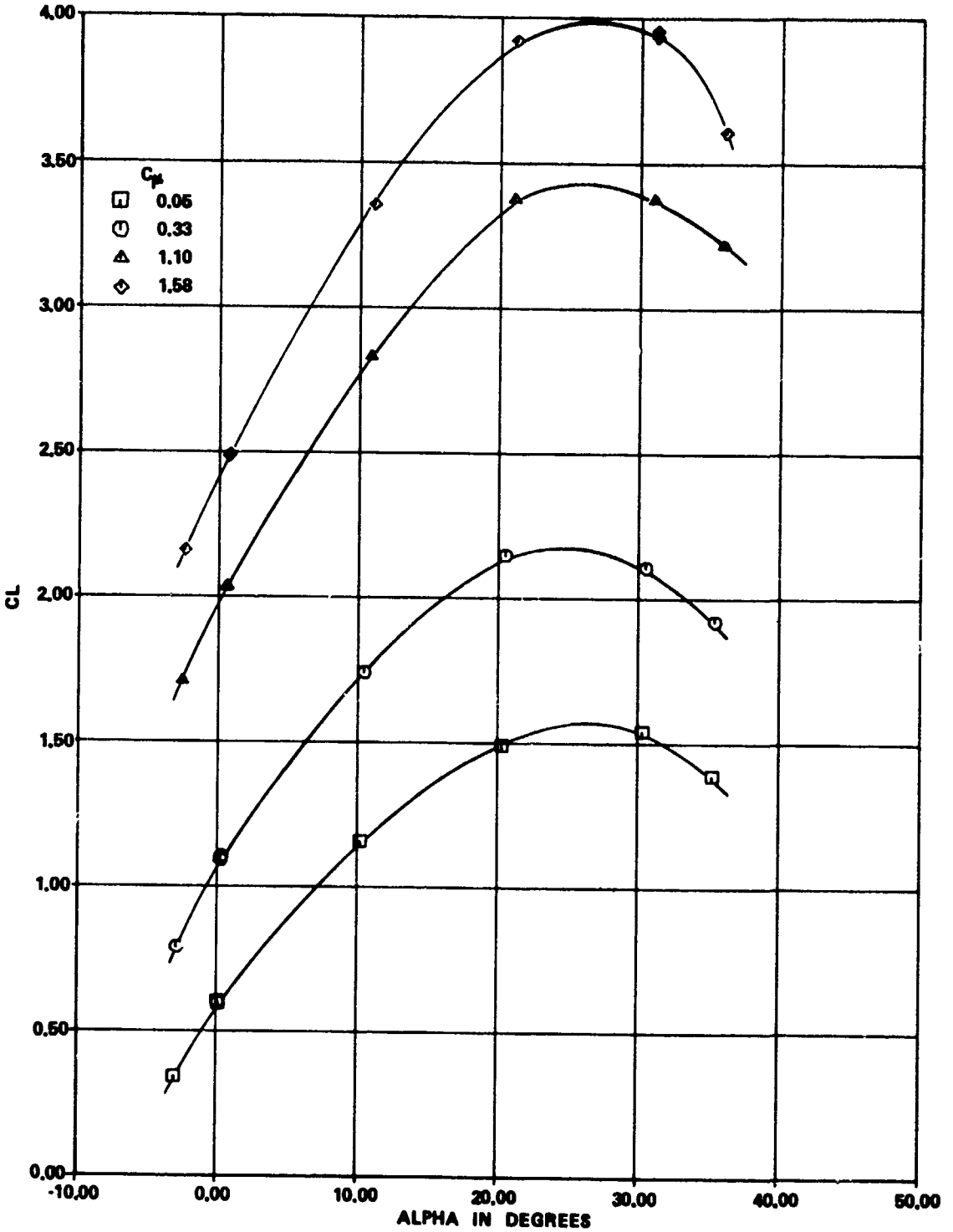

Figure 22d - Aspect Ratio 3.9 Duct with Tip Fence Installed

Figure 22 (Continued)

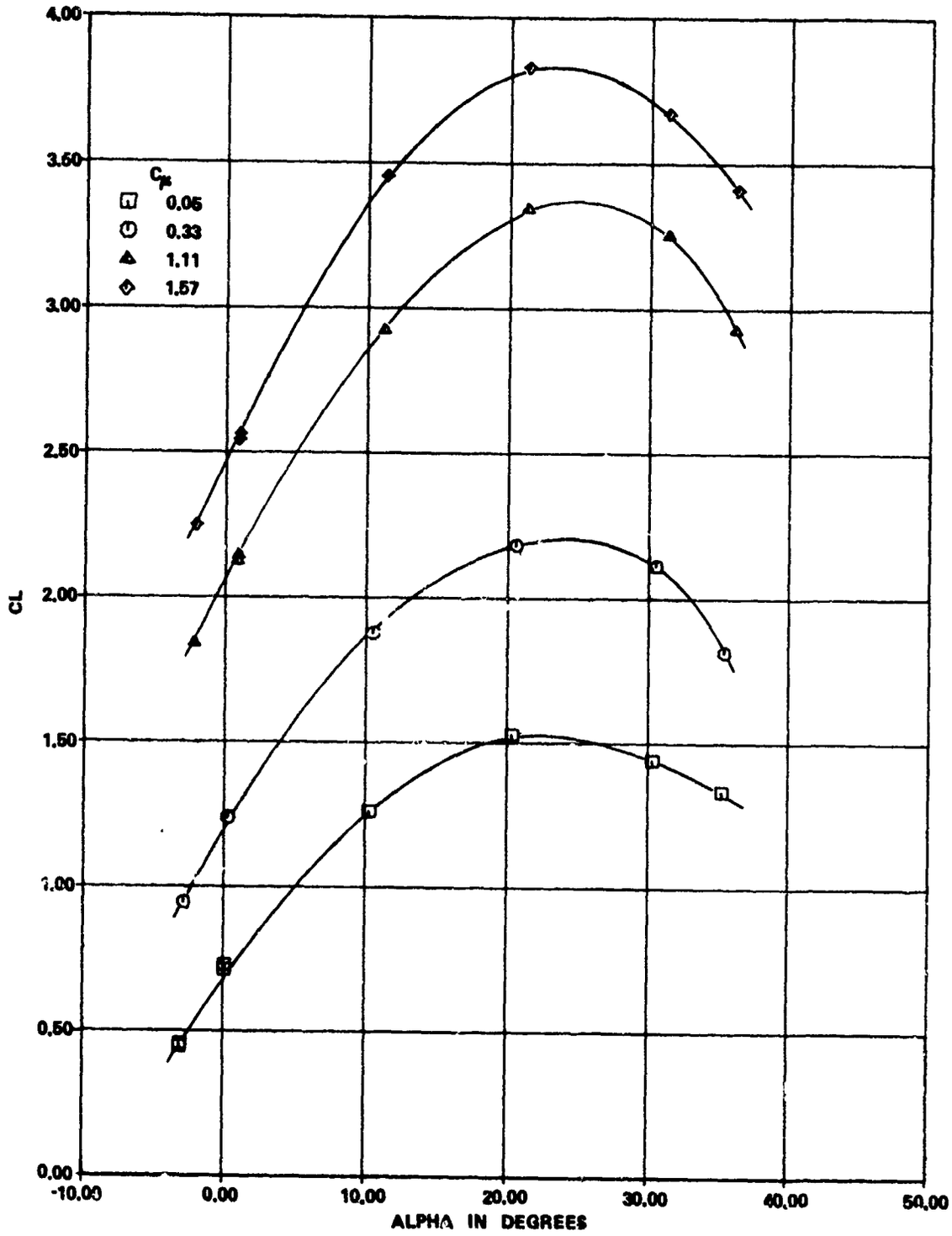

Figure 22e - Aspect Ratio 5.8 Duct with Tip Fence Installed

Figure 23 - Lift Characteristics of Aspect Ratio 3 Wing in USB Configuration with 60-Degree Flaps

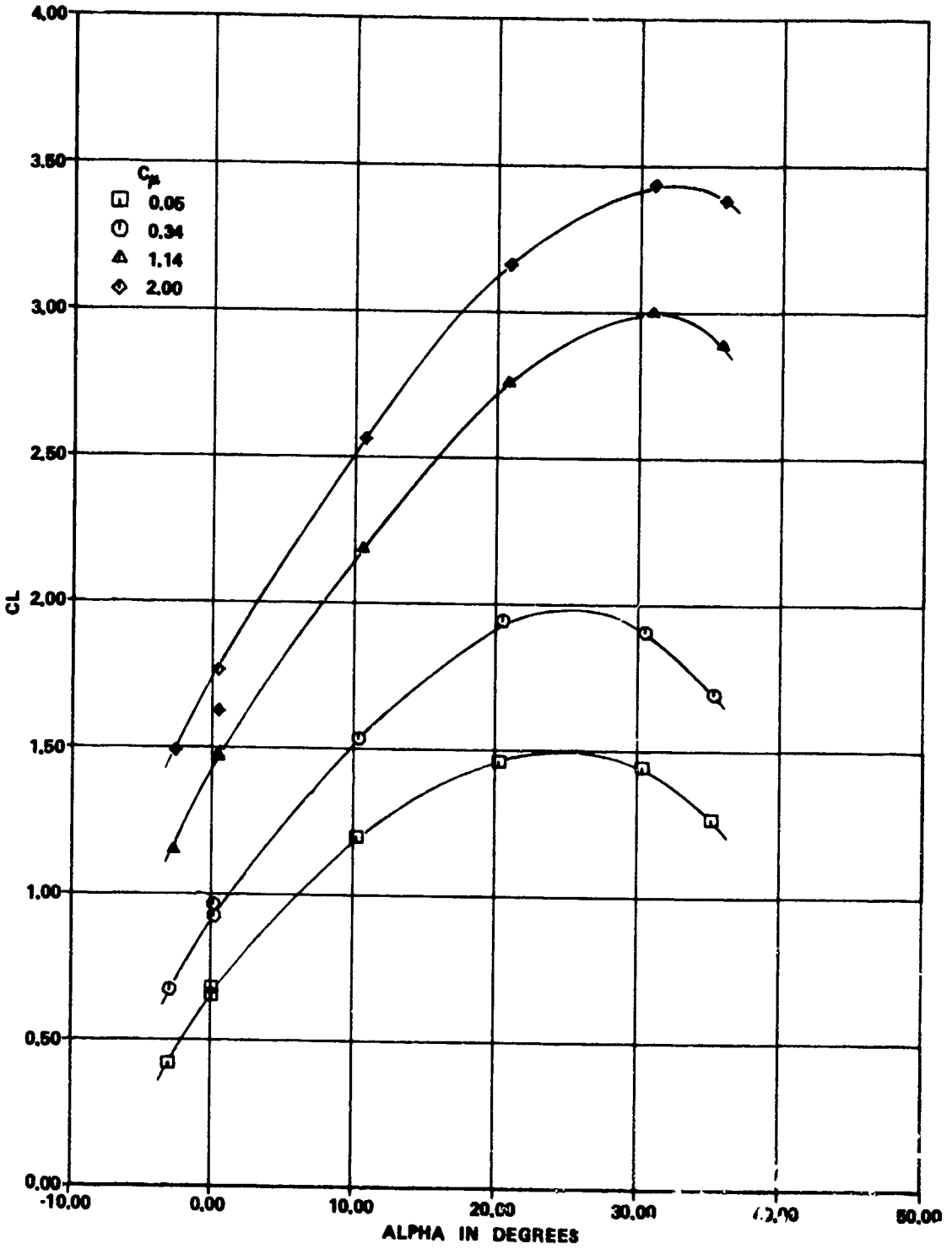

Figure 23a - Aspect Ratio 2.2 Duct

Figure 23 (Continued)

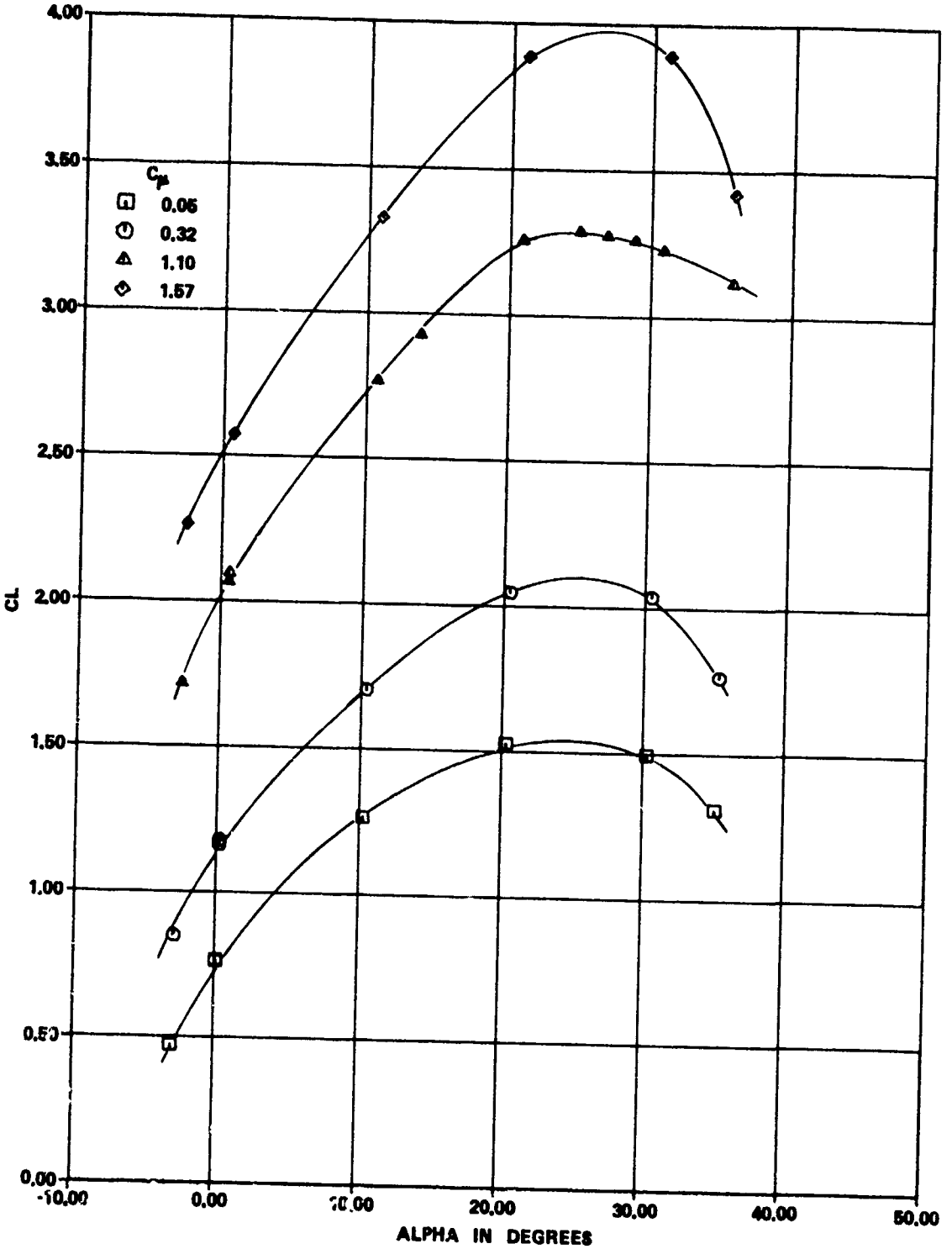

Figure 23b - Aspect Ratio 3.9 Duct

Figure 23 (Continued)

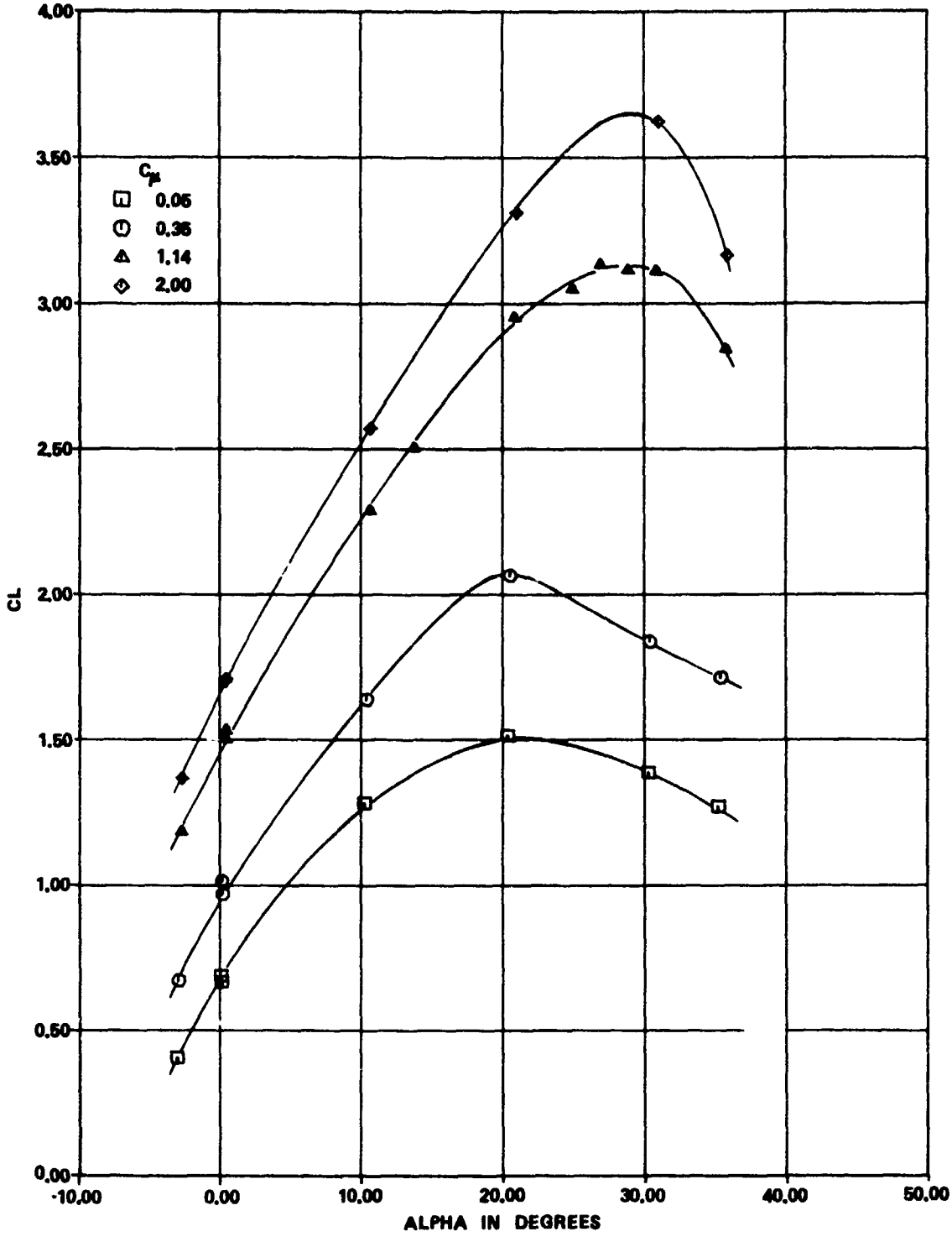

Figure 23c - Aspect Ratio 2.2 Duct with Tip Fence Installed

Figure 23 (Continued)

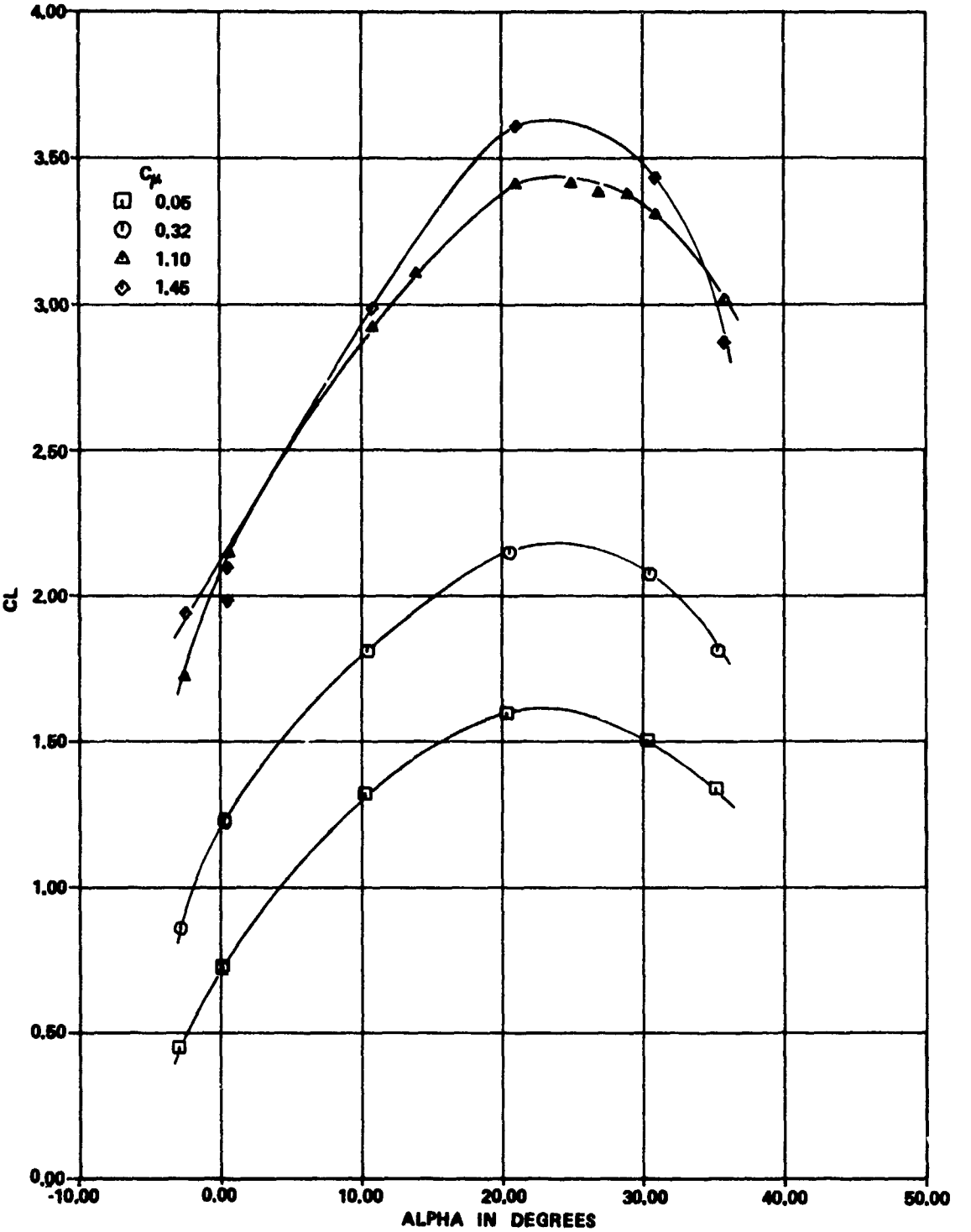

Figure 23d - Aspect Ratio 3.9 Duct with Tip Fence Installed

Figure 23 (Continued)

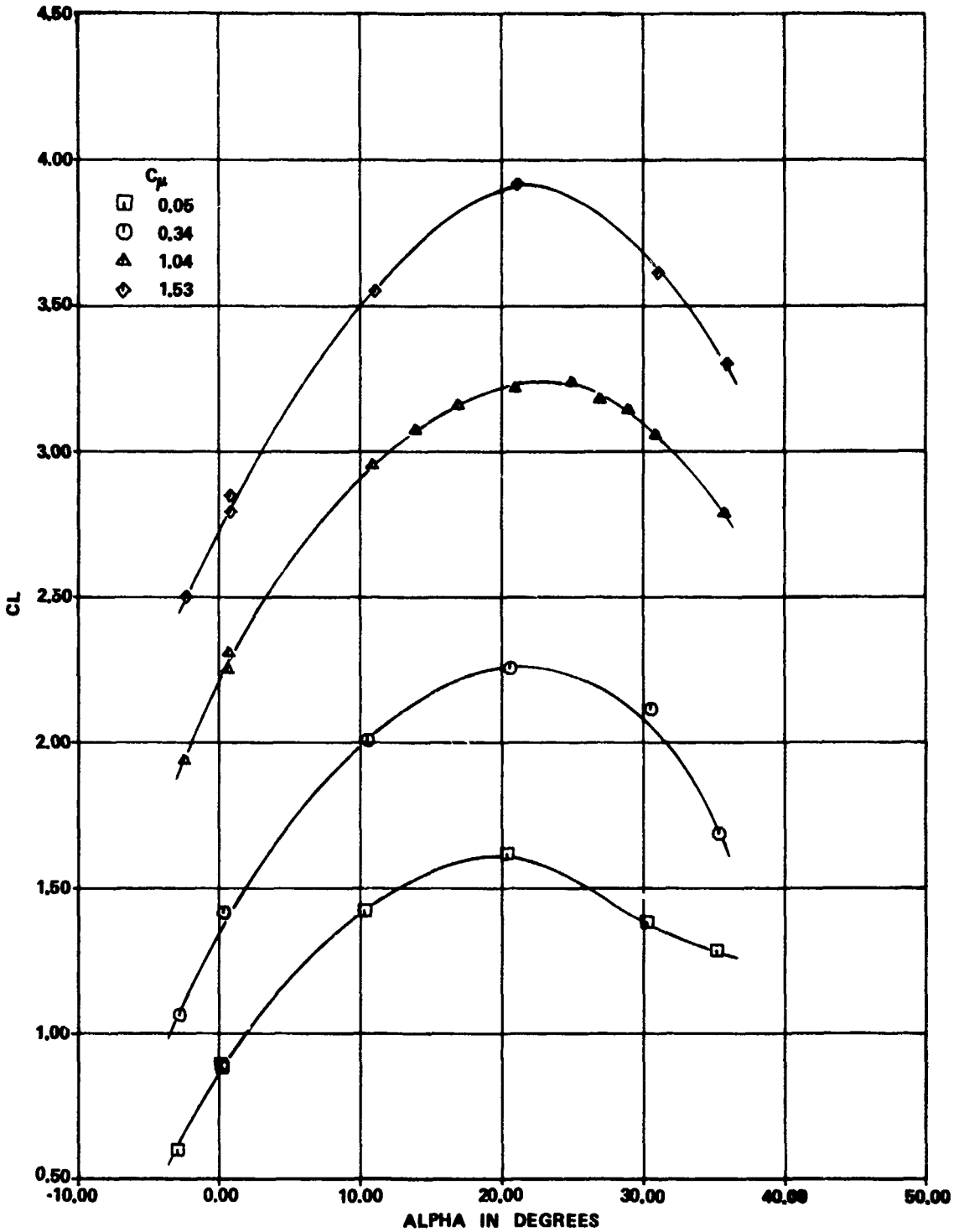

Figure 23e - Aspect Ratio 5.8 Duct with Tip Fence Installed

Figure 24 - Lift Characteristics of Aspect Ratio 4
Wing in USB Configuration with 40-Degree Flaps

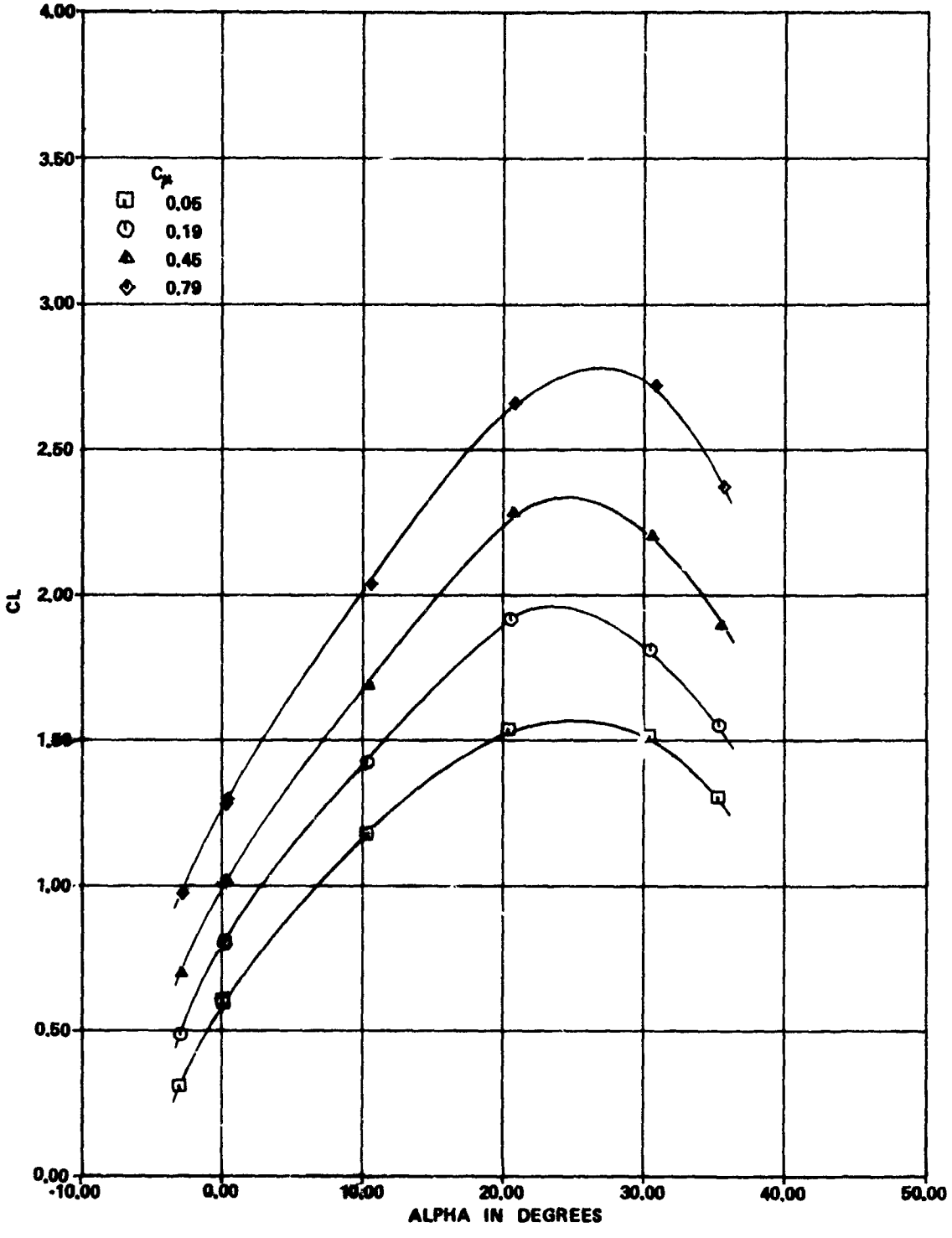

Figure 24a - Aspect Ratio 2.2 Duct

Figure 24 (Continued)

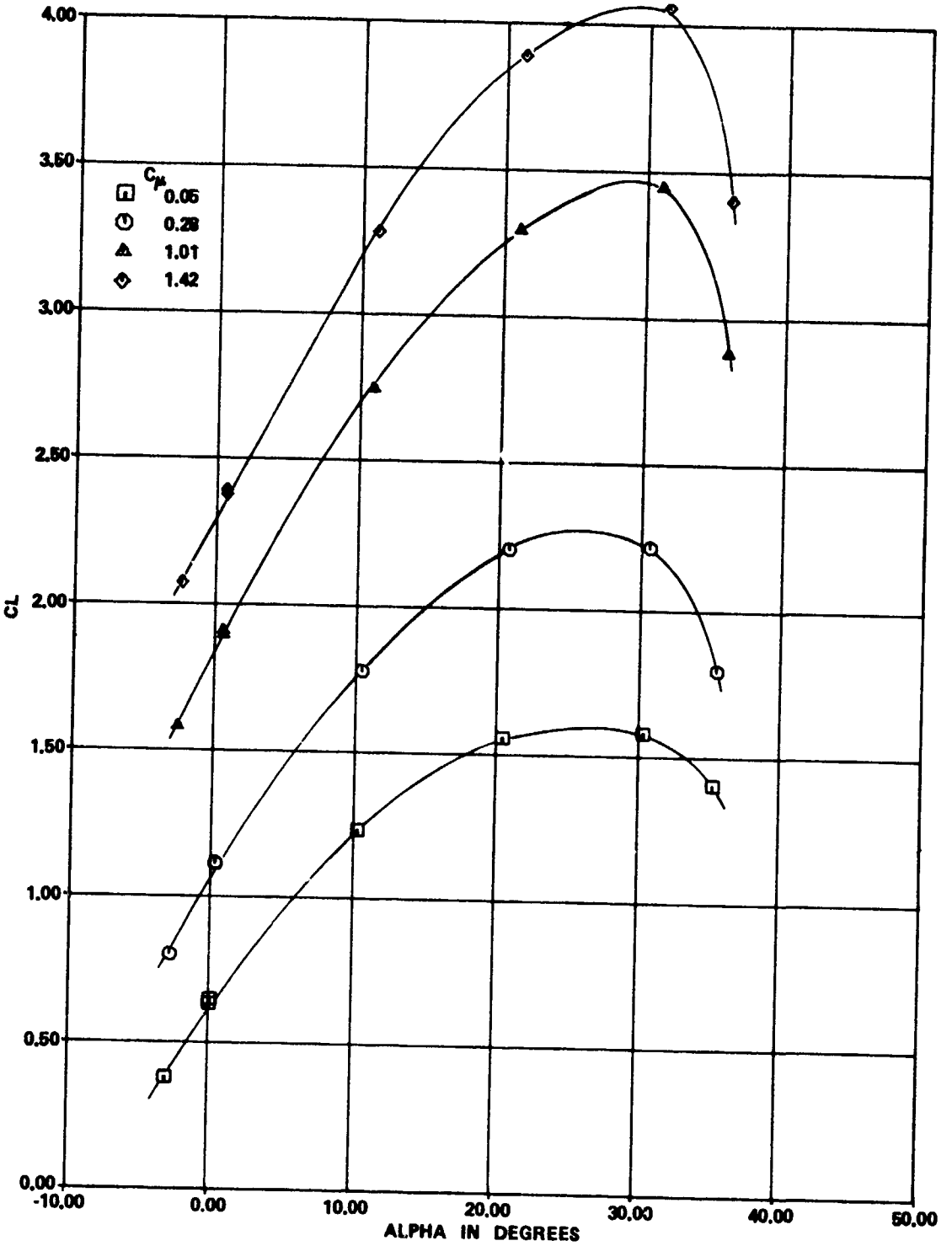

Figure 24b - Aspect Ratio 3.9 Duct

Figure 24 (Continued)

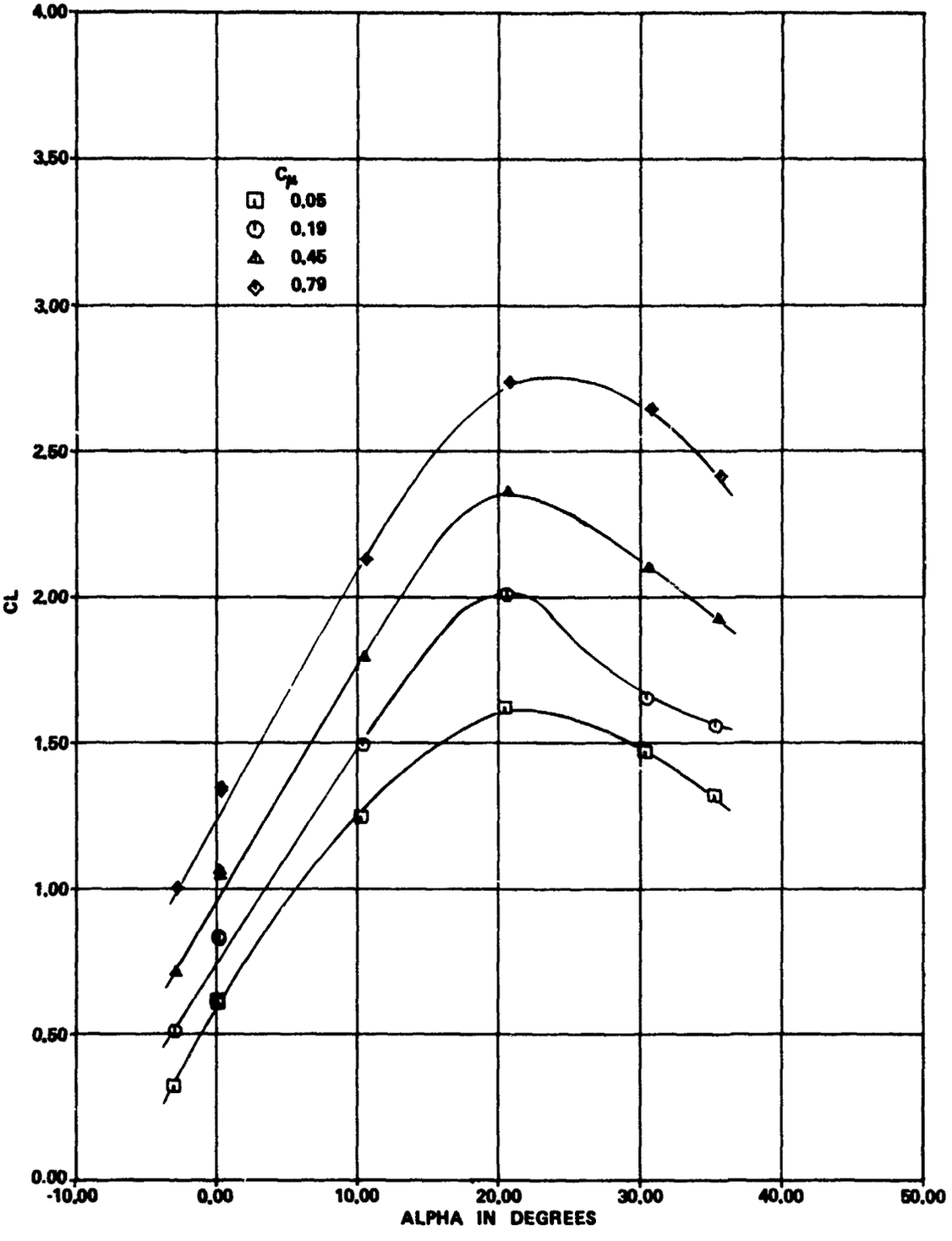

Figure 24c - Aspect Ratio 2.2 Duct with Tip Fence Installed

Figure 24 (Continued)

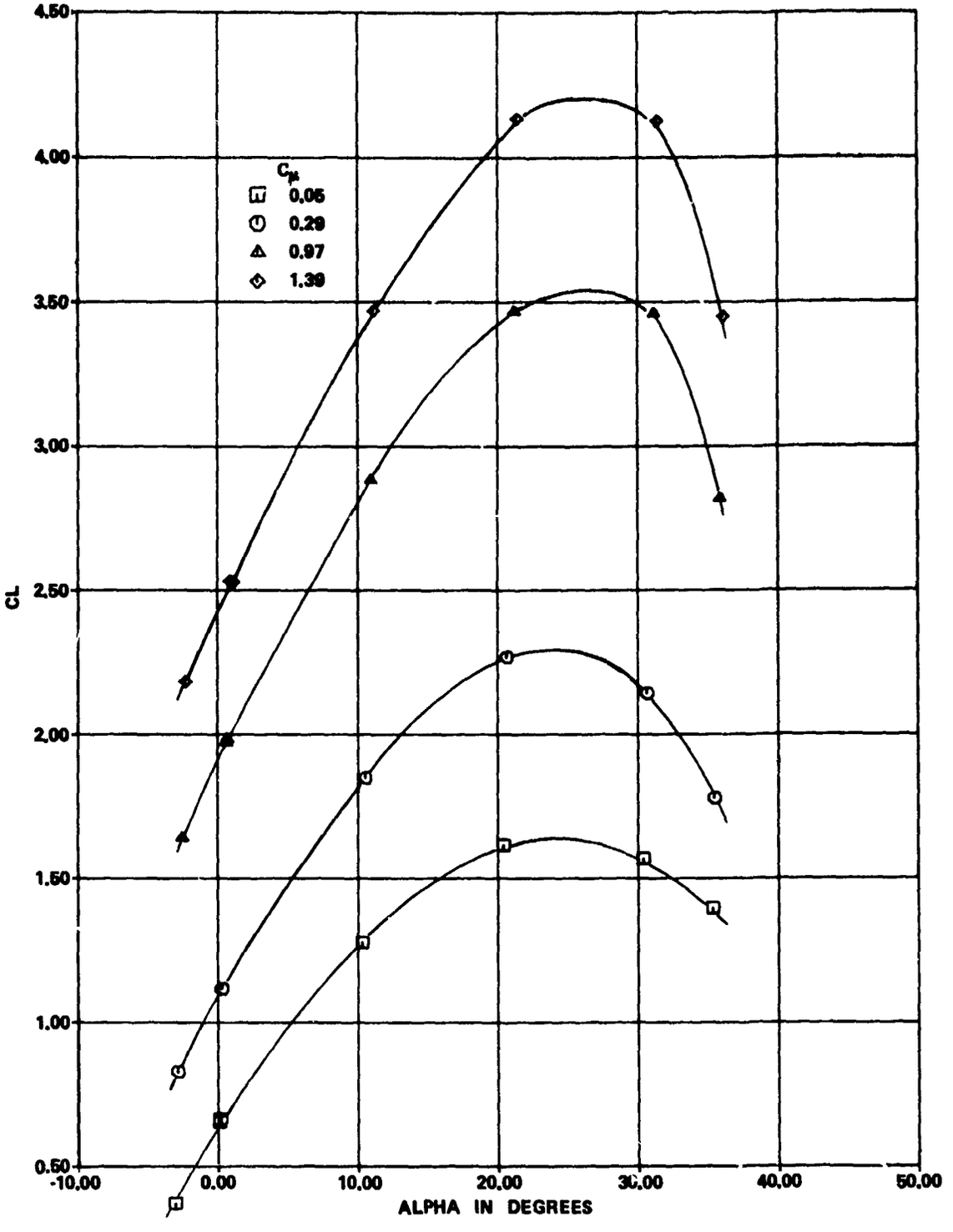

Figure 24d - Aspect Ratio 3.9 Duct with Tip Fence Installed

Figure 24 (Continued)

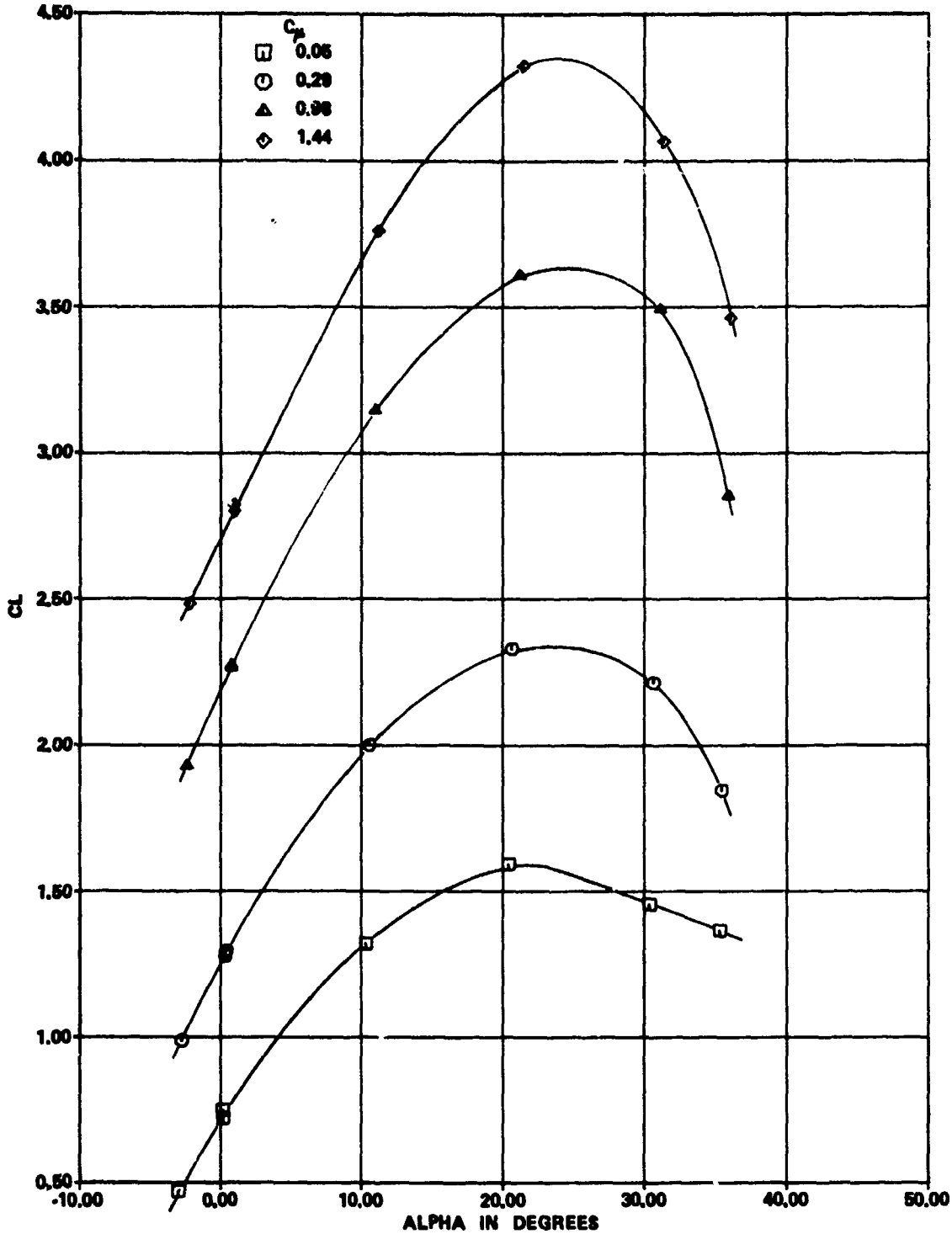

Figure 24e - Aspect Ratio 5.8 Duct with Tip Fence Installed

Figure 25 - Lift Characteristics of Aspect Ratio 4 Wing in USB Configuration with 60-Degree Flaps

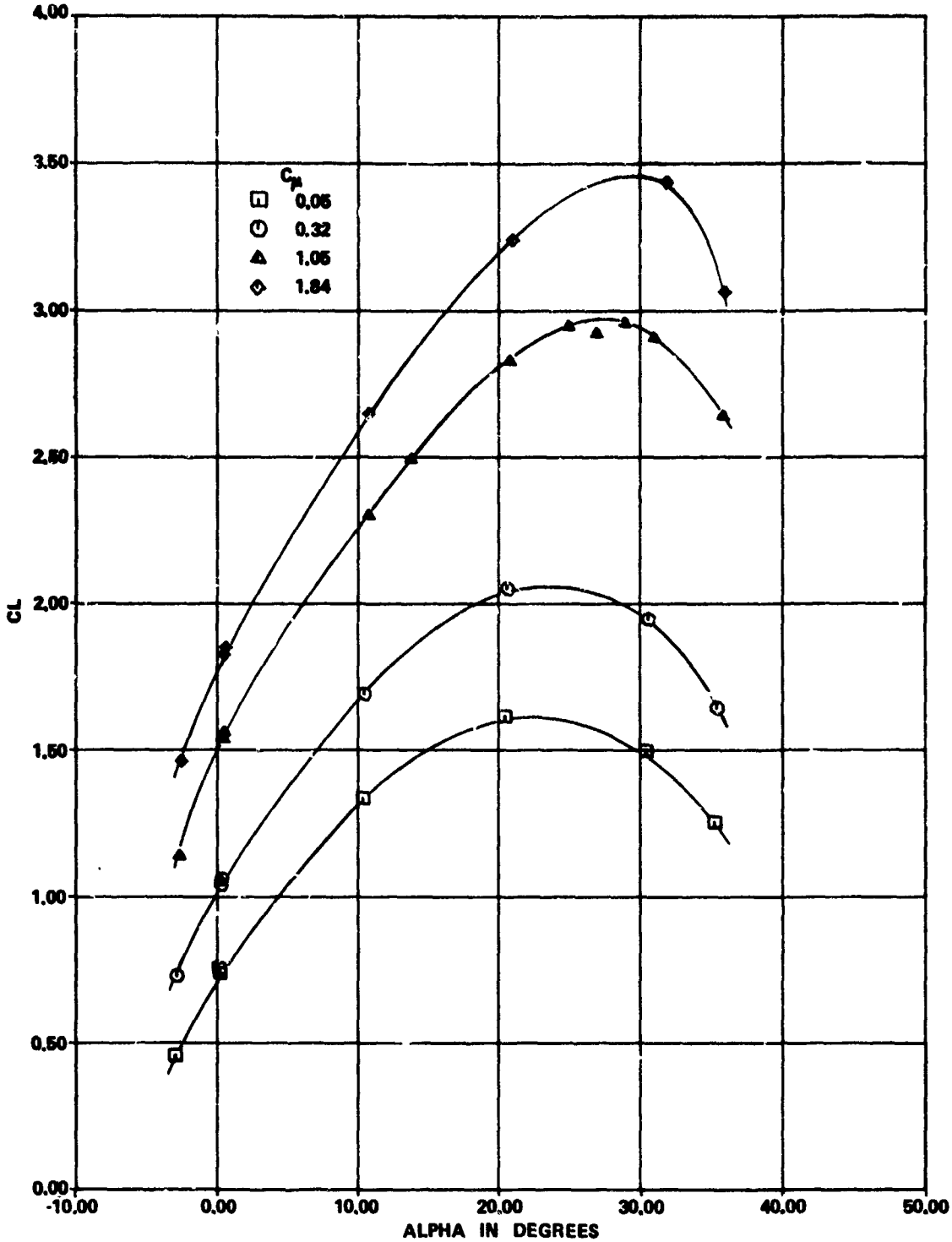

Figure 25a - Aspect Ratio 2.2 Duct

Figure 25 (Continued)

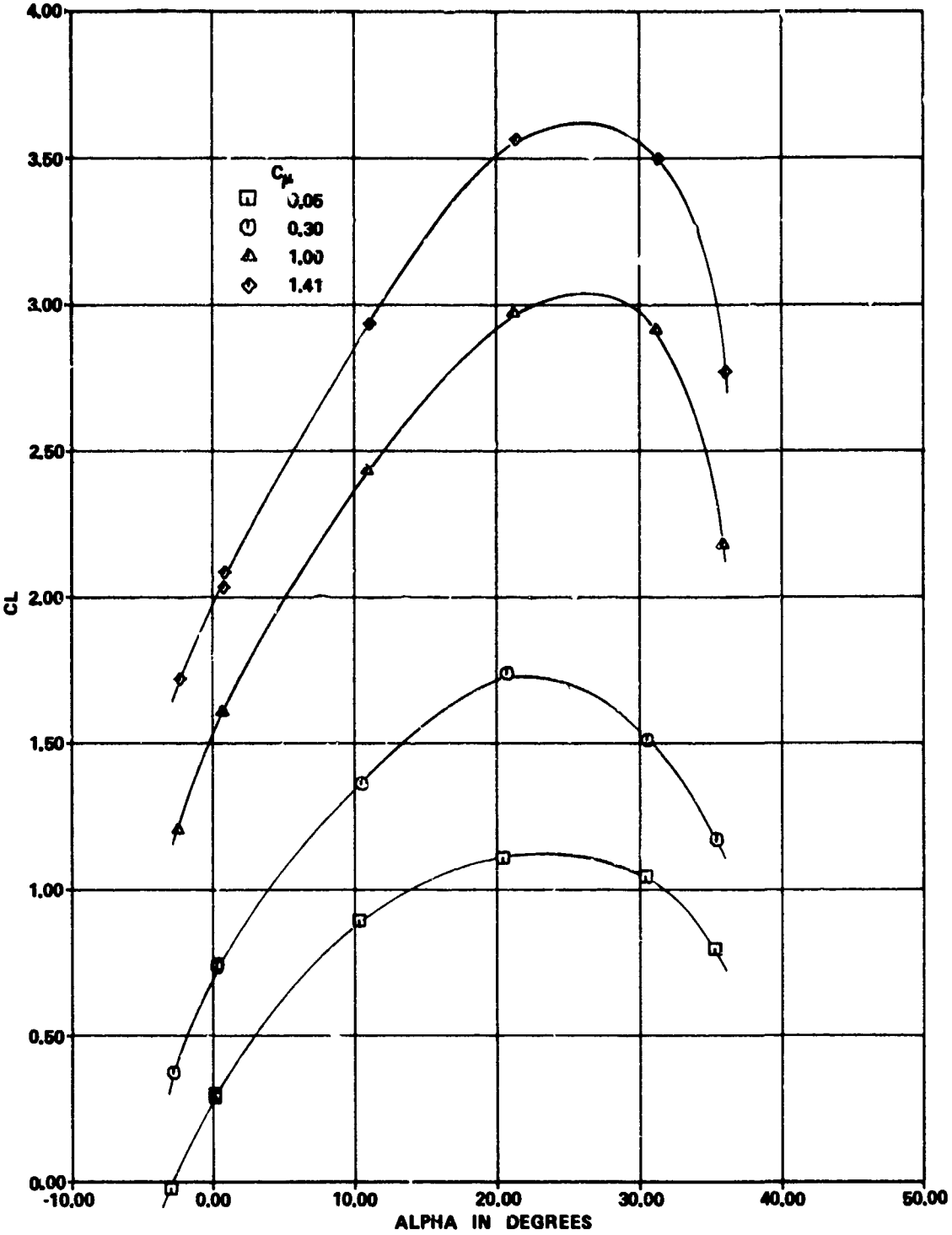

Figure 25b - Aspect Ratio 3.9 Duct

Figure 25 (Continued)

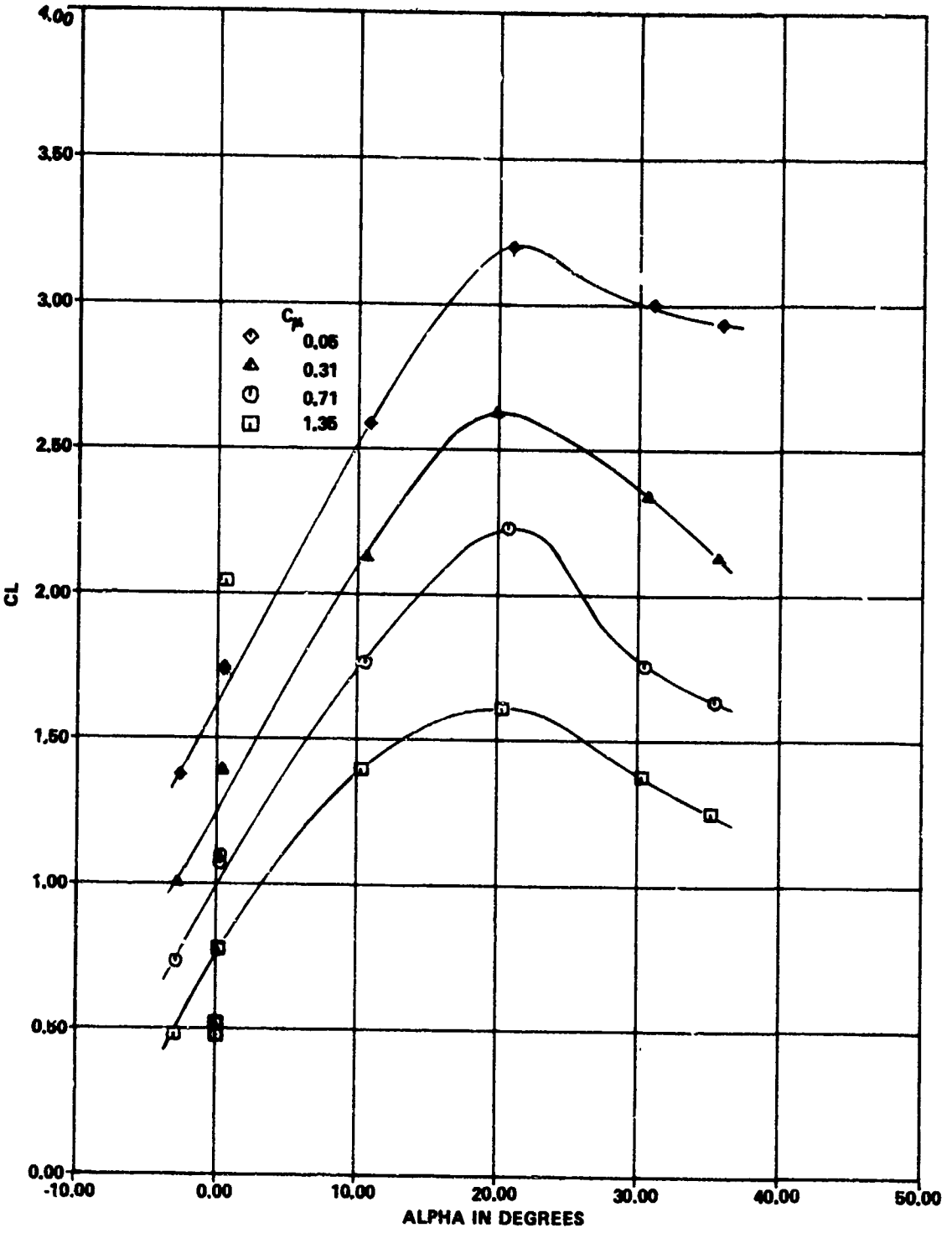

Figure 25c - Aspect Ratio 2.2 Duct with Tip Fence Installed

Figure 25 (Continued)

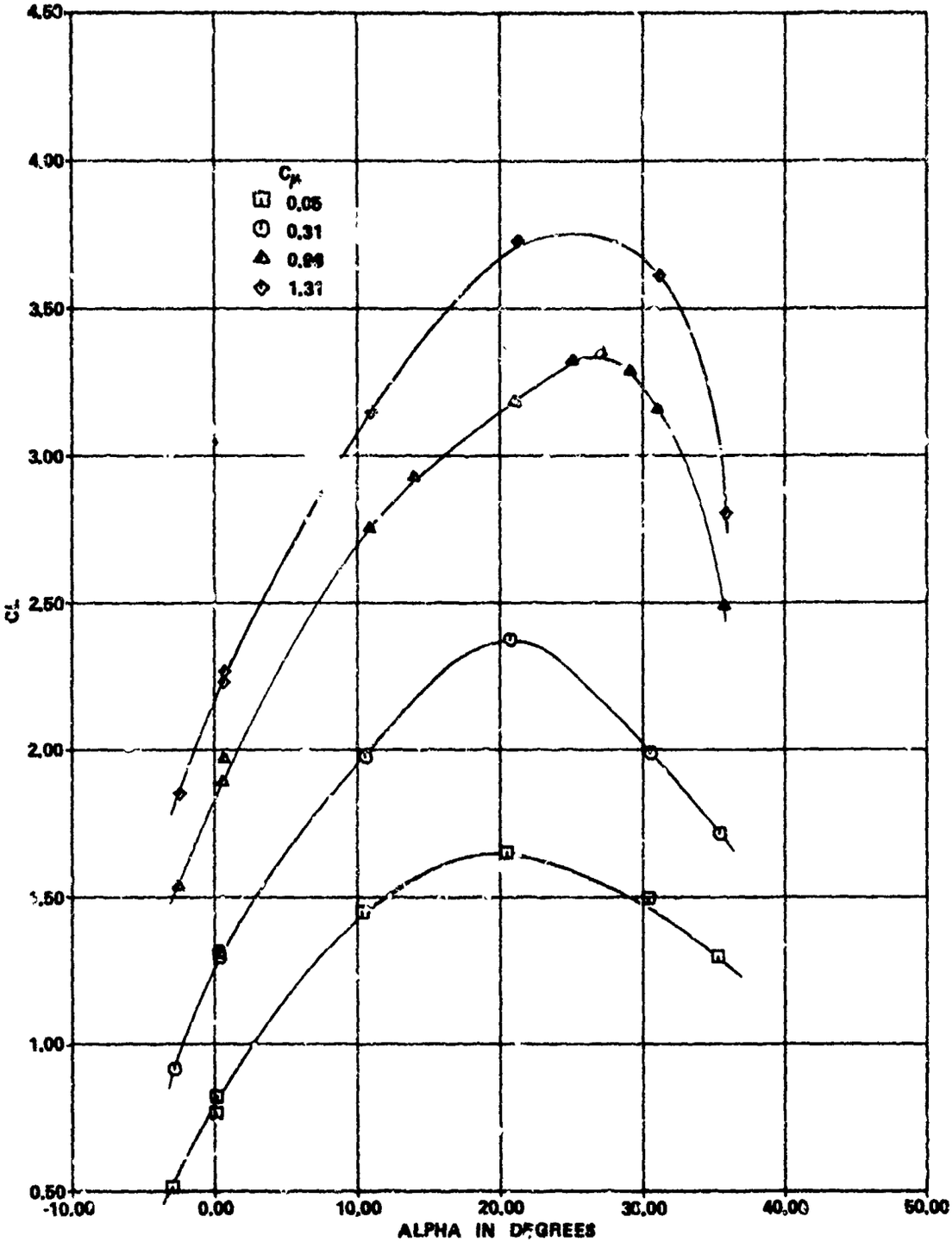

Figure 25d - Aspect Ratio 3.9 Duct with Tip Fence Installed

Figure 25 (Continuad)

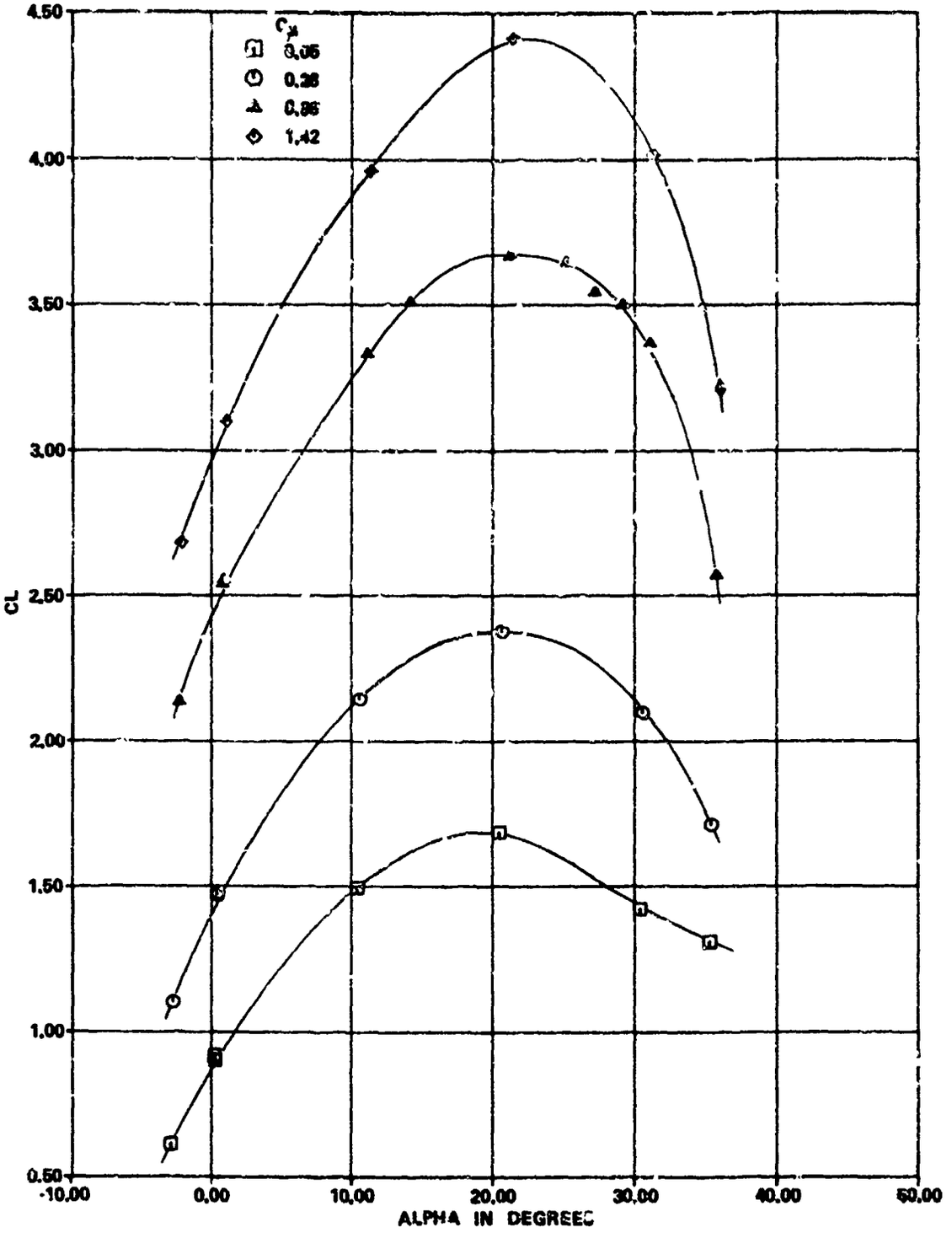

Figure 25e - Aspect Ratio 5.8 Duct with Tip Fence Installed

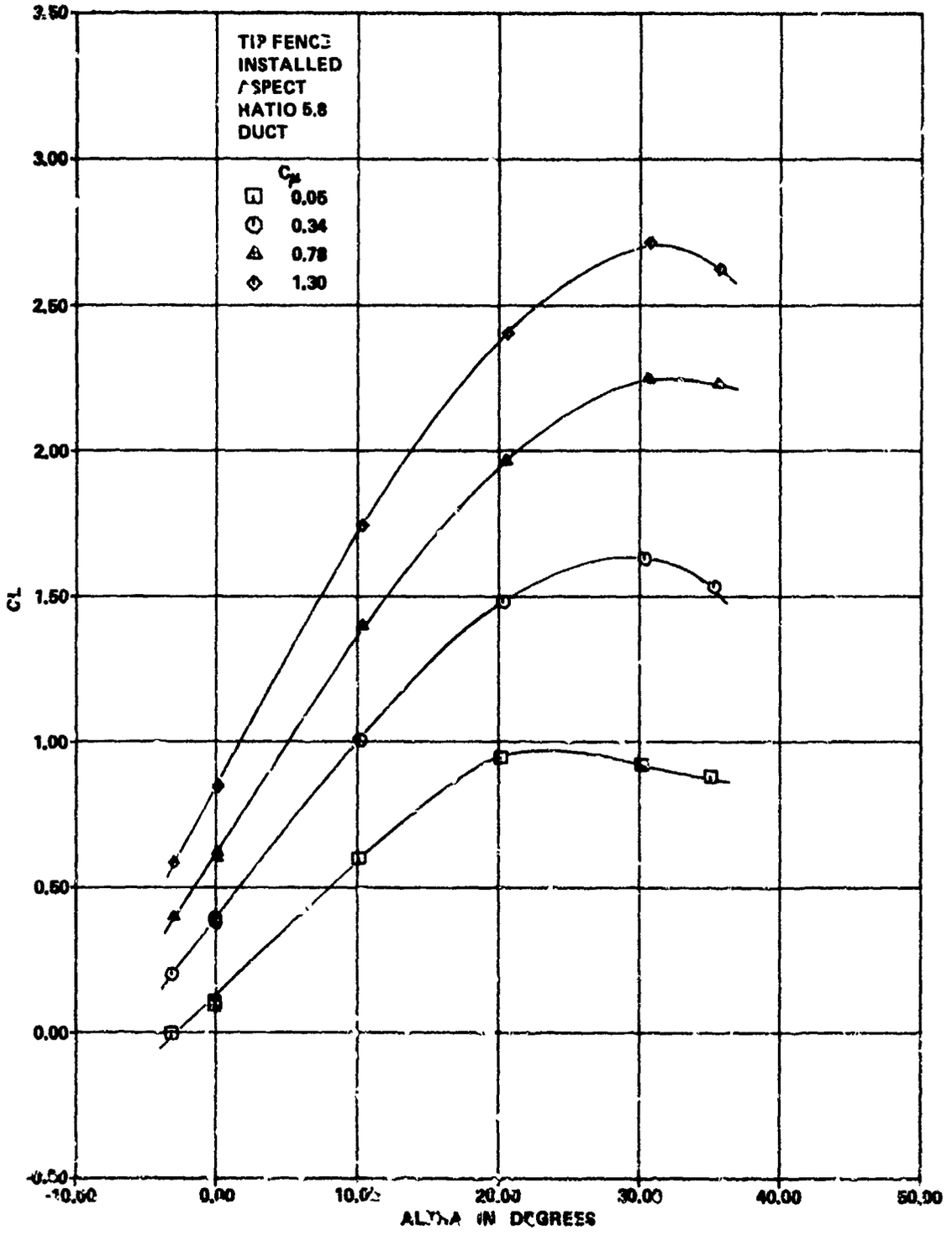

Figure 26 - Lift Characteristics of Aspect Ratio 3 Wing in USB Configuration with Zero Flap Angle

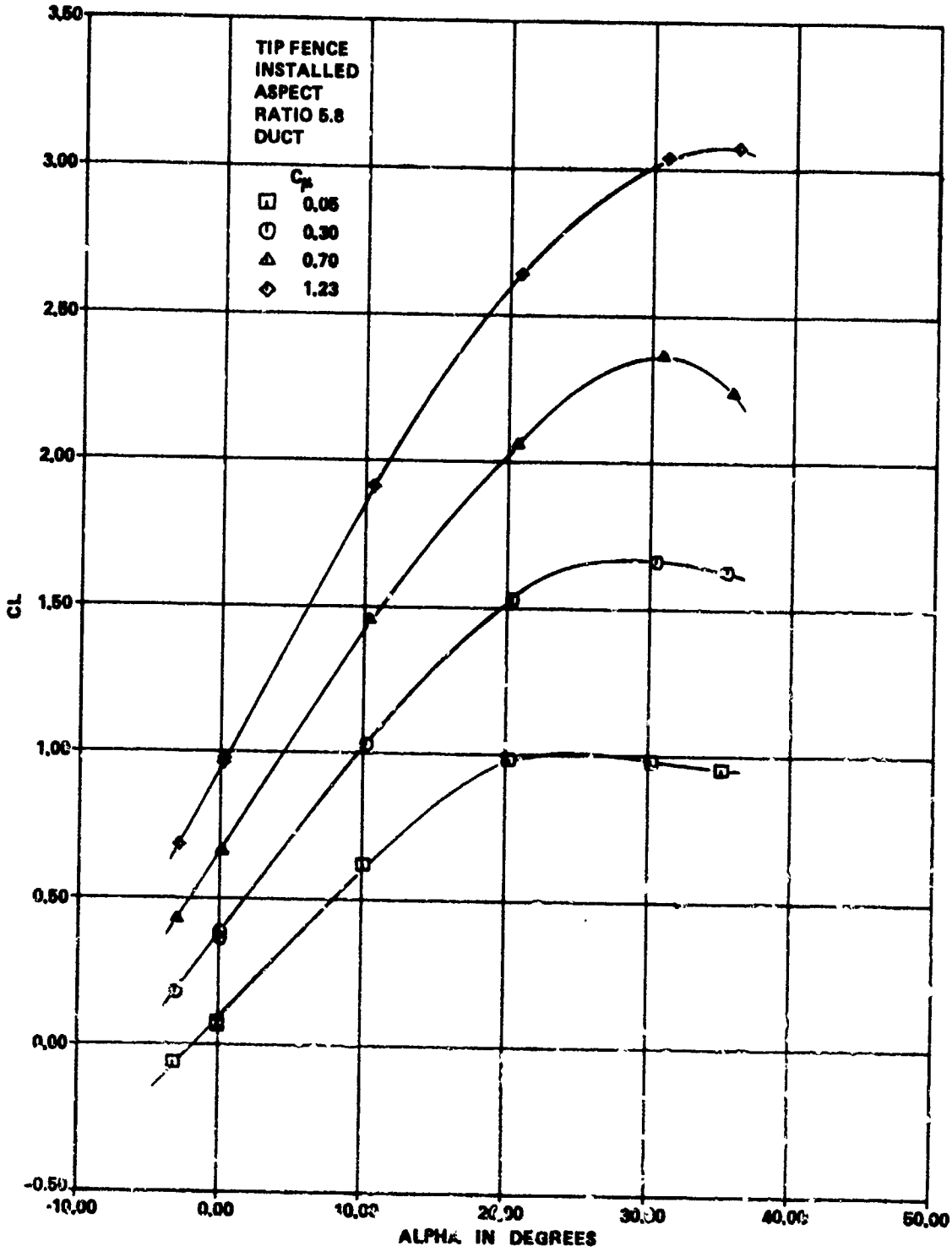

Figure 27 - Lift Characteristics of Aspect Ratio 4 Wing in USB Configuration with Zero Flap Angle

Figure 28 - Effect of Flap Slots on the Lift of a USB Configuration with 60-Degree Flaps

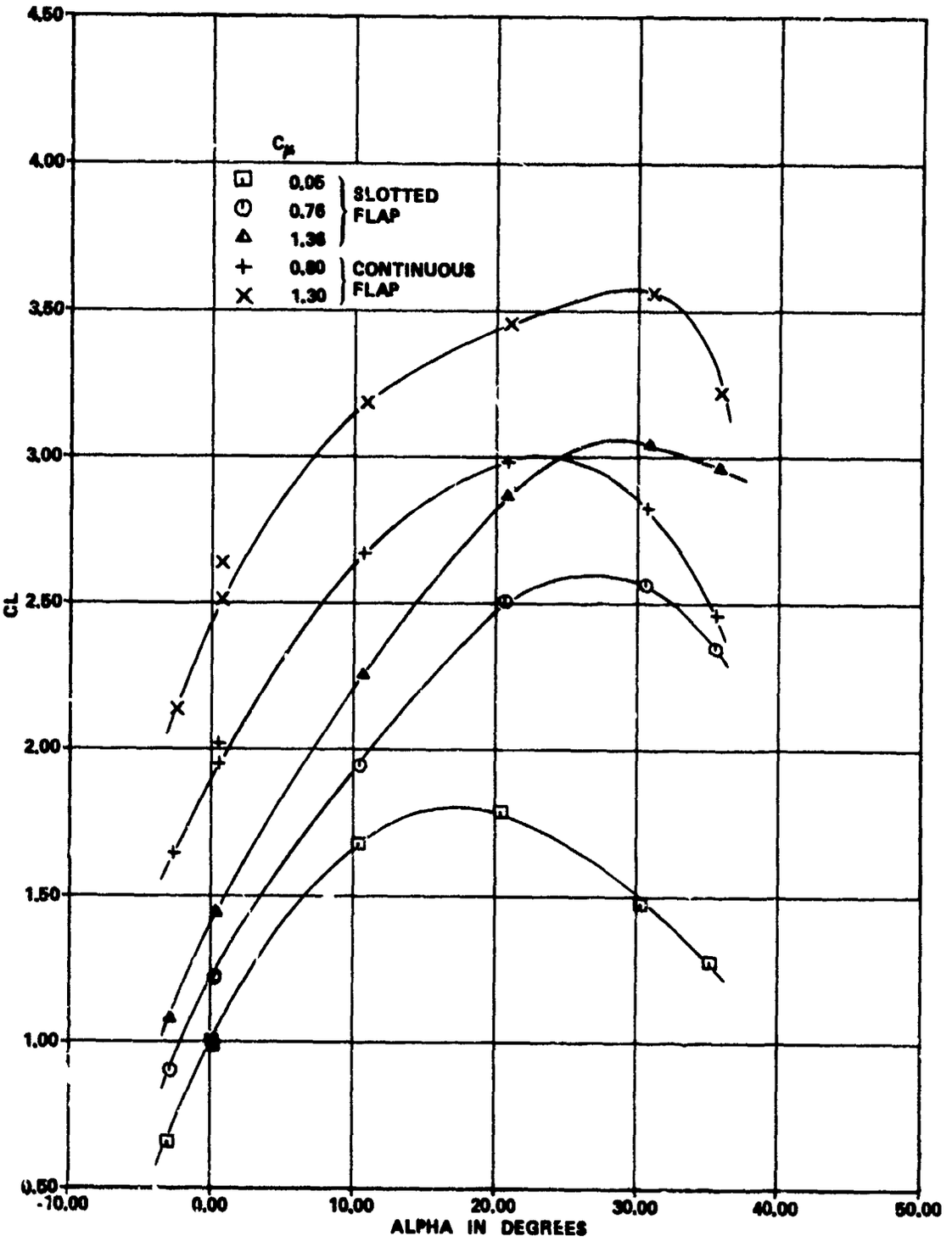

Figure 28a - Aspect Ratio 3 Wing with Tip Fences and 5.8 Aspect Ratio Duct

Figure 28 (Continued)

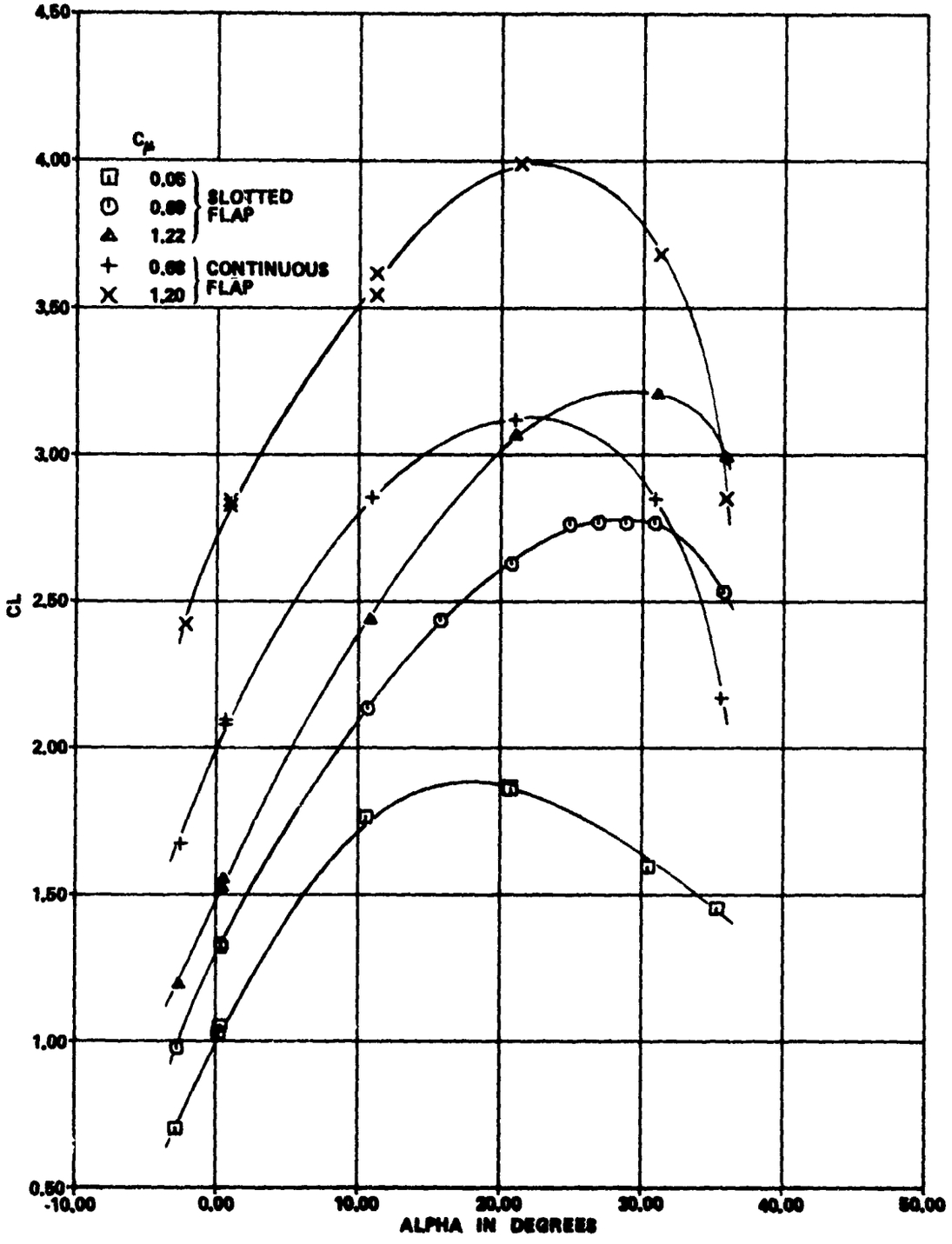

Figure 28b - Aspect Ratio 4 Wing with Tip Fences and 5.8 Aspect Ratio Duct

Figure 29 - Maximum Lift Characteristics of USB Configurations with 5.8 Aspect Ratio Duct

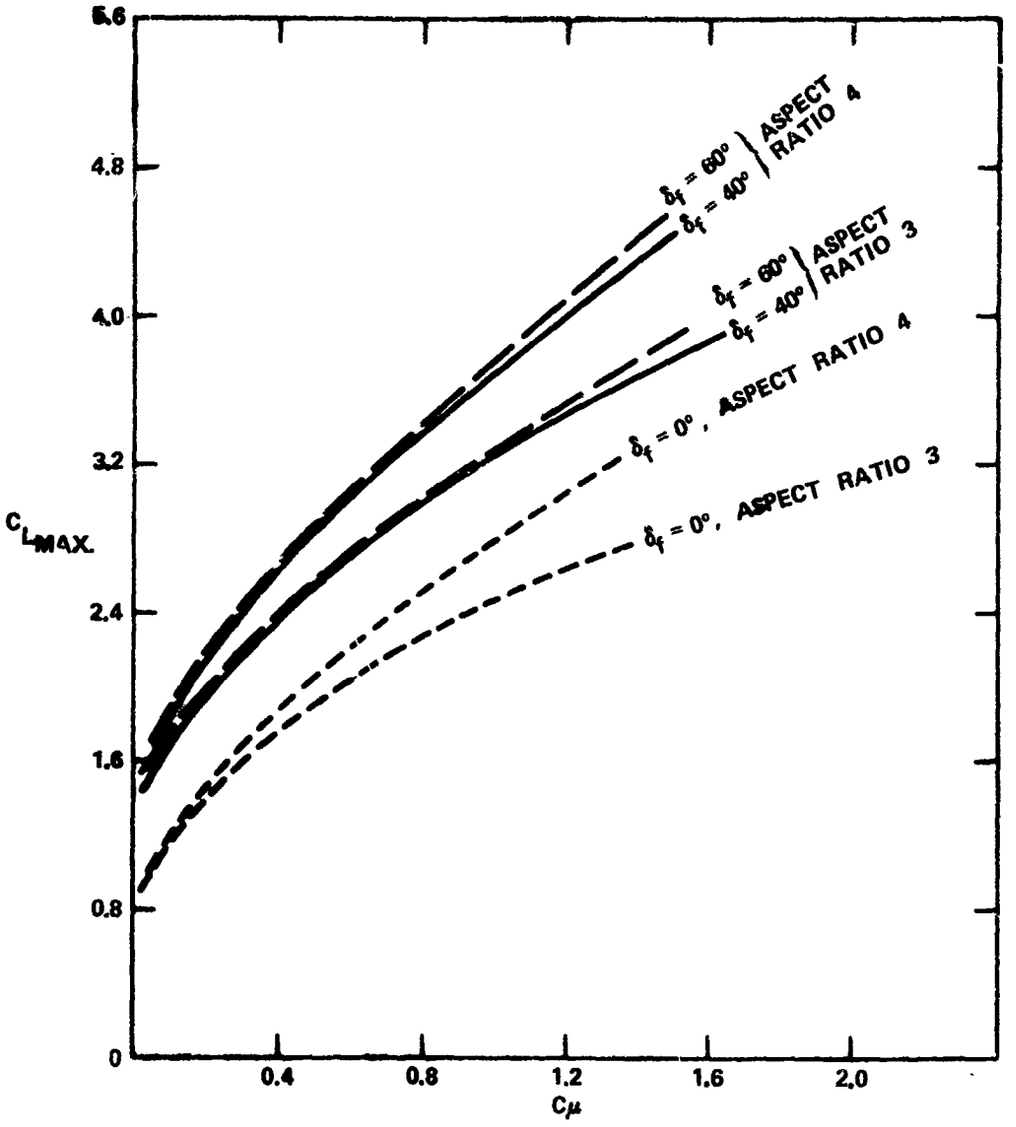

Figure 29a - With Wing Tip Fence

Figure 29 (Continued)

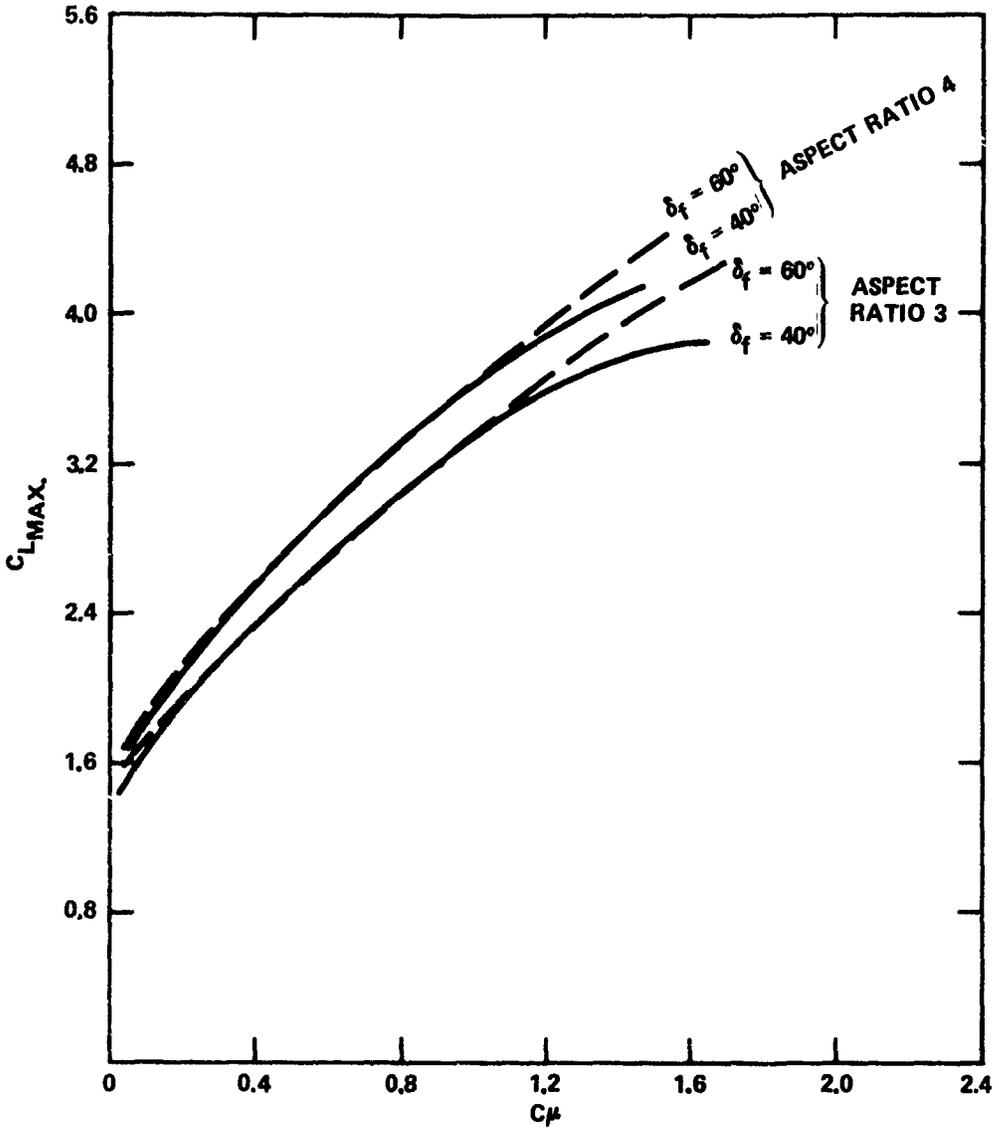

Figure 29b - Without Wing Tip Fence

DTNSRDC ISSUES THREE TYPES OF REPORTS

1. DTNSRDC REPORTS, A FORMAL SERIES, CONTAIN INFORMATION OF PERMANENT TECHNICAL VALUE. THEY CARRY A CONSECUTIVE NUMERICAL IDENTIFICATION REGARDLESS OF THEIR CLASSIFICATION OR THE ORIGINATING DEPARTMENT.

2. DEPARTMENTAL REPORTS, A SEMIFORMAL SERIES, CONTAIN INFORMATION OF A PRELIMINARY, TEMPORARY, OR PROPRIETARY NATURE OR OF LIMITED INTEREST OR SIGNIFICANCE. THEY CARRY A DEPARTMENTAL ALPHANUMERICAL IDENTIFICATION.

3. TECHNICAL MEMORANDA, AN INFORMAL SERIES, CONTAIN TECHNICAL DOCUMENTATION OF LIMITED USE AND INTEREST. THEY ARE PRIMARILY WORKING PAPERS INTENDED FOR INTERNAL USE. THEY CARRY AN IDENTIFYING NUMBER WHICH INDICATES THEIR TYPE AND THE NUMERICAL CODE OF THE ORIGINATING DEPARTMENT. ANY DISTRIBUTION OUTSIDE DTNSRDC MUST BE APPROVED BY THE HEAD OF THE ORIGINATING DEPARTMENT ON A CASE-BY CASE BASIS.